

University of Alberta

**Lewis Base Adducts of Borafluorene: En Route to Polymers and the
Discovery of New Luminescent Adducts**

by

Christopher James Berger

A thesis submitted to the Faculty of Graduate Studies and Research
in partial fulfillment of the requirements for the degree of

Master of Science

Department of Chemistry

© Christopher James Berger
Fall 2013
Edmonton, Alberta

Permission is hereby granted to the University of Alberta Libraries to reproduce single copies of this thesis and to lend or sell such copies for private, scholarly or scientific research purposes only. Where the thesis is converted to, or otherwise made available in digital form, the University of Alberta will advise potential users of the thesis of these terms.

The author reserves all other publication and other rights in association with the copyright in the thesis and, except as herein before provided, neither the thesis nor any substantial portion thereof may be printed or otherwise reproduced in any material form whatsoever without the author's prior written permission.

Abstract

A series of novel Lewis base monoadducts of 9-bromo-9-borafluorene ($\text{BrBfI}\cdot\text{LB}$, $\text{LB} = \text{IPr}$, IPrCH_2 , PPh_3) and the bisadduct $[(\text{DMAP})_2\text{BfI}]\text{Br}$ were prepared and underwent reactivity studies in the pursuit of incorporating a borafluorene unit into a polymeric scaffold for the sensing of nucleophiles in solution. This was to be accomplished through the functionalization of these adducts at boron, polymerization and subsequent removal of the Lewis base. Although initial studies indicated that the removal of the Lewis base was more difficult than anticipated, the adducts $\text{BrBfI}\cdot\text{PPh}_3$, $[(\text{DMAP})_2\text{BfI}]\text{Br}$ and $\text{BrBfI}\cdot\text{IPrCH}_2$ were found to be fluorescent. This observation was initially counterintuitive, as a borafluorene containing a four-coordinate boron environment would not be expected to possess such a property. Theoretical studies were conducted to determine the nature of the fluorescence and revealed that the Lewis base bonded to boron significantly contribute to the transitions leading to fluorescence.

Acknowledgements

The path to completing this thesis has been a long and winding road that could not have been accomplished without the involvement of many people. Specifically, I would like to thank my parents Peter & Brenda Frank and Glen Berger as well as my sister Arielle Berger for their constant support. My friends Justin Thuss, Colin Diner, Devin Reaugh, Kirsten Tomlin and the rest of my friends who's names I have apparently forgotten, thank you for your constant encouragement. My labmates past and present, especially Melanie Lui and Paul Lummis, for their support and involvement in my research. I would like to thank Dr. Christian Merten, without him I could not have provided nearly as in-depth an analysis of my chemistry. The staff of the Department of Chemistry, specifically Ryan Lewis, Bernie Hippel, Wayne Moffat and the Analytical and Instrumentation Lab staff, Mark Miskolzie and the NMR Lab staff, Dr. Robert McDonald, Dr. Michael Ferguson, Allan Chilton, Dirk Kelm and the Machine Shop, Jason Dibbs, the Mass Spectrometry Lab staff and the department administration. Without the incredible support network created by these people the quality of research leaving the Department of Chemistry would not be nearly as high. I would also like to acknowledge the contributions of Dr. Eric Rivard, Dr. Jonathan Veinot, Dr. Frederick West and Dr. Wolfgang Jäger in their role as my supervisory and evaluation committee. Thank you for taking the time to help. And to those that I have not mentioned by name, your contributions were not unnoticed.

Table of Contents

Chapter 1: Introduction	1
1.1 Brief Overview of Heterocyclic Organoborane Compounds	1
1.2 Application of Borafluorenes to Nucleophile Sensing	10
1.3 Overview of Project Goals	15
1.4 Brief Note on the Structure of this Thesis	17
1.5 References	18
Chapter 2: Synthesis, Reactivity and Photophysical Properties of Novel Lewis Base Adducts of Borafluorene	22
2.1 Introduction	22
2.2 Results and Discussion	25
2.2.1 Synthesis and Reactivity Studies of Novel Lewis Base Adducts of 9-Bromo-9-borafluorene	25
2.2.2 Photophysical Properties of the neutral 9-Bromo-9-borafluorene adducts BrBF1•PPh ₃ (10), [(DMAP) ₂ BF1]Br (12) and BrBF1•IPrCH ₂ (17)	62
2.3 Conclusions	75
2.4 Experimental Section	77
2.4.1 Experimental Methods and Procedures	77
2.4.2 Crystallographic Tables	97
2.4.3 NMR Spectra	99
2.5 References	103

Chapter 3: Summary and Future Work	110
3.1 Summary	110
3.2 Future Work Towards Incorporating Borafluorene into a Polymeric Scaffold	110
3.3 Future Research Involving Luminescent Lewis Base Adducts of Borafluorene	112

List of Tables

Table 2.2.1. Photophysical data summary for 10 , 12 and 17 .	66
Table 2.2.2. Calculated electronic transitions showing the first 12 excited states, corresponding oscillator strengths and the nature of the π - π^* /charge transfer for 10 .	73
Table 2.2.3. Calculated electronic transitions showing the first 10 excited states, corresponding oscillator strengths and the nature of the π - π^* /charge transfer for 12 .	74
Table 2.2.4. Calculated electronic transitions showing the first 10 excited states, corresponding oscillator strengths and the nature of the π - π^* /charge transfer for 17 .	75
Table 2.4.1. Attempted “unmasking” of BrBFI•IPr (2).	95
Table 2.4.2. Attempted “unmasking” of BrBFI•PPh ₃ (10).	95
Table 2.4.3. Attempted “unmasking” of [(DMAP) ₂ BFI]Br (12).	96
Table 2.4.4. Crystallographic Data for Compounds 2 , 8 and 12 .	97
Table 2.4.5. Crystallographic Data for Compounds 16 and 17 .	98

List of Figures

- Figure 1.1.1.** Parent borole showing reactive sites (left) and the isoelectronic cyclopentadienyl cation (right). 4
- Figure 1.1.2.** Representations of the parent borole (left) and parent borafluorene (right). 5
- Figure 1.1.3.** Representative examples of functionalized borafluorenes and similar boroles. 8
- Figure 1.2.1.** Structure of the nerve agents Sarin and Tabun, which, upon hydrolysis, release F^- and CN^- , respectively. 11
- Figure 2.1.1.** Representation of the general form of a borafluorene featuring the characteristic fused ring structure. 23
- Figure 2.2.1.** General schematic illustrating $N \rightarrow C$ π interactions within an NHC. 28
- Figure 2.2.2.** Thermal ellipsoid plot (30 % probability) of **2** with hydrogen atoms and CH_2Cl_2 solvate molecules omitted for clarity. 31
- Figure 2.2.3.** Thermal ellipsoid plot (30 % probability) of **8** with the hydrogen atom attached to boron presented with an arbitrarily small thermal parameter; the remaining hydrogen atoms are not shown for clarity. 36
- Figure 2.2.4.** Representative examples of organoborane species. 39
- Figure 2.2.5.** Thermal ellipsoid plot (30 % probability) of **12** with hydrogen atoms, bromide anion and CH_2Cl_2 solvate molecules omitted for clarity. 44
- Figure 2.2.6.** Representative examples of boron-nitrogen adducts with all boron-nitrogen bond lengths shown. 45

Figure 2.2.7. Thermal ellipsoid plot (30 % probability) of [IPrMe]Br (16) with the hydrogen atoms, bromide anion and CH ₂ Cl ₂ solvate molecules omitted for clarity.	53
Figure 2.2.8. Thermal ellipsoid plot (30 % probability) of 17 with the hydrogen atoms, except those at C(2), and CH ₂ Cl ₂ solvate molecules omitted for clarity.	55
Figure 2.2.9. Photophysical spectra for BrBFl•PPh ₃ (10) in CH ₂ Cl ₂ .	63
Figure 2.2.10. Photophysical spectra for [(DMAP) ₂ BFl]Br (12) in CH ₂ Cl ₂ .	64
Figure 2.2.11. Photophysical spectra for BrBFl•IPrCH ₂ (17) in CH ₂ Cl ₂ .	65
Figure 2.2.12. Representative examples of luminescent four-coordinate organoborane compounds with their quantum yields listed.	67
Figure 2.2.13. Unsubstituted parent BODIPY.	69
Figure 2.2.14. Calculated HOMO/LUMO plots for: a) BrBFl•PPh ₃ (10); b) [(DMAP) ₂ BFl]Br (12); c) BrBFl•IPrCH ₂ (17).	72
Figure 2.4.1. Crude ¹ H NMR Spectrum for (allyl)BFl•PPh ₃ (13).	99
Figure 2.4.2. Crude ¹³ C NMR Spectrum for (allyl)BFl•PPh ₃ (13).	99
Figure 2.4.3. Crude ¹¹ B{ ¹ H} NMR Spectrum for (allyl)BFl•PPh ₃ (13).	100
Figure 2.4.4. Crude ¹ H NMR Spectrum for (allyl)BFl•DMAP (14).	100
Figure 2.4.5. Crude ¹³ C NMR Spectrum for (allyl)BFl•DMAP (14).	101
Figure 2.4.6. Crude ¹¹ B{ ¹ H} NMR Spectrum for (allyl)BFl•DMAP (14).	101
Figure 2.4.7. ¹ H NMR Spectrum for HBFl•IPrCH ₂ (19).	102
Figure 2.4.8. ¹³ C NMR Spectrum for HBFl•IPrCH ₂ (19).	102
Figure 2.4.9. Proton-Coupled ¹¹ B NMR Spectrum for HBFl•IPrCH ₂ (19).	103

Figure 2.4.10. ^1H NMR spectrum for the thermal treatment of $\text{HBF}_4 \cdot \text{IPrCH}_2$

(19). 103

Figure 2.4.11. $^{11}\text{B}\{^1\text{H}\}$ NMR spectrum for the thermal treatment of

$\text{HBF}_4 \cdot \text{IPrCH}_2$ (19). 104

List of Schemes

Scheme 1.1.1. Early synthetic approaches to boroles.	2
Scheme 1.1.2. Representative examples of single electron and two electron reduction of boroles.	4
Scheme 1.1.3. Synthetic approaches to 9-Cl-9-borafluorene (ClBFl, 15) and representative reactions showing methods used to install aryl groups at boron.	7
Scheme 1.1.4. Chemical tests to probe the Lewis acidity of fluorinated borafluorenes (LB = Lewis base).	9
Scheme 1.2.1. Demonstration of the use of borafluorene derivatives to detect F ⁻ and the regeneration of the starting borafluorene.	12
Scheme 1.2.2. Preparation of the (9,9-di- <i>n</i> -octylfluorene-2,7-diyl)/[9-(4-cyanophenyl)borafluorene-2,7-diyl] random copolymer (27).	15
Scheme 1.3.1. General schematic for the synthesis of a borafluorene-containing polymer featuring the “masking” and “unmasking” process.	17
Scheme 2.1.1. General schematic for the synthesis of a borafluorene-containing polymer featuring the “masking” and “unmasking” process.	25
Scheme 2.2.2. Synthetic route to 9-bromo-9-borafluorene (1).	27
Scheme 2.2.3. Example of NHC-borane that resists intramolecular hydroboration.	28
Scheme 2.2.4. Synthesis of IPr.	28
Scheme 2.2.5. Synthesis of the carbene-bound borafluorene 2 .	29
Scheme 2.2.6. Reduction of a carbene-substituted tetraphenylborole.	33

Scheme 2.2.7. Example of an attempted reduction of 2 both with and without the use of Me ₃ SiCl as a trapping agent, along with the intended formation of an allyl-substituted species that could lead to a polymer. Included is the formation of the hydridic compound 8 .	34
Scheme 2.2.8. Successful synthesis of 8 .	35
Scheme 2.2.9. Synthesis of 9 via anionic exchange of bromide with triflate.	38
Scheme 2.2.10. Attempted “unmasking” of 1 using a) HCl, MeI, MeOTf, or b) BEt ₃ .	40
Scheme 2.2.11. Synthesis of the triphenylphosphine-borafluorene adduct 10 .	41
Scheme 2.2.12. Synthesis of the doubly substituted borafluorene, 12 , and the attempted synthesis of the monoadduct, 11 .	43
Scheme 2.2.13. Attempted removal of a) PPh ₃ and b) DMAP from 10 and 12 , respectively, in effort to liberate 1 .	47
Scheme 2.2.14. Grignard metathesis of 10 and 12 with (allyl)MgBr to form the allyl-substituted borafluorenes 13 and 14 .	48
Scheme 2.2.15. Representative canonical forms for IPrCH ₂ .	49
Scheme 2.2.16. Synthesis of an alkene-substituted phosphazene.	50
Scheme 2.2.17. Proposed synthetic pathway towards the alkene-substituted borafluorene 12 .	50
Scheme 2.2.18. Synthesis of the methylimidazolium salt 16 .	52
Scheme 2.2.19. Successful synthesis of 17 through the use of two equivalents of 1 .	54

- Scheme 2.2.20.** Attempted removal of HBr from **17** to form **15** using IPr, which resulted in the exchange of IPr with IPrCH₂ forming **2**. 57
- Scheme 2.2.21.** a) Attempted synthesis of **15** using K[N(SiMe₃)₂] as a potential base, resulting in the formation of the amino-substituted borafluorene **18**;
b) formation of **18** from the direct reaction between **1** and K[N(SiMe₃)₂]. 58
- Scheme 2.2.22.** Bromide/hydride exchange forming the hydride-substituted borafluorene **19**. Included are the decomposition reactions of **19** in CH₂Cl₂ and THF along with potential decomposition products. 60
- Scheme 2.2.23.** Attempted removal of H₂ from **19** and the potential product of a B-C hydride transfer upon stirring **19** in refluxing toluene in the presence of [Rh(COD)Cl]₂; COD = 1,5-cyclooctadiene. 61
- Scheme 3.2.1.** Representative “masking” and “unmasking” pathway utilizing pyridine as a Lewis base and featuring the incorporation of a bulky aryl group at boron. 112

List of Symbols, Nomenclature, or Abbreviations

$\{^n\text{E}\}$	Decoupled ^nE nucleus
allyl	$\text{H}_2\text{C}=\text{CH}-\text{CH}_2$
Ar	Aryl
avg.	Average
BrBF1	9-Bromo-9-borfluorene
br	Broad
BR_3	Organoborane
ClBF1	9-Chloro-9-borfluorene
COD	1,7-Cyclooctadiene
Cp	Cyclopentadienyl ligand ($\eta^5\text{-C}_5\text{H}_5$)
Cp*	Tetramethylcyclopentadienyl ligand ($\eta^5\text{-C}_5\text{Me}_5$)
d	Doublet
$D^\circ(\text{E-X})$	Bond Dissociation Energy for E-X
Dipp	2,6-Diisopropylphenyl
DMAP	<i>N,N</i> -Dimethylaminopyridine
dt	Doublet of Triplets
Et	Ethyl (C_2H_5)
Et_2O	Diethyl ether
HOMO	Highest Occupied Molecular Orbital
IPr	1,3-Bis-(2,6-diisopropylphenyl)-imidazol-2-ylidene $([(\text{HCNDipp})_2\text{C}:])$
^iPr	<i>iso</i> -propyl (Me_2CH)

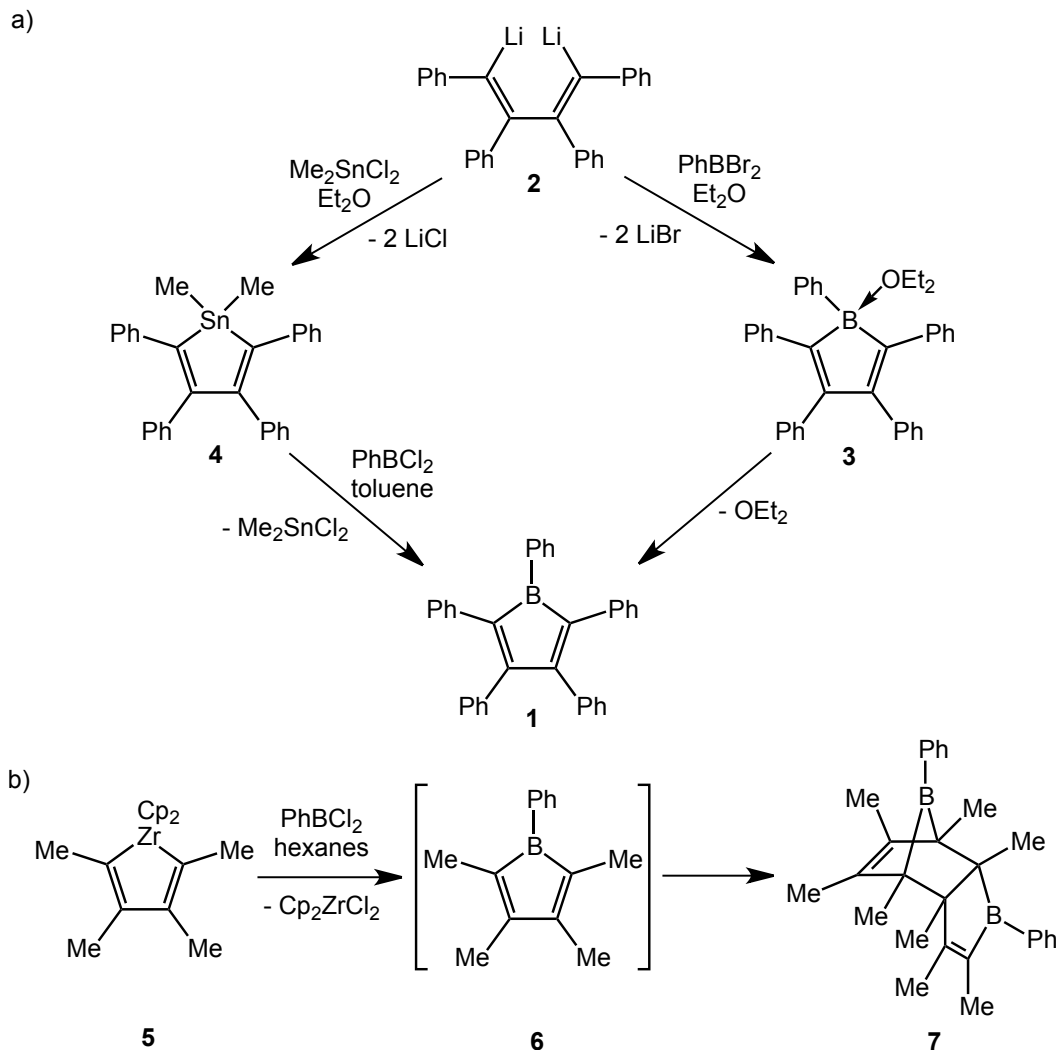
IPrCH ₂	1,3-Bis-(2,6-diisopropylphenyl)-2-methyleneimidazoline ((HCNDipp) ₂ C=CH ₂)
LA	Lewis Acid
LA•LB	Lewis Acid Base Adduct
LB	Lewis Base
LUMO	Lowest Unoccupied Molecular Orbital
Me	Methyl (CH ₃)
MeCN	Acetonitrile
Mes	2,4,6-Trimethylphenyl
Mes*	2,4,6-Tri- <i>tert</i> -butylphenyl
Na(Hg)	Sodium Mercury Amalgam
ⁿ Bu	<i>n</i> -butyl (C ₄ H ₉)
NHC	<i>N</i> -Heterocyclic Carbene
ⁿ J _{AB}	<i>n</i> -Bond coupling constant between A and B
NMR	Nuclear Magnetic Resonance Spectroscopy
OLED	Organic Light Emitting Diode
OTf	Trifluoromethanesulfonate (CF ₃ SO ₃)
Ph	Phenyl (C ₆ H ₅)
s	Singlet
t	Triplet
^t Bu	<i>tert</i> -Butyl (Me ₃ C)
td	Triplet of Doublets

TD-DFT	Time Dependant Density Functional Theorem
THF	Tetrahydrofuran
TMP	2,2,6,6-Tetramethylpiperidine
Trip	2,4,6-Tri- <i>iso</i> -propylphenyl
UV/Vis	Ultraviolet/Visible spectroscopy
δ	Chemical Shift
$\delta^{+/-}$	Partial Positive or Negative Charge
λ	Wavelength
Φ	Fluorescence Quantum Yield

Chapter 1: Introduction

1.1 Brief Overview of Heterocyclic Organoborane Compounds

The roots of the chemistry of heterocyclic organoborane compounds can be traced to the isolation of the first example of an antiaromatic borole derivative, pentaphenylborole (PhBC_4Ph_4 , **1**) by Eisch and coworkers in 1969.¹ The synthesis of PhBC_4Ph_4 , shown in Scheme 1.1.1a, could be achieved through two separate methods: 1) the direct reaction of *in situ* generated 1,4-dilithio-1,2,3,4-tetraphenylbutadiene (**2**) with PhBBr_2 in Et_2O to initially form the adduct $\text{PhBC}_4\text{Ph}_4\cdot\text{OEt}_2$ (**3**), followed by subsequent removal of Et_2O *in vacuo*; 2) through boron-tin exchange between 1,1-dimethyl-2,3,4,5-tetraphenylstanole (**4**) and PhBCl_2 . In either case, the desired borole was isolated as a deep blue solid, which was highly reactive towards to air and moisture. As a result of their highly sensitive nature, interest in boroles waned until the late 1980s when attempts were made to utilize zirconacycle transfer between $\text{Cp}_2\text{ZrC}_4\text{Me}_4$ (**5**, $\text{Cp} = \eta^5\text{-C}_5\text{H}_5^-$) and PhBCl_2 to form a less sterically encumbered borole system, PhBC_4Me_4 (**6**, Scheme 1.1.1b).² However, the target tetramethyl borole proved to be too reactive and underwent Diels-Alder [4+2] cycloaddition to yield the dimeric product **7**. This observation suggested that the steric protection offered by the carbon-bonded phenyl rings in **1** was necessary for preventing unwanted dimerization. Currently, the most common method used in the synthesis of boroles is via the boron-tin exchange pathway.^{3,4}



Scheme 1.1.1. Early synthetic approaches to boroles.

In general, boroles are planar (about the BC_4 ring), antiaromatic 4π systems that are isoelectronic with cyclopentadienyl cations (Fig. 1.1.1).³ Additionally, *ab initio* calculations on the parent borole HBC_4H_4 showed that there is a marked destabilization of the molecule upon delocalization of the four π electrons present as this would cause a shortening of the B-C and C-C bonds and distortion of the C-B-C bond angles.⁵ From the antiaromatic character, coupled with the vacant p orbital at boron, it was quickly observed that boroles could

undergo three main types of reactivity: 1) the formation of adducts with Lewis bases (resulting from both the vacant p orbital at boron and the electrophilicity stemming from the antiaromaticity); 2) potential Diels-Alder chemistry involving an activated carbon backbone; 3) undergoing two electron reductions forming formally aromatic 6π heterocyclic anions. In addition to the diverse potential for reactivity, boroles are deeply colored and typically exhibit a characteristic blue color.³ Both the potential reactivity and spectroscopic properties can be explained by the presence of a relatively high energy HOMO and relatively low energy LUMO when compared to the cyclopentadienyl cation.⁵ The resulting HOMO/LUMO configuration has several implications, including: 1) an easily accessible HOMO \rightarrow LUMO excitation consisting of a strong Laporte-allowed electronic transition; 2) facile addition of electrons to the low lying LUMO, which is primarily located at boron, to form radical anions or 6π electron aromatic anions, respectively (Scheme 1.1.2);^{6,7} 3) the LUMO is primarily centered about the vacant p orbital at boron, leaving a highly Lewis acidic site for the formation of adducts even with substrates possessing low donor strength, such as Et₂O or THF. In addition, upon bonding to a nucleophilic species, the absorbance of the borole undergoes a hypsochromic shift resulting in an often drastic color change. Although the potential for several readily accessible reaction pathways exists, interest in boroles remained somewhat stagnant for nearly 30 years with only a handful of reports published between the late 1960s and 1990s that pertained directly to the synthesis and reactivity of boroles.^{1,2,8-13}

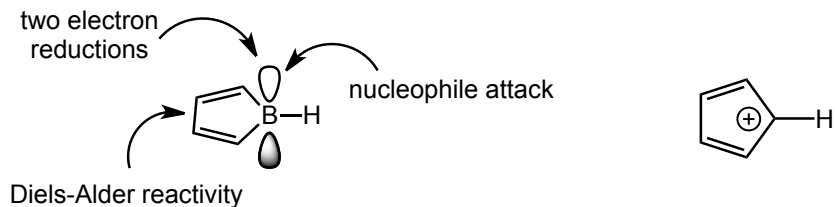
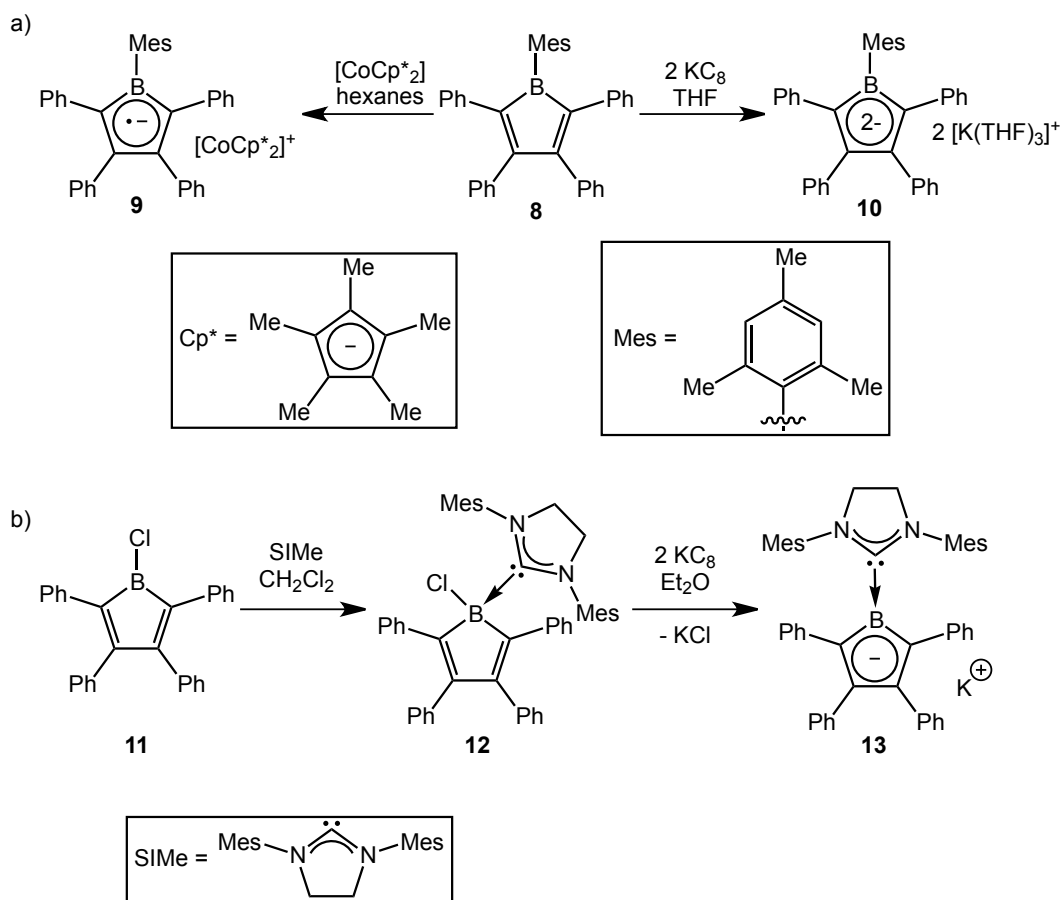


Figure 1.1.1. Parent borole showing reactive sites (left) and the isoelectronic cyclopentadienyl cation (right).



Scheme 1.1.2. Representative examples of single electron and two electron reduction of boroles.

While boroles offer an intriguing prospect in terms of redox and coordination chemistry (for possible colorimetric sensing of analytes), the dibenzo derivative, 9-borafluorene (**14**, Fig. 1.1.2), can be seen as an interesting parent system in itself. The incorporation of two fused aryl units on the periphery of the borole core adds several subtle, yet profound differences in the structure and electronic properties. The most striking difference is the luminescent properties of borafluorene units. The fluorescence of the borafluorene unit is a direct result of the interaction between the vacant p orbital at boron and the adjacent π^* system of the bound biphenyl unit present in the LUMO.¹⁴ Though similar claims can be made with single-ring boroles, for borafluorenes this interaction results in a sufficiently narrow HOMO-LUMO gap by decreasing the energy of the LUMO, and the accompanying unoccupied orbitals (e.g., LUMO+1, LUMO+2, etc.), through electron delocalization to the periphery of the molecule; this effect allows additional excited states to be accessed upon excitation, which are likely responsible for the observed luminescence.

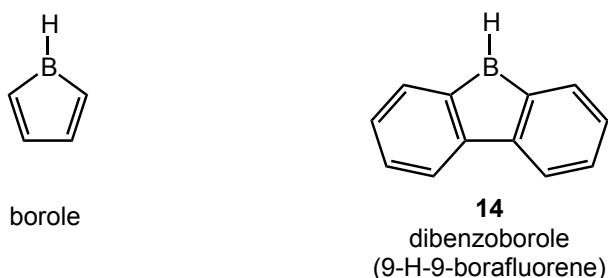
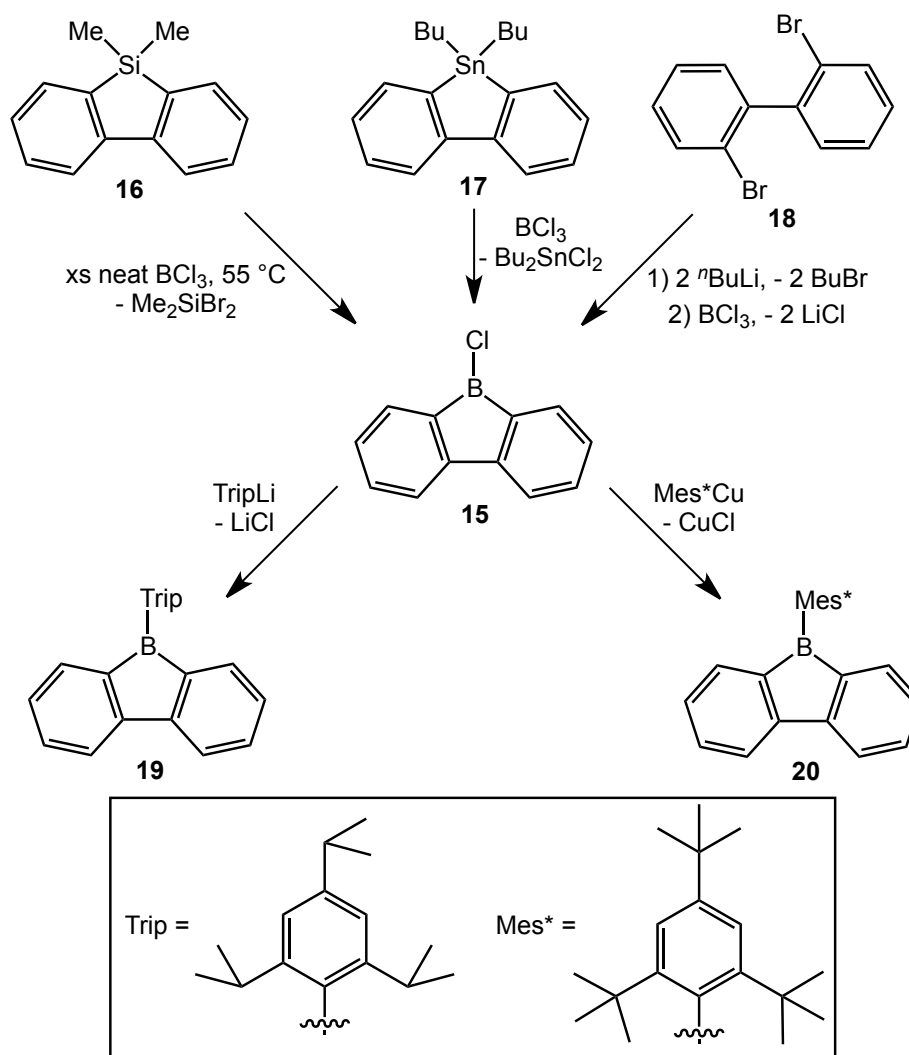


Figure 1.1.2. Representations of the parent borole (left) and parent borafluorene (right).

A convenient method for preparing borafluorene analogues is functionalization of a boron-halide bond of a halide precursor, such as 9-Cl-9-borafluorene (ClBF1 **15**, Scheme 1.1.3)). By and large, three main synthetic approaches exist for the synthesis of **15** and each are presented in Scheme 1.1.3; similar reaction pathways can be used to yield BrBF1 when BBr₃ is used in place of BCl₃ as a reagent. The three synthetic approaches to **15** are: 1) from the reaction of a precursor silafluorene (**16**) with a large excess of BCl₃,¹⁵ 2) Sn/B transmetallation chemistry between a diorganostannylfluorene (**17**) and BCl₃,¹⁶ 3) treatment of 2,2'-dibromobiphenyl (**18**) with ⁿBuLi, to generate the dilitho species *in situ*, followed by a reaction with BCl₃.¹⁷ The presence of the chloro group allows for further functionalization of the borafluorene unit at boron through the use of organolithium¹⁶ or organocopper¹⁸ reagents typically to install bulky aryl groups, such as tri-*iso*-propylphenyl (Trip) or tri-*tert*-butylphenyl (Mes*) groups, to protect the reactive boron center from attack by oxygen and moisture (Scheme 1.1.3). Thus, haloboranes such as ClBF1 (**15**) and BrBF1 can be viewed as useful precursors from which borafluorene chemistry can develop. Furthermore, under suitable synthetic conditions, the borafluorene ring system can be extended to form more complex systems such as those listed in Figure 1.1.3.^{16,19} Functionalization of the borafluorene core in this fashion leads to changes in both the color of the compound and emission profile through an extension of the electronic conjugation.^{15,19-24} In addition, the installation of groups with increased π donating ability will force electron density from the periphery of the molecule toward the π accepting borafluorene core in a push/pull manner increasing the

charge transfer character in the excited state and resulting in a red-shift of the fluorescence emission maxima and increased fluorescence quantum yields.



Scheme 1.1.3. Synthetic approaches to 9-chloro-9-borafluorene (ClBFI, **15**) and representative reactions showing methods used to install aryl groups at boron.

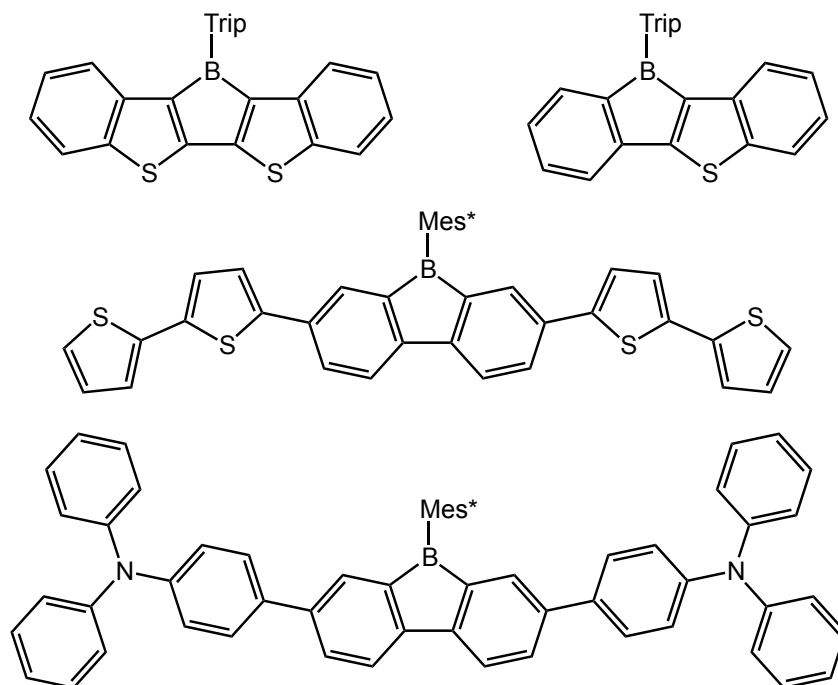
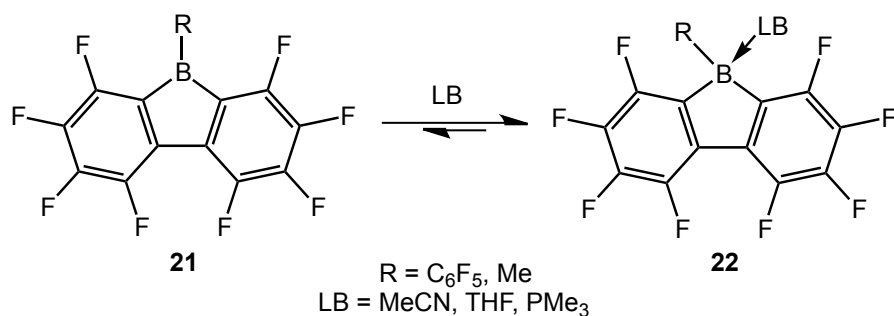


Figure 1.1.3. Representative examples of functionalized borafluorenes and similar boroles.

Borafluorene units exhibit rather strong Lewis acidity as a consequence of the vacant p orbital on boron. The Lewis acid strength of fluorinated borafluorene systems, relative to the known strong Lewis acid $B(C_6F_5)_3$,²⁵ was probed by Piers and coworkers in 2005 (Scheme 1.1.4).²⁶ By combining the Lewis bases MeCN, THF and PMe_3 with the fluorinated borafluorenes **21** and **22**, they determined that in all cases the borafluorene derivatives **21** and **22** were either comparable to or surpassed the Lewis acid strength of $B(C_6F_5)_3$ using both the methods of Childs^{27,28} and that of Laszlo and Teston²⁹ to evaluate the Lewis acidity. By and large, the comparatively higher Lewis acidity of the borafluorene unit can be attributed to two main factors: 1) the planarity of the borafluorene fused ring array which reduces steric repulsion between the borafluorene and the incoming Lewis

base; 2) lower back strain energies upon pyramidalization as a result of the planar borafluorene unit being a fixed structure. In contrast, coordinating a Lewis base to $B(C_6F_5)_3$ forces the C_6F_5 moieties into closer proximity leading to increased steric strain. Overall, this clearly demonstrates that the borafluorene unit can be considered as a strong Lewis acidic system. Moreover, it was observed that the observed bright color of the borafluorenes studied ($R = C_6F_5$, orange; $R = Me$, green) completely disappeared upon complexation with Lewis bases. This phenomenon is common throughout four-coordinate borafluorene systems and can be attributed to a disruption of the $p-\pi^*$ conjugation present in the LUMO of a three-coordinate borafluorene resulting in an increase HOMO-LUMO gap leading to hypsochromic shifts of the absorption maxima into the UV region; in addition, fluorescence is often quenched within four-coordinate borafluorenes.^{14,26} This further implies that borafluorene systems are ideal candidates for use as nucleophile detectors as, upon binding the incoming nucleophile, a visible color change will occur and fluorescence quenching can be monitored.



Scheme 1.1.4. Chemical tests to probe the Lewis acidity of fluorinated borafluorenes (LB = Lewis base).

1.2 Application of Borafluorenes to Nucleophile Sensing

In today's society, the presence of the fluoride anion has become ubiquitous as it has been well documented to be quite beneficial to both dental and skeletal health, and fluoride is even being used in the treatment of osteoporosis.^{30,31} Fluoride is so beneficial in these applications that it can be found, typically in the form of NaF, as an additive to drinking water, toothpaste, as well as vitamin and other dietary supplements. Although the benefits are clear, the potential for over exposure can cause concern as either dental or skeletal fluorosis can occur. Moreover, the presence of fluoride anions can be used as an indication that more harmful compounds, such as the phosphorofluoridate nerve agent Sarin (Fig. 1.2.1), that liberate F^- upon hydrolysis, may be present.³² In a similar vein, cyanide (CN^-) is also a commonly encountered and potentially harmful anion. While the insidious nature of this species is apparent through the use of HCN or nerve agents, such as Tabun (Fig. 1.2.1), as chemical warfare agents,³² CN^- is still commonly used in many industrial processes such as gold extraction³³ and in the manufacturing of adiponitrile, a precursor to nylon.³⁴ While instances of cyanide poisoning are rare, cessation of cellular respiration can occur within seconds after exposure and ultimately lead to death.³⁵ With these aspects of the F^- and CN^- anions in mind, it is evident that a convenient and quantifiable detection system is paramount in the determination of any potential hazards.

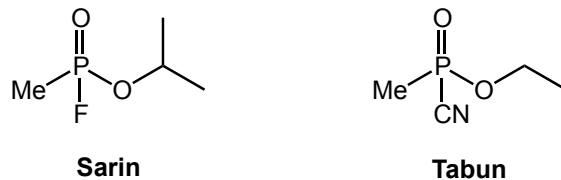
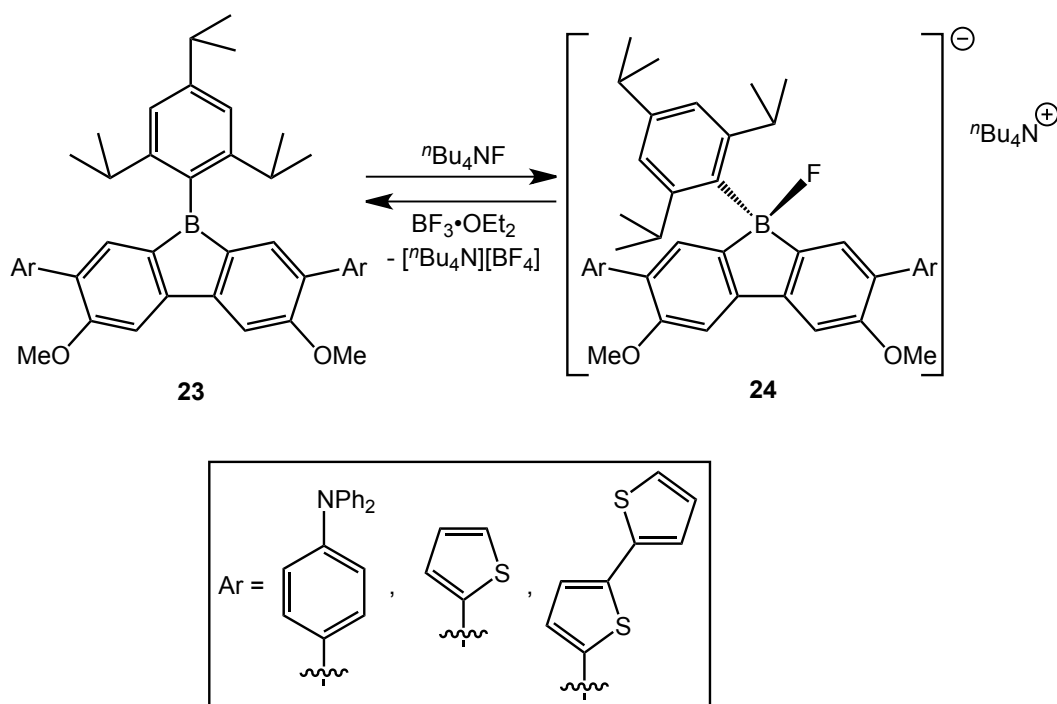


Figure 1.2.1. Structure of the nerve agents Sarin and Tabun, which, upon hydrolysis, release F^- and CN^- , respectively.

As discussed in the previous section, the borfluorene unit is a powerful Lewis acid in terms of forming adducts with incoming nucleophiles. While the Lewis acidic property of borfluorene-containing species may allow for these species to be used in several applications, such as an activator for single-site olefin polymerization catalysts,³⁶ the development of weakly-coordinating anions (akin to $B(C_6F_5)_4^-$)²⁵ or in the initiation of cationic polymerization,^{37,38} a much more attractive means of employing borfluorenes in a practical sense is found in the detection of nucleophilic species. The changes in absorbance and fluorescence maxima upon complexation with incoming nucleophiles are typically so pronounced that they can be detected with the naked eye. That is, the structural change from a three-coordinate to four-coordinate boron is accompanied with a visible color change from, for example, bright orange or green to colorless along with a quenching of the fluorescence.¹⁴ The spectroscopic changes that occur when borfluorenes bind nucleophilic species can be adapted for use in the detection of potentially harmful anions, as demonstrated by Yamaguchi and coworkers in their seminal study in 2002 (Scheme 1.2.1).¹⁴ Specifically, the *iso*-propylphenyl-substituted borfluorene (**23**) was successfully employed as a

solution-based detector of fluoride anions (F^-), wherein the decolorization and fluorescence quenching in **23** in the presence of F^- (forming the four-coordinate borafluorene **24**), is both a visual indicator and a quantifiable spectroscopic property. Furthermore, the bonded F^- could be removed from **24** through the addition of the halide acceptor $BF_3 \cdot OEt_2$, to regenerate the original three-coordinate borafluorene **23**.



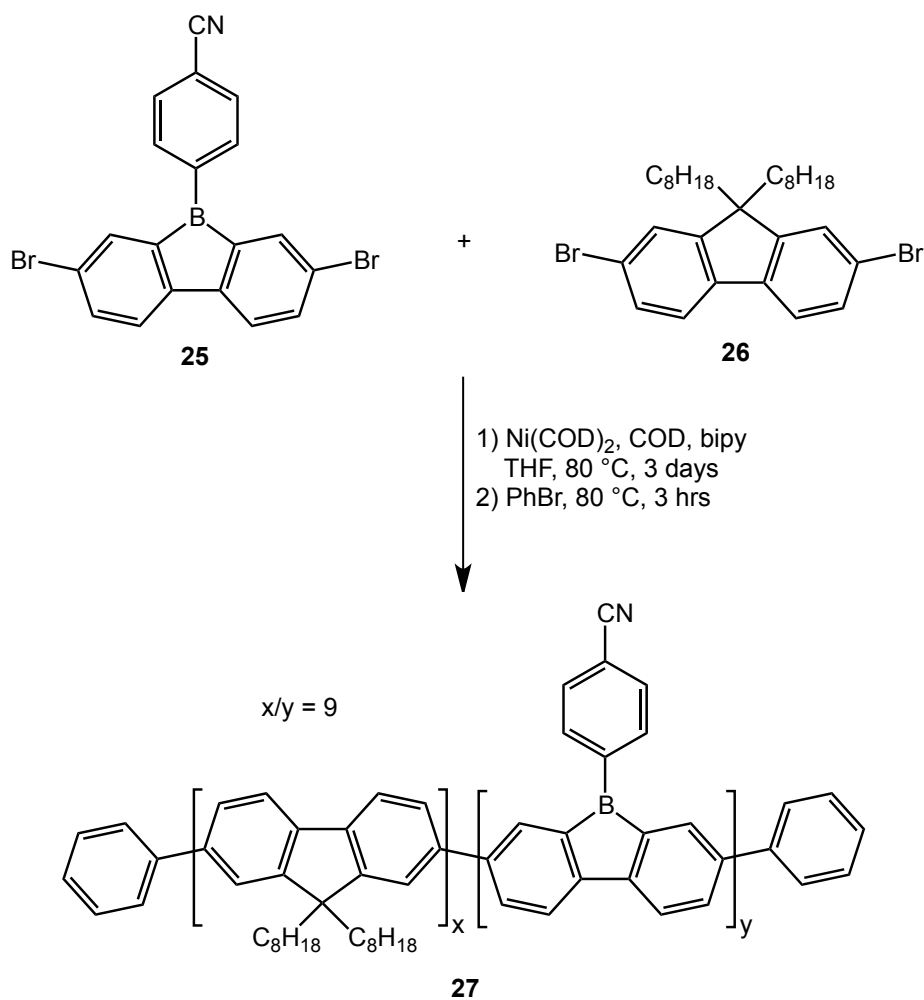
Scheme 1.2.1. Demonstration of the use of borafluorene derivatives to detect F^- and the regeneration of the starting borafluorene.

The borafluorene-based system depicted in Scheme 1.2.1 was shown to effectively detect F^- (from nBu_4NF) in a THF solution over a wide range of concentrations.¹⁴ With borafluorene concentrations as low as $0.38 \mu M$, F^- could be

detected at concentrations as low as 1.3 μM , as evidenced by detectable variations in the fluorescence emission intensity. At lower concentrations of F^- , the quenching effect was less pronounced than at higher concentrations. This clearly illustrates the capability of the borafluorene unit to exhibit quantifiable changes in their photophysical properties, which could be extrapolated to determine the concentration of F^- in an unknown solution provided the borafluorene concentration and fluorescence quantum yield were known.

In 2008, Bonifácio *et al.* successfully incorporated the borafluorene unit into the backbone of a random copolymer with dioctylfluorene (**27**, Scheme 1.2.2).³⁹ This polymer was formed with a modest molecular weight of 4.07 kDa and a polydispersity index of 1.78. The polymer was found to be air- and water-stable. To test its ability as a sensor for F^- and CN^- , submicrometer thick films of the polymer were drop-cast from 0.025 w/v% toluene solutions onto a glass slide and submersed in ethanol solutions of either ${}^n\text{Bu}_4\text{NF}$ or ${}^n\text{Bu}_4\text{NCN}$ at various concentrations for 60 seconds. Their findings indicated that the polymer was capable of exhibiting detectable fluorescence quenching at concentrations as low as 120 μM (for F^-) and 60 μM (for CN^-). It is worth noting that only incomplete quenching was observed for two reasons: 1) incomplete occupancy of every available boron site; 2) presence of the still fluorescent dioctylfluorene comonomer along the polymer backbone. Although the concentrations required to induce measurable quenching, with respect to F^- , seemed to indicate that the polymer system may not be as sensitive as Yamaguchi's previously reported species (Scheme 1.2.1),¹⁴ their work demonstrated that not only could the

borafuorene unit be incorporated into the backbone of a polymer, but this conjugated unit could be used within a solid/liquid interface detection system. Bonifácio also noted that increasing the boron content of the polymer could result in increased sensitivity at lower concentrations. Moreover, the polymer only exhibited significant quenching in the presence of F^- and CN^- , a lower degree of quenching in the presence of I^- and no observed quenching in the presence of Br^- or Cl^- . Thus, the conclusion can be drawn that the borafuorene unit can be used as a semi-selective detector when analyzing mixtures of analyte anions. A subsequent study was conducted by Bonifácio and coworkers in 2010 using the same system to detect F^- in aqueous solutions.⁴⁰ In this study, it was determined that thin-films (358 ± 3 nm thickness) of the polymer **27** exhibited measurable increased electrical impedance upon binding F^- that could be observed at concentrations of nBu_4NF as low as 10^{-5} μM in aqueous solutions. At the lowest measured concentration (10^{-5} μM) of nBu_4NF , the electrical impedance increased by ca. 4 k Ω relative to that of the film in pure water. The increased impedance is due to decreased electrical conductivity of the polymer **27** as a result of the binding of F^- at boron serving to decrease the overall conjugation of the polymer. This further solidifies the claims that the borafuorene unit, once incorporated into a polymer, is quite an effective tool for the detection of potentially harmful anions in solution.

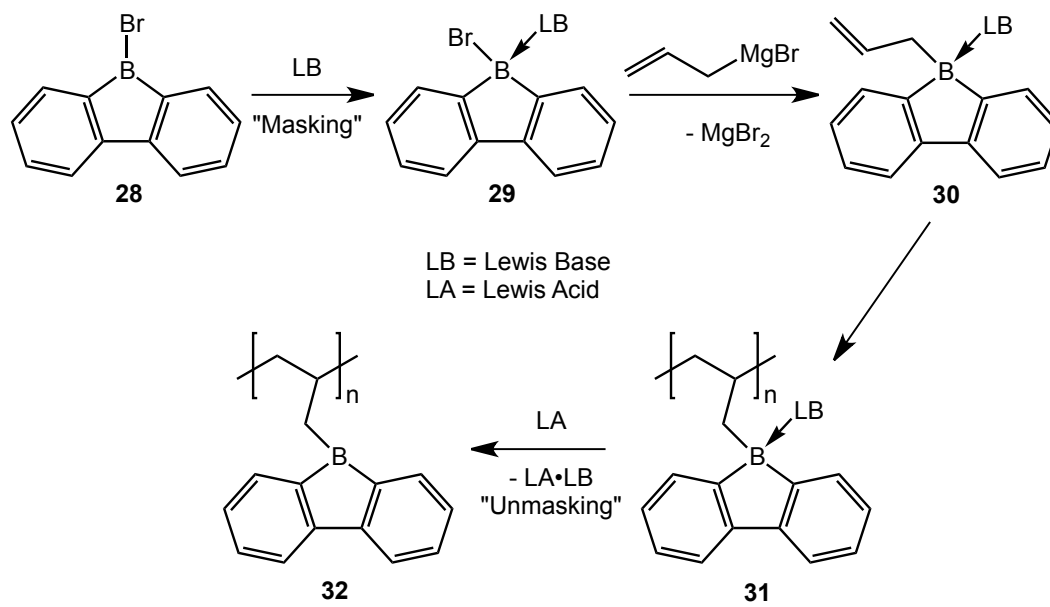


Scheme 1.2.2. Preparation of the (9,9-di-*n*-octylfluorene-2,7-diyl)/[9-(4-cyanophenyl)borafluorene-2,7-diyl] random copolymer (**27**).

1.3 Overview of Project Goals

The pioneering work of Yamaguchi and Bonifácio offers striking evidence that the borafluorene unit has a high potential in the future development of both molecular- and polymer-based anion detectors. It was with this in mind that the initial goals of this project were defined. The overall goal, shown in Scheme 1.3.1, involved the incorporation of the borafluorene unit as a pendent group of a linear

polyalkene. The initial hypothesis was that, upon incorporation of pendent borfluorene units, the sensing ability could be enhanced, as the boron center would be less sterically encumbered and the attached alkyl group may allow for more flexibility in solution allowing the boron to more easily adopt a four-coordinate environment upon complexation with incoming anions. The method chosen to achieve this involved the installation of an alkenyl group at boron (e.g., **30**, Scheme 1.3.1) and subsequent radical polymerization. However, the issue remained that upon addition of a radical initiator to a borfluorene solution may react with the boron and prevent the desired polymerization from occurring. It has been documented that the incoming radical species (R^{\bullet}) can bind irreversibly with boranes to give boryl radicals (RBR'_3)^{41,42} or even substitute the group bonded to boron.⁴³ To overcome this potential limitation, the thought had occurred to form a Lewis base adduct with borfluorene prior to the installation of the alkenyl group, allowing radical polymerization to occur. Subsequently, the boron-bound Lewis base would be removed via the addition of a Lewis acid, forming a new Lewis acid-base adduct as a byproduct, thus returning the boron to the desired three-coordinate environment for sensing applications. The overall term for the use of Lewis bases as protecting groups is “masking/unmasking”.



Scheme 1.3.1. General schematic for the synthesis of a borafluorene-containing polymer featuring the “masking” and “unmasking” process.

Through the course of experimentation to find a suitable Lewis base to carry out the desired “masking/unmasking” process, it was discovered that adducts of borafluorene formed using PPh_3 , DMAP and IPrCH_2 are fluorescent in their own right. This unexpected result was initially counter-intuitive, as the four-coordinate borafluorene species would be expected to be non-fluorescent as described earlier in this chapter. This prompted further study into the nature of the observed fluorescence and will be the main subject of this thesis.

1.4 Brief Note on the Structure of this Thesis

It is a policy within our research group that each research based chapter of this thesis is written as a self-contained paper prepared for publication in a peer reviewed journal. All sections of this thesis were drafted by myself and no

portions contained herein have been submitted for publication at the time of submission.

1.5 References

- (1) Eisch, J. J.; Hota, N. K.; Kozima, S. *J. Am. Chem. Soc.* **1969**, *91*, 4575.
- (2) Fagan, P. J.; Burns, E. G.; Calabrese, J. C. *J. Am. Chem. Soc.* **1988**, *110*, 2979.
- (3) Braunschweig, H.; Kupfer, T. *Chem. Commun.* **2011**, *47*, 10903.
- (4) Fan, C.; Piers, W. E.; Parvez, M. *Angew. Chem. Int. Ed.* **2009**, *48*, 2955.
- (5) Malar, E. J. P.; Jug, K. *Tetrahedron* **1986**, *42*, 417.
- (6) Braunschweig, H.; Dyakonov, V.; Jimenez-Halla, J. O. C.; Kraft, K.; Krummenacher, I.; Radacki, K.; Sperlich, A.; Wahler, J. *Angew. Chem. Int. Ed.* **2012**, *51*, 2977.
- (7) Braunschweig, H.; Chiu, C.-W.; Radacki, K.; Kupfer, T. *Angew. Chem. Int. Ed.* **2010**, *49*, 2041.
- (8) Groves, J. T.; Ma, K. W. *J. Am. Chem. Soc.* **1975**, *97*, 4434.
- (9) Herberich, G. E.; Hengesbach, J.; Kölle, U.; Oschmann, W. *Angew. Chem. Int. Ed.* **1977**, *16*, 42.
- (10) Herberich, G. E.; Buller, B.; Hessner, B.; Oschmann, W. *J. Organomet. Chem.* **1980**, *195*, 253.
- (11) Eisch, J. J.; Galle, J. E.; Kozima, S. *J. Am. Chem. Soc.* **1986**, *108*, 379.
- (12) Eisch, J. J.; Galle, J. E.; Shafii, B.; Rheingold, A. L. *Organometallics* **1990**, *9*, 2342.

- (13) Fagan, P. J.; Nugent, W. A.; Calabrese, J. C. *J. Am. Chem. Soc.* **1994**, *116*, 1880.
- (14) Yamaguchi, S.; Shirasaka, T.; Akiyama, S.; Tamao, K. *J. Am. Chem. Soc.* **2002**, *124*, 8816.
- (15) Gross, U.; Kaufmann, D. *Chem. Ber.* **1987**, *120*, 991.
- (16) Wakamiya, A.; Mishima, K.; Ekawa, K.; Yamaguchi, S. *Chem. Commun.* **2008**, *0*, 579.
- (17) Biswas, S.; Oppel, I. M.; Bettinger, H. F. *Inorg. Chem.* **2010**, *49*, 4499.
- (18) Li, H.; Sundararaman, A.; Venkatasubbaiah, K.; Jäkle, F. *J. Am. Chem. Soc.* **2007**, *129*, 5792.
- (19) Iida, A.; Yamaguchi, S. *J. Am. Chem. Soc.* **2011**, *133*, 6952.
- (20) Eisch, J. J.; Shafii, B.; Odom, J. D.; Rheingold, A. L. *J. Am. Chem. Soc.* **1990**, *112*, 1847.
- (21) Byun, Y. G.; Saebo, S.; Pittman, C. U. *J. Am. Chem. Soc.* **1991**, *113*, 3689.
- (22) Sugihara, Y.; Yagi, T.; Murata, I.; Imamura, A. *J. Am. Chem. Soc.* **1992**, *114*, 1479.
- (23) Araneda, J. F.; Neue, B.; Piers, W. E.; Parvez, M. *Angew. Chem. Int. Ed.* **2012**, *51*, 8546.
- (24) Thanthiriwatte, K. S.; Gwaltney, S. R. *J. Phys. Chem. A* **2006**, *110*, 2434.
- (25) Piers, W. E. *Adv. Organomet. Chem.* **2004**, *52*, 1.
- (26) Chase, P. A.; Romero, P. E.; Piers, W. E.; Parvez, M.; Patrick, B. O. *Can. J. Chem.* **2005**, *83*, 2098.
- (27) Childs, R. F.; Mulholland, D. L.; Nixon, A. *Can. J. Chem.* **1982**, *60*, 801.

- (28) Childs, R. F.; Mulholland, D. L.; Nixon, A. *Can. J. Chem.* **1982**, *60*, 809.
- (29) Laszlo, P.; Teston, M. *J. Am. Chem. Soc.* **1990**, *112*, 8750.
- (30) Aaseth, J.; Shimshi, M.; Gabrilove, J. L.; Birketvedt, G. S. *J. Trace Elem. Exp. Med.* **2004**, *17*, 83.
- (31) Carton, R. *J. Fluoride* **2006**, *39*, 163.
- (32) Burnworth, M.; Rowan, S. J.; Weder, C. *Chem. Eur. J.* **2007**, *13*, 7828.
- (33) Acheampong, M.; Paksirajan, K.; Lens, P. L. *Environ. Sci. Pollut. Res.* **2013**, *20*, 3799.
- (34) Lloyd, L. *Handbook of Industrial Catalysts*; Springer Science + Business Media, LLC: New York, NY, USA, 2011.
- (35) Li, H.; Lalancette, R. A.; Jäkle, F. *Chem. Commun.* **2011**, *47*, 9378.
- (36) Chen, E. Y.-X.; Marks, T. J. *Chem. Rev.* **2000**, *100*, 1391.
- (37) Lewis, S. P.; Taylor, N. J.; Piers, W. E.; Collins, S. *J. Am. Chem. Soc.* **2003**, *125*, 14686.
- (38) Lewis, S. P.; Henderson, L. D.; Chandler, B. D.; Parvez, M.; Piers, W. E.; Collins, S. *J. Am. Chem. Soc.* **2005**, *127*, 46.
- (39) Bonifácio, V. D. B.; Morgado, J.; Scherf, U. *J. Polym. Sci., Part A: Polym. Chem.* **2008**, *46*, 2878.
- (40) Ribeiro, C.; Brogueira, P.; Lavareda, G.; Carvalho, C. N.; Amaral, A.; Santos, L.; Morgado, J.; Scherf, U.; Bonifácio, V. D. B. *Biosens. Bioelectron.* **2010**, *26*, 1662.
- (41) Sainsbury, T.; Satti, A.; May, P.; Wang, Z.; McGovern, I.; Gun'ko, Y. K.; Coleman, J. *J. Am. Chem. Soc.* **2012**, *134*, 18758.

(42) Braïda, B.; Derat, E.; Chaquin, P. *ChemPhysChem* **2013**, DOI:
10.1002/cphc.201300361.

(43) Zhang, Z.-C.; Chung, T. C. M. *Macromolecules* **2006**, *39*, 5187.

Chapter 2: Synthesis, Reactivity and Photophysical Properties of Novel Lewis Base Adducts of Borafluorene

2.1 Introduction

Over the past three decades, the detection and recognition of anions has developed into a major research theme in chemistry.¹ Of specific interest is the sensing of fluoride (F^-) and cyanide (CN^-) anions. Fluoride can be found in many common household products such as toothpaste, vitamins and dietary supplements; however other sources can include insecticides and rodenticides (such as NaF or SO_2F_2), the ingestion of which can be quite dangerous and even fatal.² Cyanide, on the other hand, is a much more sinister species that is still used in several industrial processes such as gold extraction³ or in the manufacturing of adiponitrile, a precursor to nylon.⁴ Although poisoning from cyanides is rare, serious dysfunction arising from the cessation of cellular respiration can occur within seconds after exposure.² More importantly, both anions are generated upon the decomposition of certain phosphonate-based chemical warfare agents.⁵

Organoboranes (BR_3) represent an attractive class of molecules for the detection of anions as a result of their high affinity and binding selectivity towards small anions such as F^- and CN^- .⁶⁻⁸ π -Conjugated borafluorenes (Fig. 2.1.1) represent a promising class of molecular boranes due to their high Lewis acidity⁹ coupled with their brilliantly colored and fluorescent nature,¹⁰ allowing for facile colorimetric detection of nucleophilic species (such as anions).⁶ The high Lewis acidity of these species is derived from the vacant p -orbital situated at the boron allowing for the complexation of an incoming nucleophile.¹¹ Furthermore, the

highly colored nature of borafluorenes, arising from a transition from the π -conjugated HOMO delocalized over the biphenyl moiety to the LUMO that is delocalized over the vacant boron p -orbital and the π^* system of the biphenyl, allows for drastic changes in color upon coordination of various nucleophilic species resulting causing a pronounced hypsochromic shift in the absorbance.¹¹ For example, Tamao and coworkers used conjugated borafluorene derivatives to detect fluoride anions via “On/Off” detection through which an observable change color (from orange to colorless) and a quenching of the fluorescence upon F^- binding due to disruption of the conjugation within the borafluorene unit.⁶ The result of this is a facile means to detect analytes with the naked eye.

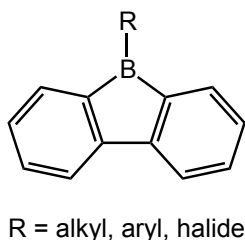
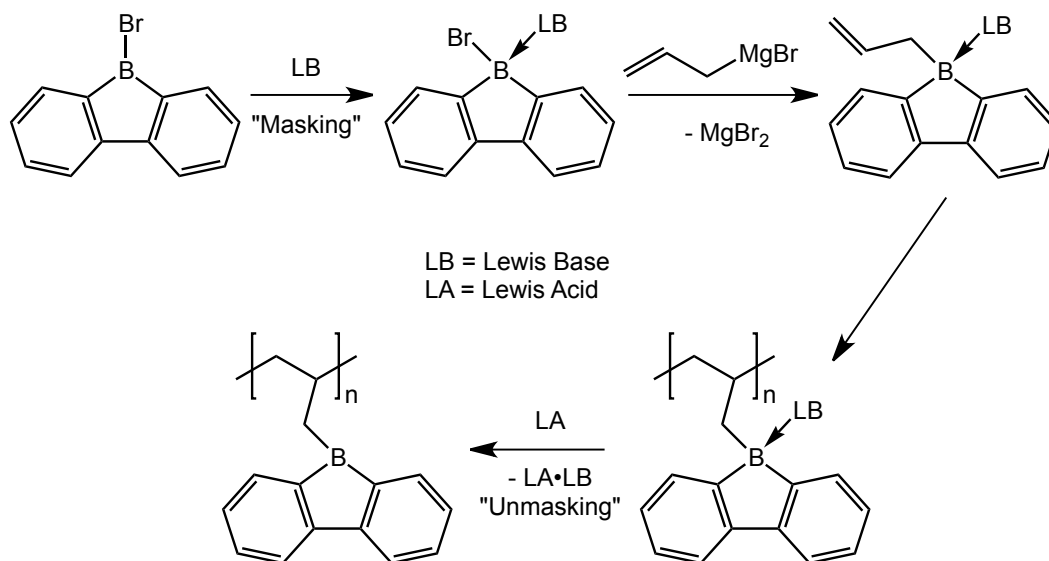


Figure 2.1.1. Representation of the general form of a borafluorene featuring the characteristic fused ring structure.

With this in mind, the initial inspiration of this project was to incorporate borafluorene as a pendent group within a polymer to allow for the rapid detection of potentially harmful anions. Scheme 2.1.1 shows a general schematic of how this goal was to be achieved. The synthetic method explored involved first the “masking” of a halogenated borafluorene with a Lewis basic “masking agent” to block any potential side reactions with the empty p -orbital boron during

subsequent radical polymerization chemistry. Specifically, the unprotected trivalent boron could potentially form an adduct with the radical initiator^{12,13} or substitute a group (e.g., Br) at the boron,¹⁴ thus preventing the desired polymerization from occurring. Next, replacement of the halide with a group that could be polymerized was planned, followed by the polymerization of the Lewis base coordinated borafluorene. The final stage of this scheme features the “unmasking” of the now polymerized borafluorene through removal of the Lewis base with a suitable Lewis acid. This would restore the color and fluorescent characteristics of the three-coordinate borafluorene unit while leaving vacant boron *p*-orbitals accessible for incoming anions in solution. During the course of this study, a series of new luminescent compounds based on Lewis base (PPh₃, DMAP and IPrCH₂) adducts of the borafluorene unit were discovered. The findings seem to indicate a complex communication between the borafluorene centered occupied molecular orbitals and the Lewis base centered unoccupied molecular orbitals, which may be giving rise to the observed fluorescent characteristics of these adducts. Furthermore, this represents a new class of emissive organoborane compounds featuring a four-coordinate boron.



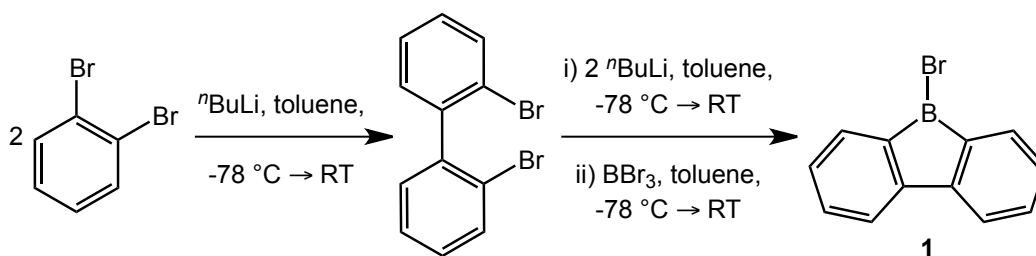
Scheme 2.1.1. General schematic for the synthesis of a borafluorene-containing polymer featuring the “masking” and “unmasking” process.

2.2 Results and Discussion

2.2.1 Synthesis and Reactivity Studies of Novel Lewis Base Adducts of 9-Bromo-9-borafluorene

Initial investigations into the feasibility of incorporating a borafluorene into a polymeric scaffold were focused on the formation of an *N*-heterocyclic carbene borafluorene adduct. This was accomplished first through the synthesis of the necessary precursor, 9-bromo-9-borafluorene, BrBF1 (**1**). Motivated by the previously reported synthesis of 9-chloro-9-borafluorene by Biswas, *et al.*,¹⁵ the synthesis of **1** was carried out in a similar manner with replacement of BCl₃ with BBr₃ in the synthetic protocol (Scheme 2.2.2). To begin, 2,2'-dibromobiphenyl was prepared and isolated according to the procedure reported by Dougherty, *et al.*,¹⁶ involving the *in situ* reaction of 1,2-dibromobenzene with one half

equivalent of $n\text{BuLi}$. This reaction most likely transpires via the formation of a benzyne intermediate followed by intermolecular coupling of the benzyne intermediate with a second equivalent of 1,2-dibromobenzene to yield 2,2'-dibromobiphenyl.^{17,18} In a second step, a double lithiation of the remaining two bromine sites in 2,2'-dibromobiphenyl was conducted to generate the 2,2'-dilithiated biphenyl which was then combined with BBr_3 to yield **1** as a bright yellow solid in a yield of 90 %. The rationale behind the use of BBr_3 over BCl_3 , as used by Biswas, *et al.*, took root upon examination of the boron-halide (B-X; X = Br or Cl) bond dissociation energies ($D^\circ(\text{B-X})$) of BX_3 in the gaseous phase: $D^\circ(\text{B-Br}) = 396 \text{ kJ mol}^{-1}$; $D^\circ(\text{B-Cl}) = 511 \text{ kJ mol}^{-1}$.¹⁹ This indicates the B-Br bond is weaker than the B-Cl bond, and further implies that bromine will be more easily displaced than chlorine by incoming nucleophiles leading to improved functionalization at boron, especially with respect to the formation of a boron-carbon bond ($D^\circ(\text{B-C}) = 448 \text{ kJ mol}^{-1}$). As it will be of importance in later discussions, it should be mentioned that the $^{11}\text{B}\{^1\text{H}\}$ NMR chemical shift of **1** (broad singlet due to the quadrupole broadening of boron)²⁰ occurs at 65.8 ppm, and this chemical shift value is in the range observed with other three-coordinate boron borafluorene compounds,^{10,21-23} indicating that the boron atom in **1** remained in a three-coordinate state.



Scheme 2.2.2. Synthetic route to 9-bromo-9-borfluorene (**1**).

Once **1** had been synthesized in a satisfactory yield and purity, the next step was to determine which Lewis base was to be used as a masking agent for **1** in an effort to block any unwanted reactivity at the boron center, especially during subsequent polymerization attempts (e.g., in radical polymerization). Attention quickly turned toward using an *N*-heterocyclic carbene (NHC) as a Lewis base/masking agent. Carbenes of this nature are strong σ -donors and weak π -acceptors (Fig. 2.2.1). The presence of two nitrogen atoms (each with a lone pair of electrons) bound directly to the carbene carbon offer both a means to stabilize a singlet state at carbon as well as help to minimize the potential π -accepting ability of the formally vacant *p*-orbital on carbon.²⁴ Furthermore, when coordinated to a boron atom, NHCs will not readily undergo any 1,2-migrations, such as an intramolecular hydroboration, with the carbene carbon (Scheme 2.2.3).^{20,25} It was with these factors in mind, along with knowledge of the Lewis acidic nature of the borfluorene unit, that the selection of 1,3-bis-(2,6-diisopropylphenyl)-imidazol-2-ylidene, IPr (IPr = [(HCNDipp)₂C:]; Dipp = 2,6-*i*Pr₂C₆H₃), was made as a starting point for the “masking” of borfluorene. IPr can be synthesized quite

readily through the deprotonation of its corresponding hydrochloride salt according to a procedure developed by Nolan and coworkers (Scheme 2.2.4).²⁶

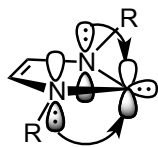
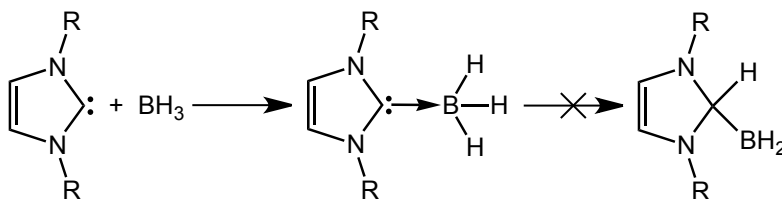
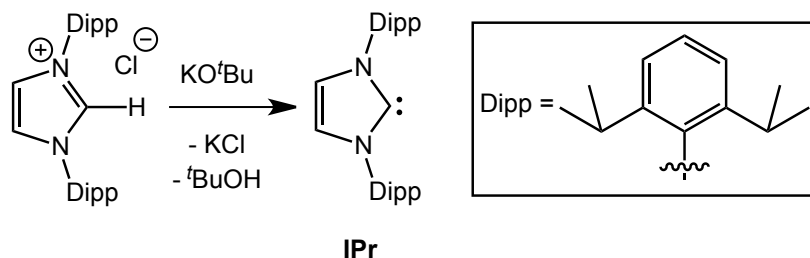


Figure 2.2.1. General schematic illustrating $N \rightarrow C$ π interactions within an NHC.



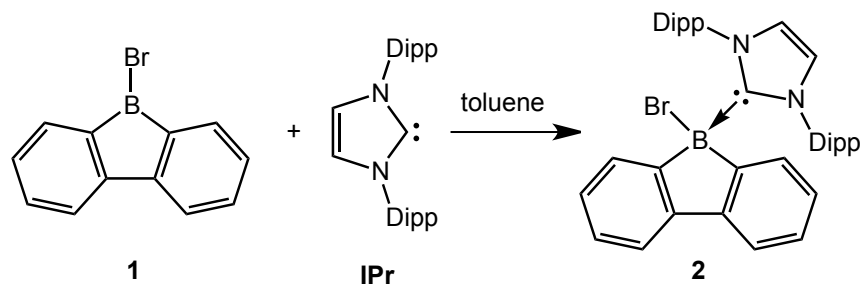
Scheme 2.2.3. Example of NHC-borane that resists intramolecular hydroboration.



Scheme 2.2.4. Synthesis of IPr.

After the Lewis base had been chosen, the synthesis of the IPr adduct of **1**, $\text{BrBF}_4 \cdot \text{IPr}$ (**2**), was pursued (Scheme 2.2.5). This was accomplished through a rather facile set-up that involved adding toluene (in which both **1** and IPr are soluble) to a mixture of the two solid precursors. Upon solvent addition, a bright yellow solution, likely due to the initial presence of **1**, was observed. The color of

the solution quickly began to fade and the formation of a colorless precipitate (**2**) transpired. The supernatant was decanted from the precipitate, and the remaining solid was dried *in vacuo* to afford **2** in a remarkably high yield (> 90 %); the formation of **2** was confirmed through NMR spectroscopic analysis (^1H , $^{13}\text{C}\{^1\text{H}\}$ and $^{11}\text{B}\{^1\text{H}\}$). The loss of color in the final product is due to the loss of conjugation between the flanking aryl moieties and the boron center in **1** as a result of the carbene lone pair now occupying the once vacant boron *p*-orbital. This is a common occurrence in borafluorene chemistry and forms the basis on “On/Off” detection as demonstrated by Yamaguchi and coworkers.⁶



Scheme 2.2.5. Synthesis of the carbene-bound borafluorene **2**.

The presence of a coordinated IPr unit in **2** was readily confirmed through ^1H NMR spectroscopy. The chemical shift of the protons located along the unsaturated backbone ($-\text{N}-\text{CH}=\text{CH}-\text{N}-$) occurs as a singlet at 6.28 ppm. Perhaps even more compelling evidence for the generation of **2** was found through analysis of the $^{11}\text{B}\{^1\text{H}\}$ NMR spectrum. As mentioned before, **1** shows a single broad resonance at 65.8 ppm; however, the boron resonance of **2** appears at -6.4 ppm. This drastic shift in resonance frequency clearly shows that the boron center

in **2** was now in a considerably different bonding environment. In addition, the upfield shifted resonance in **2** is consistent with resonances known in the literature corresponding to four-coordinate boron environments featuring NHCs (i.e., NHC•BR₃).²⁰ The adduct **2** exhibits remarkable thermal stability, with no visible decomposition or melting up to 340 °C under nitrogen. It should be noted that, unlike **1**, compound **2** was stable in moisture rich environments as the addition of H₂O to a solution of **2** in C₆D₆ did not result in hydrolysis. Further structural characterization of **2** was accompanied by X-ray analysis performed on a crystal obtained from a mixture of CH₂Cl₂ and hexanes at -35 °C and the refined structure is presented in Figure 2.2.2.

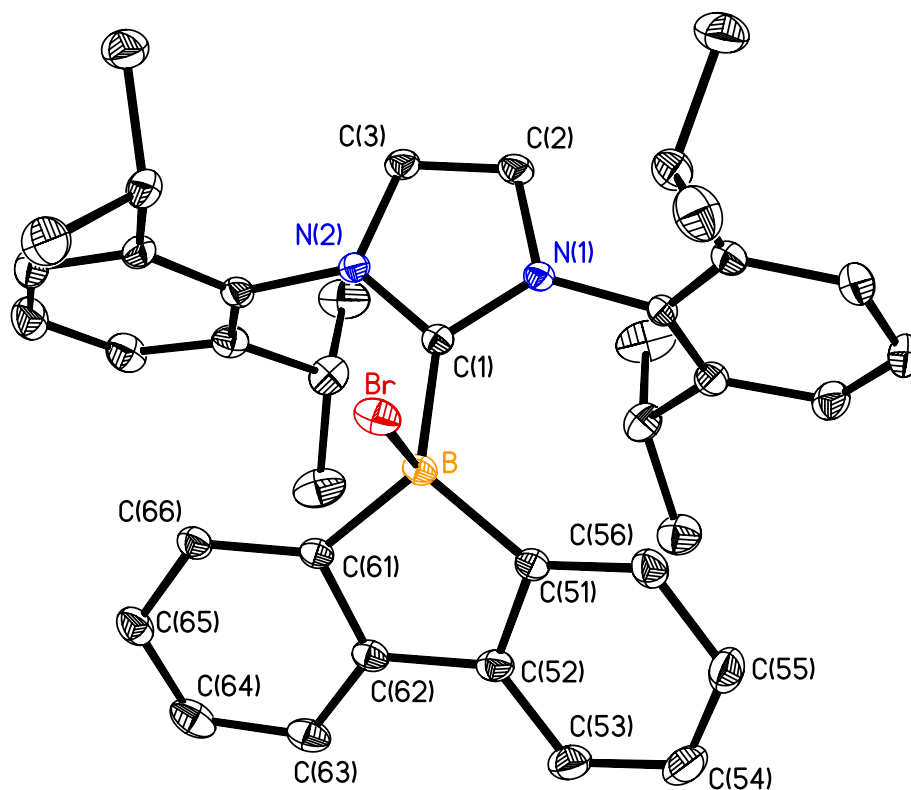


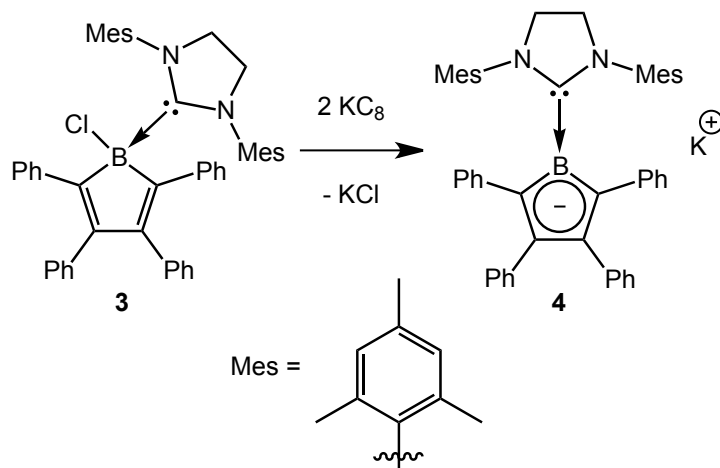
Figure 2.2.2. Thermal ellipsoid plot (30 % probability) of **2** with hydrogen atoms and CH₂Cl₂ solvate molecules omitted for clarity. Selected bond lengths (Å) and angles (°): B-Br 2.114(2), B-C(1) 1.639(3), B-C(51) 1.619(3), B-C(61) 1.619(3); Br-B-C(1) 101.47(13), Br-B-C(51) 108.32(14), Br-B-C(61) 111.65(14), C(51)-B-C(61) 110.14(17), C(1)-B-C(51) 119.11(18), C(1)-B-C(61) 116.27(17); C(52)-C(51)-B-Br torsion angle 125.63(16), C(56)-C(51)-B-Br torsion angle -47.6(3).

The solid state structure of **2** clearly shows the bonding environment about boron has changed when compared to that found in compound **1**.²⁷ Perhaps the most striking difference in the structure of **2**, as compared to **1**, is the boron center is now in a more tetrahedral environment, whereas **1** has a trigonal planar environment at boron. The boron-bromine bond length in **2** has increased by

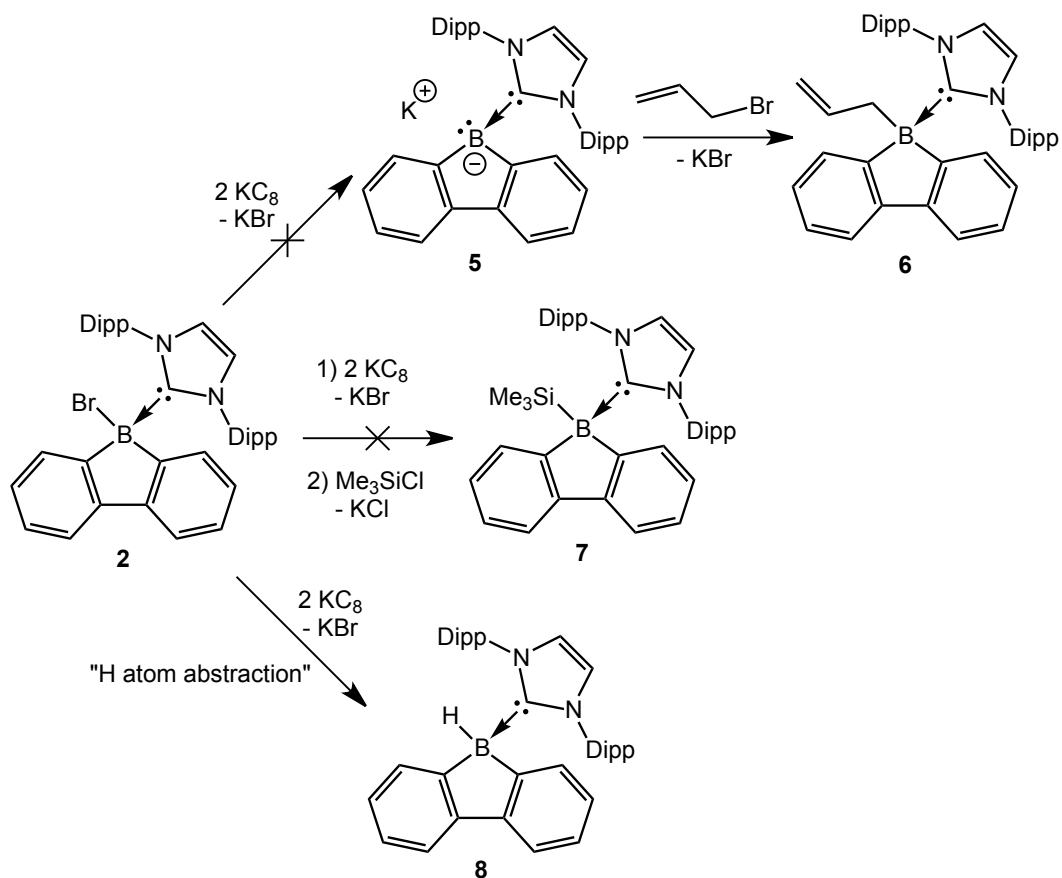
approximately 0.2 Å (1.909(10) Å in **1**, 2.114(2) in **2**) and the bromine atom is now positioned significantly above the plane formed by the borafluorene unit. The boron-carbon bond distances within the borafluorene array of **2** have been increased by approximately 0.1 Å (1.554(12) Å and 1.557(12) Å in **1** to 1.639(3) Å and 1.619(3) Å in **2**). The boron-carbene carbon bond distance of **2** (1.639(3) Å) is comparable with other organoborane-NHC adducts in the literature (1.541(2) – 1.655(3) Å).^{28,29}

To begin probing the potential reactivity of **2**, inspiration was drawn from work published by Braunschweig, *et al.*, in 2010.²⁹ This work involved the reduction of the carbene-substituted tetraphenylchloroborole SIMes•ClBC₄Ph₄ (**3**) with KC₈ to form a stable π -boryl anion (**4**, Scheme 2.2.6). Following this chemistry, it was hoped that a related borafluorene anion (**5**) could be used as a nucleophile for further derivatization of the borafluorene unit, with the ultimate goal being the incorporation of polymerizable groups at boron (**6**, Scheme 2.2.7). The work of Braunschweig, *et al.*, revealed that the ¹¹B NMR resonance of the reduced species was shifted considerably downfield from the starting material (shifting from -3.3 ppm to 12.7 ppm), however this was not the case in the attempted reductions of **2**. Whenever **2** was treated with KC₈, the ¹¹B NMR resonance of the reaction mixture was observed to shift upfield from -6.4 ppm to -19.1 ppm, thus implying that the formation of the target boron anion **5** had not occurred. Multiple attempts to reduce **2** with KC₈ under various solvent and temperature conditions gave identical results. Assuming that KC₈ was too strong a reducing agent for **2**, milder reducing agents including sodium naphthalide and

5 % Na(Hg) were examined. However, in these cases, no reaction was observed. It was not until a proton coupled ^{11}B NMR experiment was conducted that any light was shed on the potential product of the KC_8 reduction. Specifically, the new resonance at -19.1 ppm split into a doublet upon running a proton-coupled ^{11}B NMR experiment ($^1J_{\text{BH}} = 84$ Hz), indicating that a hydrogen atom had been acquired and effectively exchanged in place with the bromine atom in **2**. Further efforts were made to trap the anionic borafluorene **5** through addition of trimethylsilyl chloride (Me_3SiCl) to the reaction mixture as shown in Scheme 2.2.7. However, the results were identical to those observed in the reaction of **2** with KC_8 in the absence of Me_3SiCl .



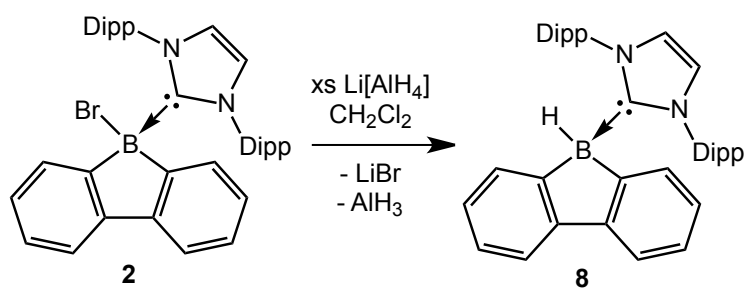
Scheme 2.2.6. Reduction of a carbene-substituted tetraphenylborole.



Scheme 2.2.7. Example of an attempted reduction of **2** both with and without the use of Me_3SiCl as a trapping agent, along with the intended formation of an allyl-substituted species that could lead to a polymer. Included is the formation of the hydridic compound **8**.

To confirm that the boron-bonded bromide group in **2** was replaced with a hydride, the hydridic product, **8**, was prepared independently (Scheme 2.2.8) by reacting **2** with the hydride transfer agent $\text{Li}[\text{AlH}_4]$. Attempts to prepare **8** by reacting **2** with Et_3SiH ,²³ $\text{Li}[\text{Et}_3\text{BH}]$, $\text{Na}[\text{BH}_4]$, and $\text{Li}[\text{BH}_4]$ gave no reaction. Upon stirring a mixture of **2** with an excess of $\text{Li}[\text{AlH}_4]$ in CH_2Cl_2 for up to five days, the desired hydridic species, $\text{HBFI}\cdot\text{IPr}$ (**8**), was isolated in a moderate yield

of 27 % as a colorless solid. The formation of this species was confirmed through ^1H , $^{13}\text{C}\{^1\text{H}\}$ and proton-coupled ^{11}B NMR spectroscopy. The most compelling and readily identifiable evidence for the formation of **8** was found in the ^1H resonance of the backbone protons ($\delta = 7.10$ ppm, shifted from 6.28 ppm in **2**) and the proton-coupled ^{11}B NMR spectrum, which showed the presence of a B-H unit ($\delta = -19.1$ ppm, d, $^1J_{\text{BH}} = 84$ Hz). Crystals suitable for X-ray analysis were grown from a mixture of CH_2Cl_2 and hexanes at -35 °C (see Fig. 2.2.3 for a representative view of **8**).



Scheme 2.2.8. Successful synthesis of **8**.

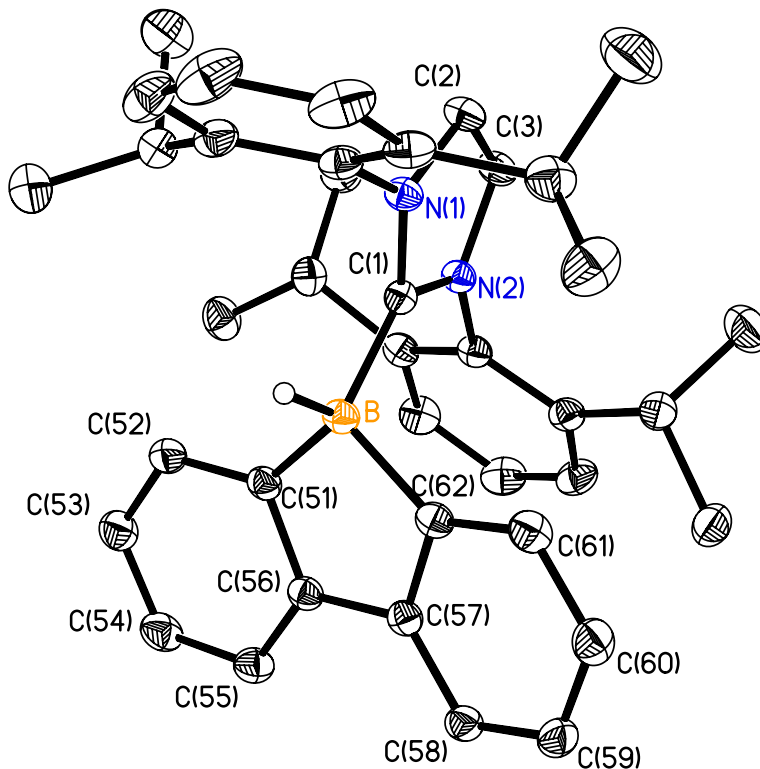


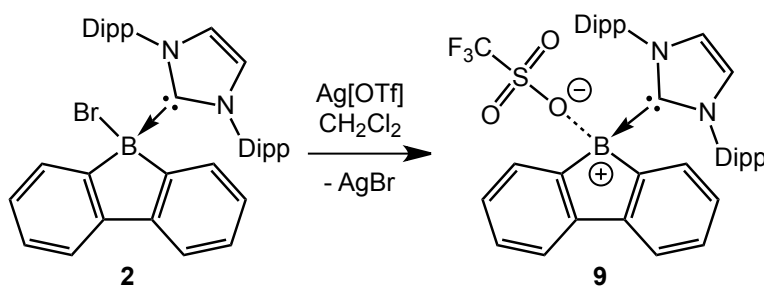
Figure 2.2.3. Thermal ellipsoid plot (30 % probability) of **8** with the hydrogen atom attached to boron presented with an arbitrarily small thermal parameter; the remaining hydrogen atoms are not shown for clarity. Selected bond lengths (Å) and angles (°): B-H(1B) 1.135(14), B-C(1) 1.6232(16), B-C(51) 1.6232(17), B-C(62) 1.6258(17); H(1B)-B-C(1) 105.8(7), H(1B)-B-C(51) 109.4(7), Br-B-C(62) 110.6(7), C(51)-B-C(62) 99.31(9), C(1)-B-C(51) 117.85(9), C(1)-B-C(62) 113.80(9).

When compared to the solid state structure of **2**, the structure of **8** clearly shows a profound difference in the orientation of the IPr moiety relative to the borafluorene plane. The IPr unit of **8** twists approximately 90° about the boron-carbene carbon bond relative to **2** effectively creating an umbrella-like cover over

the boron-bound hydride, while all bond angles and distances remain fairly similar between **2** and **8**. The boron-carbene carbon bond distance in **8** is only ca. 0.02 Å shorter than in **2**, indicating that the different orientations of the IPr units in these two species with respect to the borafluorene array does not perturb the boron-carbene carbon interaction to a large degree.

Knowing now that the bromine of **2** could be exchanged, and keeping with a desire to form **5** via the reduction of **2**, the thought had occurred that exchanging the bromine for a different leaving group might assist in the reduction and prevent the formation of **8**. To test this, the triflate-substituted borafluorene, IPr•B(OTf)FI (**9**), was prepared from the reaction of **2** with Ag[OTf] in CH₂Cl₂ (Scheme 2.2.9) in a 45 % yield. As in the synthesis of **8**, the ¹H resonance of the carbene backbone protons had shifted downfield in **9** (7.11 ppm) relative to that found in **2** (6.28 ppm). The ¹¹B resonance was shifted downfield to 2.3 ppm with no additional coupling observed. This chemical shift implies that **9** contains a three-coordinate borenium cation (i.e., [IPr•BFI]⁺), however the ¹⁹F NMR spectrum showed a singlet resonance at -77.8 ppm which indicates that the triflate anion may be bound to boron in solution as this value agrees well with previously reported four-coordinate organoborane species with a OTf group at boron (Fig. 2.2.4a).³⁰ Rigorously three-coordinate borenium cations (Fig. 2.2.4b-d) found in the literature typically exhibit ¹¹B resonances at chemical shifts > 20 ppm,^{31,32} although upon coordination of a Lewis base (becoming four-coordinate), this resonance can be shifted downfield as shown by Bonnier, *et al.*, involving the DMAP adduct of a BODIPY derived borenium cation, which exhibits an ¹¹B

resonance at -1.6 ppm (Fig. 2.2.4e).³¹ Several attempts were made to grow X-ray quality crystals of **9** from various combinations of arene, halogenated and ethereal solvents with no success. Mass spectrometry indicated that the triflate anion was present in the $[M]^+$ ($m/z = 700.31221$) providing further support that **9** had been formed and that the triflate anion was directly bound to the boron center. Reduction attempts similar to those investigated with compound **2** (Scheme 2.2.6) were made with **9**; in all cases, treatment of **9** with KC_8 invariably led to the formation of **8**.



Scheme 2.2.9. Synthesis of **9** via anionic exchange of bromide with triflate.

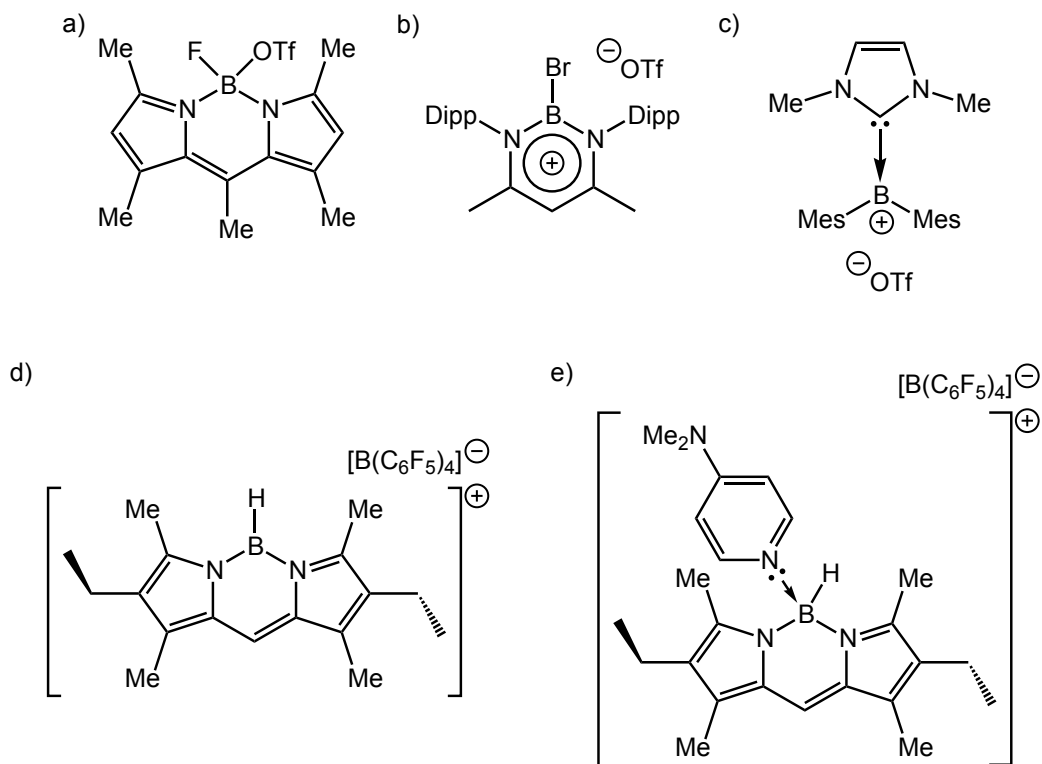
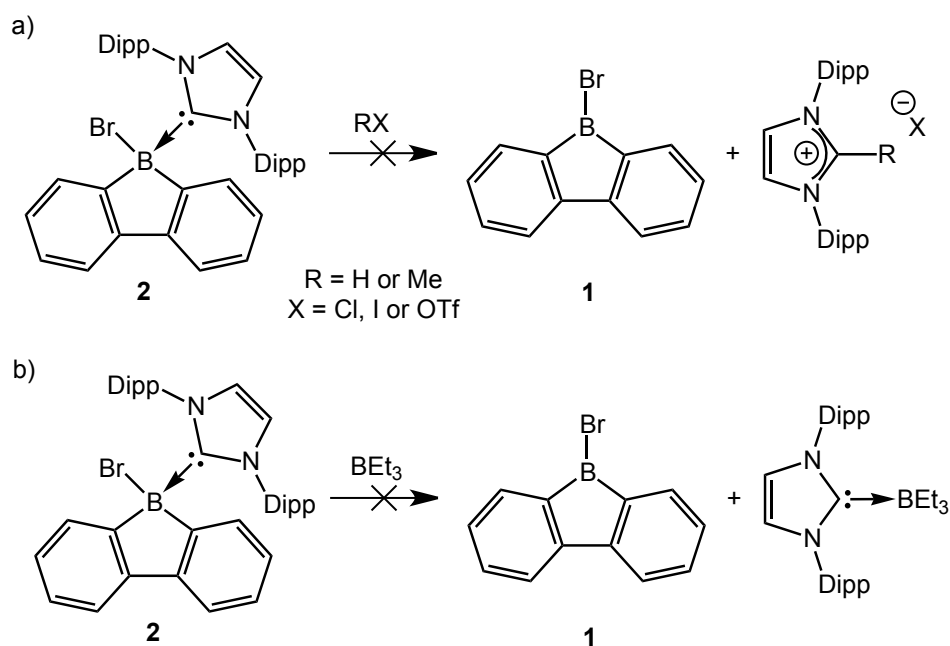


Figure 2.2.4. Representative examples of organoborane species featuring: a) a bound triflate group; b) borenium cation with a triflate anion; c) a three-coordinate borenium cation bound to an *N*-heterocyclic carbene; d) a three-coordinate borenium cation; e) a four-coordinate borenium cation.

Considering the synthetic difficulties forming the anionic species, $[\text{BF}_1\cdot\text{IPr}]^-$ (**5**, Scheme 2.2.7), attention was turned back to an original goal of the project: the “masking” and “unmasking” of boraf luorene as indicated in Section 2.1. Specifically, compound **2** was combined with either Brønsted acidic, methylating, or Lewis acidic (BET_3) reagents (Scheme 2.2.10) in an effort to remove the IPr unit and recover the carbene-free boraf luorene **1**. Multiple attempts were conducted under various conditions, including at room temperature or at reflux in either CH_2Cl_2 or in toluene overnight or for up to three days in both

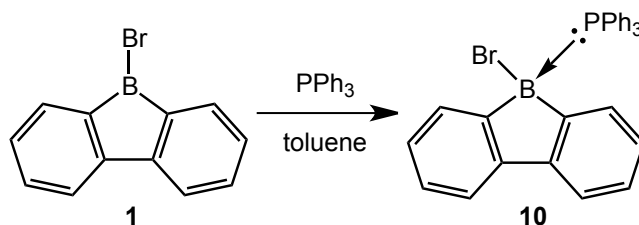
stoichiometric and excess mole ratios of the H^+ and methyl sources. However, in all cases, uncomplexed **1** was not recovered and the starting material **2** was observed; similar results were obtained when **2** was combined with BEt_3 . With this in mind, the conclusion drawn was that the carbene-boratrafluorene interaction was too strong and that less strongly donating Lewis bases (relative to carbene) were required to enable controlled “masking” and “unmasking” chemistry to occur, *en route* to a functionalized boratrafluorene polymer.



Scheme 2.2.10. Attempted “unmasking” of **1** using a) HCl , MeI , $MeOTf$, or b) BEt_3 .

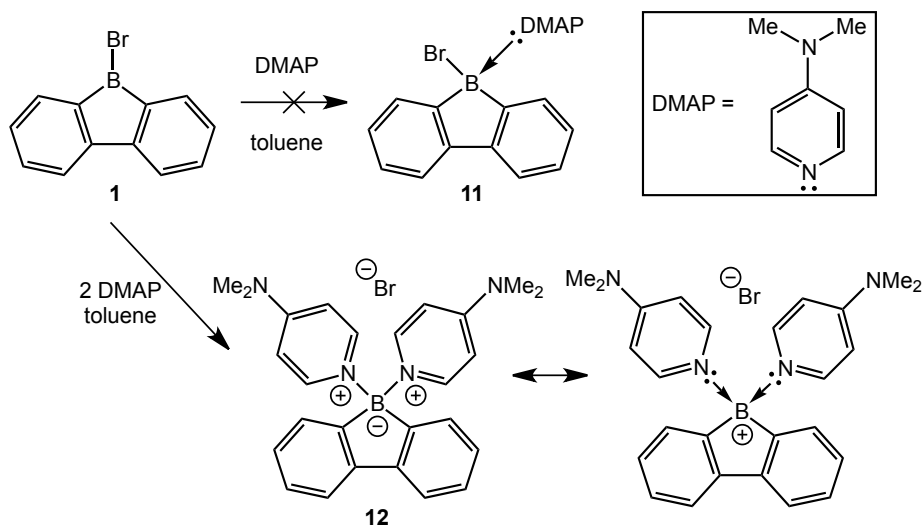
Stemming from recent success within our group with regard to isolating Lewis base (LB) adducts of aminodiboranes (e.g., $LB \cdot H_2BNH_2 \cdot BH_3$),³³ the decision was made to move away from carbenes and focus on triphenylphosphine

(PPh₃) and the pyridine-derived donor *N,N*-dimethylaminopyridine (DMAP). The synthesis of the triphenylphosphine adduct of **1**, BrBFl•PPh₃ (**10**), proceeded as expected (Scheme 2.2.11) through the addition of toluene to a 1:1 mixture of **1** and PPh₃. Upon dissolution of the reagents, the initially bright yellow solution quickly discolored and the formation of a white precipitate was noted. Removal of the volatile components and subsequent washing of the precipitate with hexanes afforded **10** as a colorless solid in a 92 % yield. Although the ¹H and ¹³C{¹H} NMR spectra were not entirely diagnostic that **10** had formed, more compelling evidence was offered through ¹¹B{¹H} and ³¹P{¹H} NMR spectroscopy. The ³¹P NMR spectrum showed a singlet at 1.8 ppm, which was found to have shifted slightly downfield from the resonance due to free PPh₃ (δ = -5.3 ppm). Moreover, the ¹¹B{¹H} NMR spectrum of **10** showed a broad singlet at -7.4 ppm, representing a significant upfield shift from that of free **1** (δ = 65.8 ppm), consistent with the formation of a four-coordinate boron center, as previously discussed. Repeated attempts to grow crystals suitable for X-ray analysis were unsuccessful; however, additional confirmation for the formation of **10** was provided through mass spectrometry.



Scheme 2.2.11. Synthesis of the triphenylphosphine-borafluorene adduct **10**.

The formation of a DMAP adduct of **1** was carried out in tandem with the synthesis of **10** in an effort to compare the viability of the two Lewis bases (PPh₃ and DMAP) for the “masking” and “unmasking” synthetic approach to polymeric borafluorenes (Scheme 2.2.12). Upon analysis of the crude products of a 1:1 reaction of **1** and DMAP, the ¹H NMR spectrum seemed to indicate that two DMAP molecules had become bound to **1** as evidenced by the integration of the ¹H resonances and the presence of significant quantities of free **1** in the reaction mixture. The methyl groups of DMAP in the new product showed a singlet at 3.16 ppm that was shifted from that of free DMAP ($\delta = 2.95$ ppm) with an integration of 6:1 relative to the borafluorene arylH resonances, rather than the 3:1 ratio expected from a monoadduct such as BrBFl•DMAP (**11**). This hypothesis was confirmed by carrying out a reaction of two equivalents of DMAP with one equivalent of **1** in toluene (Scheme 2.2.12). The initially bright yellow solution almost immediately faded to a colorless solution and the formation of a white solid occurred which gave similar spectroscopic parameters as the product described above.



Scheme 2.2.12. Synthesis of the doubly substituted borafluorene, **12**, and the attempted synthesis of the monoadduct, **11**.

Crystals of **12** suitable for X-ray analysis were grown from a mixture of THF and CH_2Cl_2 at $-35\text{ }^\circ\text{C}$ and clearly shows the incorporation of two DMAP donors at boron to yield the borafluorenium salt $[(\text{DMAP})_2\text{BFI}]\text{Br}$, **12**, with a distorted tetrahedral geometry at boron (Fig. 2.2.5). The boron-carbon bond distances within the borafluorene unit are the same within experimental error as those seen in compounds previously discussed (see Fig. 2.2.2 and Fig. 2.2.3). The boron-nitrogen bond distances (*avg.* $1.581(9)\text{ \AA}$) were identical within experimental error and matched dative boron-nitrogen bond lengths reported in the literature (Fig. 2.2.6).^{33,34} It is worth noting that three independent crystallographic forms of **12** are present with only slight variations in the relative orientation of the DMAP unit to the borafluorene plane. Regardless, each of the three crystallographic forms show similar bond lengths and distances with respect to each other.

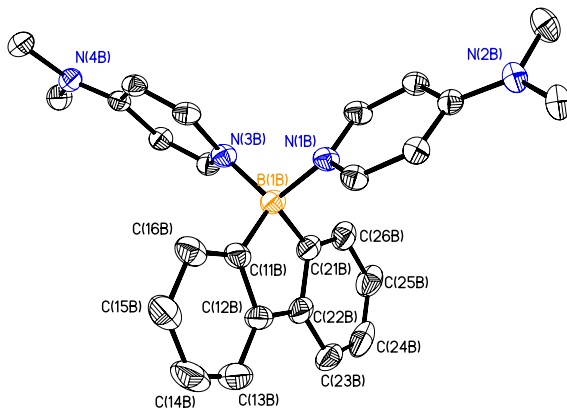


Figure 2.2.5. Thermal ellipsoid plot (30 % probability) of **12** with hydrogen atoms, bromide anion and CH₂Cl₂ solvate molecules omitted for clarity. Three distinct crystallographic forms of **12** exist, only one of which is shown for simplicity. Bond lengths and angle are consistent amongst all crystallographic forms. Selected bond lengths (Å) and angles (°) with values for the two other molecules in the asymmetric unit in square brackets: B(1B)-N(1B) 1.582(5) [1.584(5), 1.576(5)], B(1B)-(N3B) 1.582(5) [1.597(5), 1.604(5)], B(1B)-C(11B) 1.609(6) [1.606(6), 1.620(6)], B(1B)-C(21B) 1.632(6) [1.606(6), 1.629(6)]; N(1B)-B(1B)-N(3B) 108.2(3) [105.8(3), 102.2(4)], C(11B)-B(1B)-C(21B) 100.6(3) [100.8(3), 100.2(3)], N(1B)-B(1B)-C(11B) 112.6(3) [114.0(3), 110.2(3)], N(1B)-B(1B)-C(21B) 108.6(3) [110.8(3), 113.4(3)], N(3B)-B(1B)-C(11B) 111.8(3) [112.5(4), 114.3(4)], N(3B)-B(1B)-C(21B) 115.0(3) [113.0(3), 109.0(5)]; C(12B)-C(11B)-B(1B)-N(1B) torsion angle -110.6(4) [-117.3(4), 114.7(3)], C(22B)-C(21B)-B(1B)-N(1B) torsion angle 113.4(4) [118.9(4), 130.0(4)], C(12B)-C(11B)-B(1B)-N(3B) torsion angle 127.4(3) [122.2(4), -129.2(5)], C(22B)-C(21B)-B(1B)-N(3B) torsion angle -125.3(4) [-122.5(4), 130.0(4)].

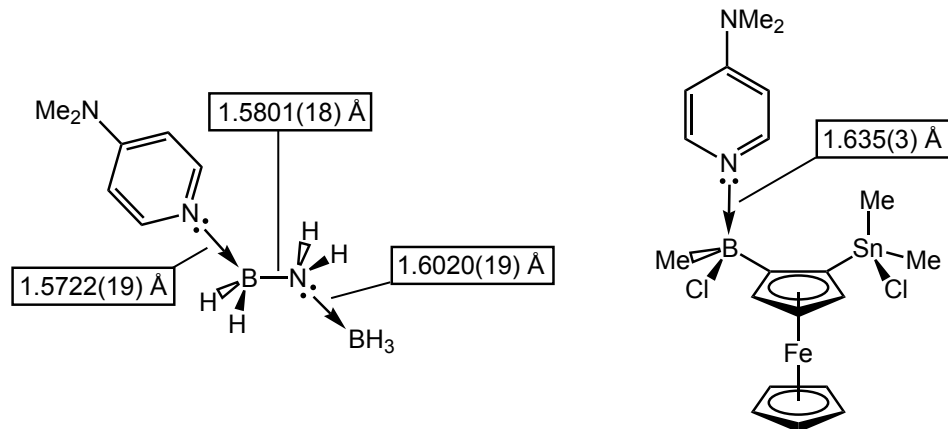
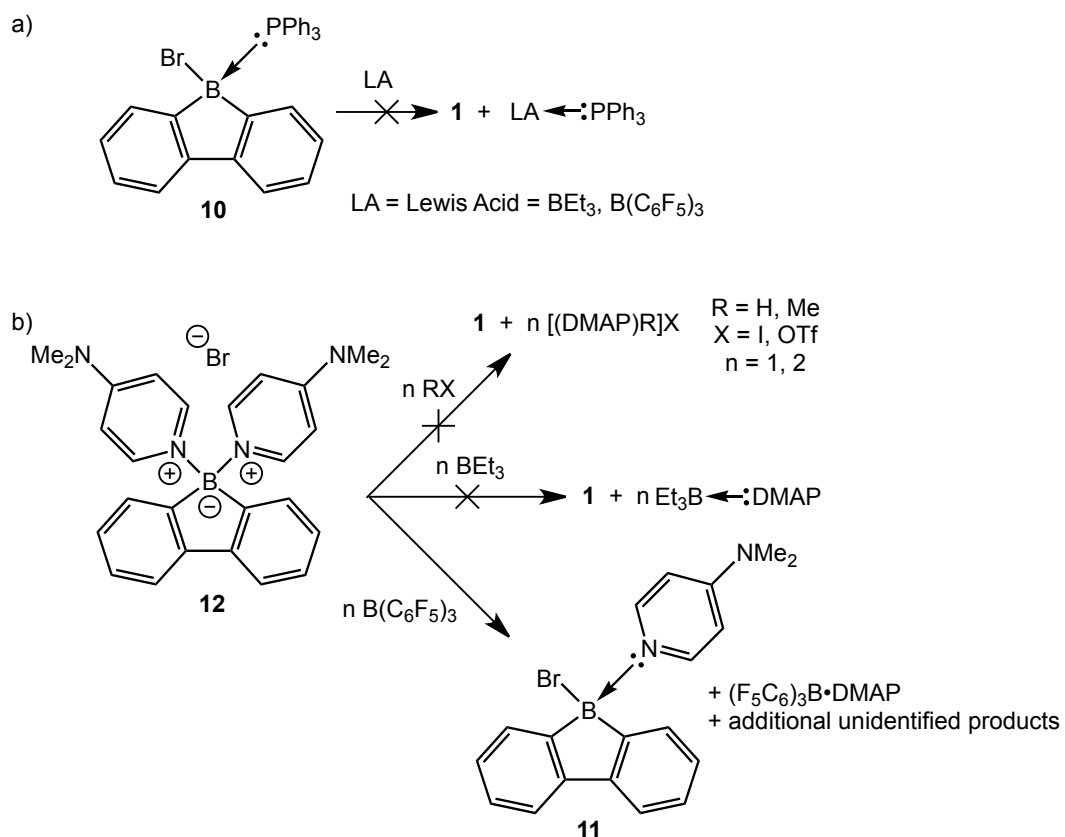


Figure 2.2.6. Representative examples of boron-nitrogen adducts with all boron-nitrogen bond lengths shown.

Attention once again turned toward the removal of the Lewis bases from both **10** and **12** as the eventual target polymeric species requires the restoration of a three-coordinate boron atom within the borafluorene units. Scheme 2.2.13 shows representative reactions involving the attempted removal of the Lewis base (PPh_3 or DMAP) from either **10** or **12**. Additions of HCl, MeI or MeOTf in either one or two equivalents to **12** did not result in any observed reactivity. Additions of BEt_3 to either **10** or **12** also resulted in no reaction. It was not until the very Lewis acidic borane, $\text{B}(\text{C}_6\text{F}_5)_3$,⁹ was used that any reactivity was observed. Upon addition of $\text{B}(\text{C}_6\text{F}_5)_3$ to **10**, an unidentified product was observed along with over 80 % starting material in the crude reaction mixture as determined by $^{11}\text{B}\{^1\text{H}\}$ and $^{31}\text{P}\{^1\text{H}\}$ NMR spectroscopy. The unidentified product did not correspond to the expected byproduct, $(\text{F}_5\text{C}_6)_3\text{B}\cdot\text{PPh}_3$,³⁵ and neither free **1** nor free PPh_3 were observed. The addition of either one or two equivalents of $\text{B}(\text{C}_6\text{F}_5)_3$ to **12** did

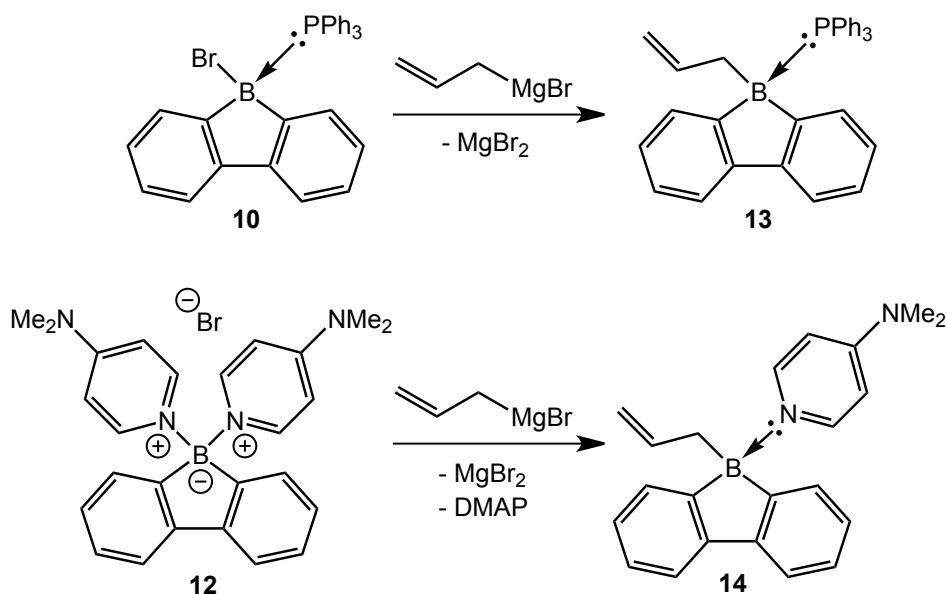
result in the removal of at least one of the DMAP units. Evidence of this was provided through the observation that $(F_5C_6)_3B \cdot DMAP$ had been formed by 1H and $^{11}B\{^1H\}$ NMR spectroscopy,³⁶ although $^{19}F\{^1H\}$ NMR spectroscopy indicated that additional products may have formed; and attempts to isolate pure products via fractional crystallization were unsuccessful. A second product was observed that may correspond to the formal 1:1 adduct of **1** and DMAP, $BrBF_4 \cdot DMAP$, although efforts to form this species by a separate methods were not successful. Future investigations (see Chapter 3) will focus on exploring the use of other pyridinyl-based Lewis bases (such as pyridine, picoline or lutidine) in efforts to optimize the “unmasking” of **1** along with investigations involving allyl-substituted borafluorene species. Upon stirring a mixture of $BrBF_4 \cdot PPh_3$ (**10**) with two equivalents of DMAP in CH_2Cl_2 for 24 hours, free PPh_3 and **12** were found to be in the crude reaction mixture. This provides evidence that DMAP has a stronger binding affinity for borafluorene and will readily displace PPh_3 .



Scheme 2.2.13. Attempted removal of a) PPh_3 and b) DMAP from **10** and **12**, respectively, in effort to liberate **1**.

As outlined in Scheme 2.1.1, an initial goal of this project was to form allyl-substituted borafluorene polymer precursors. A direct reaction of allylmagnesium bromide with BrBFI (**1**) resulted in a complex mixture of products. To this end, the installation of an allyl group at boron through the functionalization of the boron-bromine bond in **10** and **12** was seen as a logical step toward the incorporation of borafluorene unit into a polymer. In order to form allyl-substituted borafluorenes, both **10** and **12** were combined with allylmagnesium bromide (Scheme 2.2.14). At this stage, evidence for the successful incorporation of the allyl unit at boron in **13** and **14** can be found by

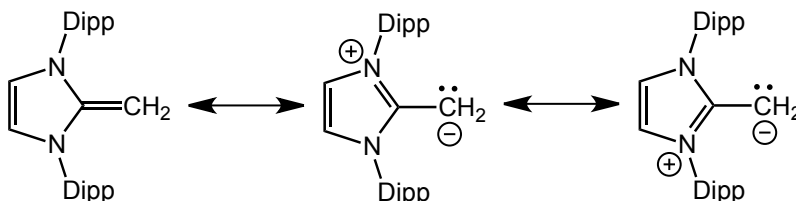
NMR spectroscopy; however, attempts to grow crystals of suitable quality for X-ray crystallography have been unsuccessful thus far. For **14**, only one DMAP donor was present as revealed by inspection of the ^1H integration and the presence of free DMAP as a byproduct in the crude reaction mixture was noted. In the reaction of **10** with allylmagnesium bromide, the resulting product **13** contained coordinated PPh_3 as determined by a shift in the ^{31}P resonance ($\delta = 11.2$ ppm) from that of **10** ($\delta = 1.8$ ppm).



Scheme 2.2.14. Grignard metathesis of **10** and **12** with (allyl) MgBr to form the allyl-substituted borafluorenes **13** and **14**.

In the hope of isolating novel borafluorene adducts with potential luminescent properties, attention turned to the use of the nucleophilic olefin, IPrCH_2 ($\text{IPrCH}_2 = (\text{HCNDipp})_2\text{C}=\text{CH}_2$; $\text{Dipp} = 2,6\text{-}^i\text{Pr}_2\text{C}_6\text{H}_3$) as a Lewis base was explored. This species has recently found success as a donor ligand, analogous to

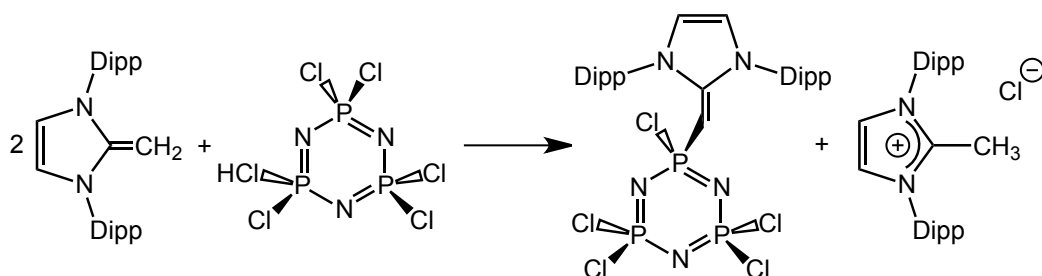
NHCs, in low oxidation state main group chemistry.^{33,37-40} The nucleophilic character of IPrCH₂ can be described by the canonical forms represented in Scheme 2.2.15 whereby, through resonance, the methylene (CH₂) carbon can possess lone pair character thus becoming nucleophilic.^{39,40}



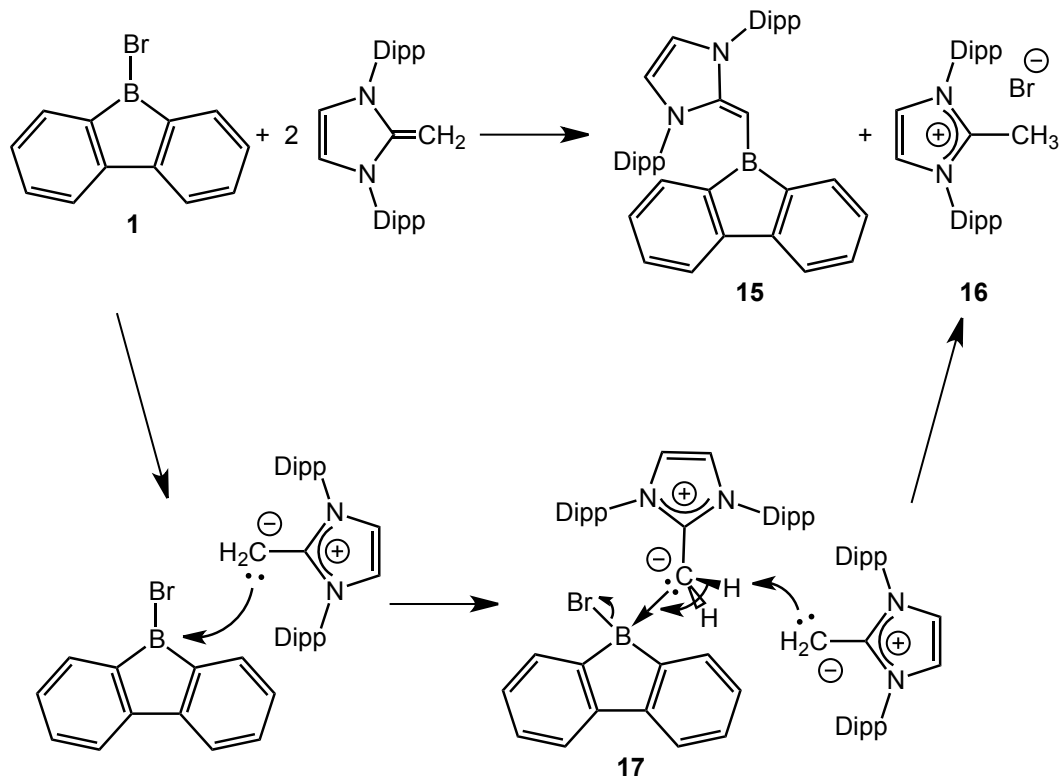
Scheme 2.2.15. Representative canonical forms for IPrCH₂.

As demonstrated by our group, IPrCH₂ can be used to remove chloride from phosphorus within hexachlorotriphosphazene, [Cl₂PN]₃, to afford a new alkene substituted species via deprotonation and the formal elimination of HCl (Scheme 2.2.16).³⁸ With this in mind, similar reactivity using **1** was explored (Scheme 2.2.17). The proposed mechanism of this reaction initially involves the coordination of IPrCH₂ to **1**, followed by subsequent deprotonation of the intermediate **17**, in Scheme 2.2.17, by a second equivalent of IPrCH₂ to form the olefin-bound borafluorene **15** and the methylimidazolium salt **16** as a byproduct. As many heterocyclic boron-containing systems exhibit intriguing photophysical properties, as described in previous sections, it was believed that the target alkenyl-borafluorene **15** might prove to be a new class of luminescent compound in its own right as a so-called “push-pull” system.⁴¹⁻⁴³ In these systems, the presence of both an electron-donating group and an electron-accepting group

serve to form a molecular dipole typically resulting in highly colored chromophores.



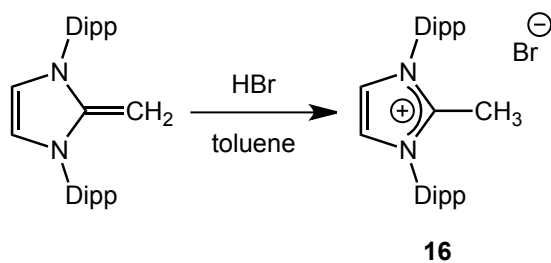
Scheme 2.2.16. Synthesis of an alkene-substituted phosphazene.



Scheme 2.2.17. Proposed synthetic pathway towards the alkene-substituted borafluorene **12**.

Several attempts to prepare **15** were made under various conditions including, but not limited to: the addition of toluene to a mixture of IPrCH₂ and **1**, the slow addition of a toluene solution of IPrCH₂ to a toluene solution of **1**, combination of the reagents at -78 °C or through the use of a cold well by freezing the solutions in liquid N₂ and allowing them to thaw just prior to mixing. In all cases, the same mixture of three new products was noted as evidenced by ¹H NMR spectroscopy and two new boron resonances through ¹¹B{¹H} NMR spectroscopy. The observed boron resonances from the reaction mixture had shifted upfield to 2.2 and -1.4 ppm (as a broad singlets) from a value of 65.8 ppm noted in free **1**. This initially indicated the new products formed with a boron center in a four-coordinate environment, as seen in previous adducts. However, this was inconsistent with the predicted ¹¹B chemical shift for the three-coordinate boron in **15** as other alkyl or aryl substituted three-coordinate typically show chemical shifts greater than 0 ppm.^{2,10,44} Attention turned to ¹H NMR spectroscopy in order to determine if **15** was successfully synthesized. A new ¹H resonance located at 2.66 ppm was initially assigned to the IPr=CH group in **15**; however, inspection of the integration of this resonance revealed that two protons were present compared to the IPr unit. Thus, it appeared this new boron-containing species had an intact IPrCH₂ unit bound at boron. Analysis of the aromatic region of the ¹H NMR spectrum of the crude reaction mixture seemed to indicate the emergence of two new borafluorene environments shown through the presence of two triplet resonances (at 6.69 and 6.56 ppm) and two doublet resonances (at 6.12 and 5.94 ppm) which are unique to borafluorene. Two singlets

were observed at 7.22 ppm and 8.15 ppm in the ^1H NMR spectrum of the crude product and are consistent with the presence of two different carbene backbone environments, the most downfield resonance was identified as belonging to $[\text{IPrMe}]\text{Br}$ (**16**), based on a previous synthesis of $[\text{IPrMe}]\text{Cl}$.³⁸ To confirm that **16** was formed as a product in this reaction, a direct synthesis of this product was carried out by bubbling HBr gas through a toluene solution of IPrCH_2 (Scheme 2.2.18). Crystals suitable for X-ray analysis were grown from a mixture of CH_2Cl_2 and hexanes at $-35\text{ }^\circ\text{C}$, and Figure 2.2.7 shows a representative view of the solid state structure of **16**. Upon characterization of the product from this reaction, **16** could now be confirmed to be present in the reaction mixture from the reaction of IPrCH_2 with **1** in a 2:1 ratio.



Scheme 2.2.18. Synthesis of the methylimidazolium salt **16**.

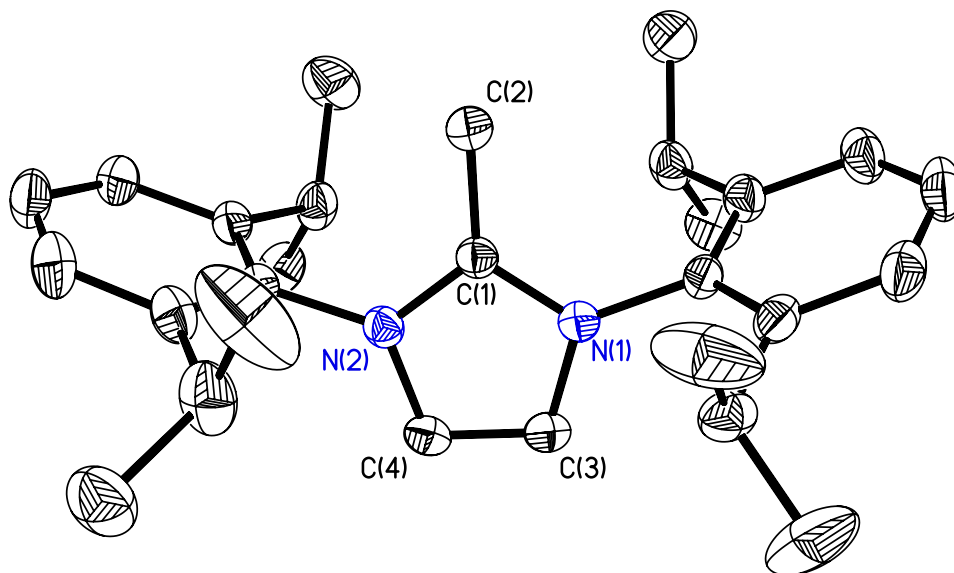
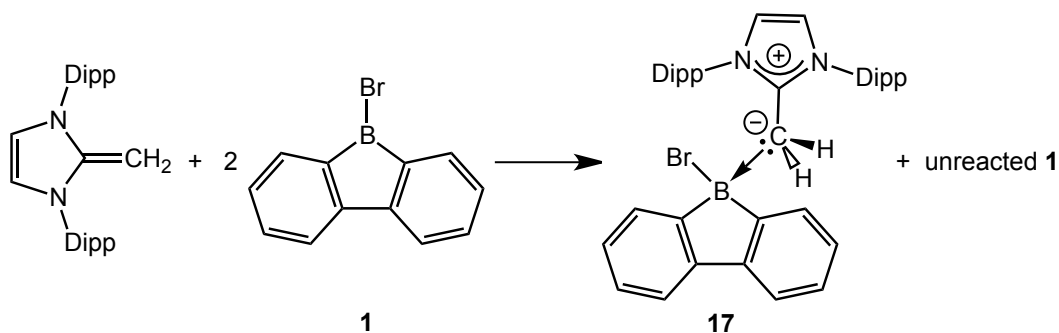


Figure 2.2.7. Thermal ellipsoid plot (30 % probability) of [IPrMe]Br (**16**) with the hydrogen atoms, bromide anion and CH₂Cl₂ solvate molecules omitted for clarity. Selected bond lengths (Å) and angles (°): C(1)-C(2) 1.477(3), C(1)-N(1) 1.337(3), C(1)-N(2) 1.338(3), N(1)-C(3) 1.385(3), N(2)-C(4) 1.388(3), C(3)-C(4) 1.345(4); N(1)-C(1)-C(2) 126.3(2); N(2)-C(1)-C(2) 126.1(2), N(1)-C(1)-N(2) 107.6(2), C(1)-N(1)-C(3) 109.162, C(1)-N(2)-C(4) 109.1(2).

To achieve a better understanding of the previously discussed reaction, IPrCH₂ and **1** were combined in a 1:2 ratio in toluene (essentially the opposite mole ratio as attempted previously) in an attempt to isolate the intermediate **17** (Scheme 2.2.17). The reaction proceeded immediately as evidenced by the formation of a white precipitate that was isolated and washed with toluene to afford BrBfI•IPrCH₂ (**17**) in a 96 % yield (Scheme 2.2.19), and the structure of the product was confirmed by X-ray crystallography (Fig. 2.2.8). Analysis of the ¹H NMR spectrum in CDCl₃ showed a resonance at 2.66 ppm, which could now

be confirmed as belonging to the methylene group of the IPrCH₂ group bound to boron, while the ¹¹B resonance at -1.4 ppm can now be clearly assigned to the boron center in the monoadduct BrBF1•IPrCH₂ (**17**). Moreover, one of the unknown products from the reaction listed in Scheme 2.2.17 could now be identified as **17** by comparison of the ¹H, ¹³C{¹H} and ¹¹B{¹H} NMR spectra. It should be noted that the third product, which may have been IPrCHBF1 (**15**), from the 2:1 reaction between IPrCH₂ and **1** could not be fully characterized as repeated efforts to separate the mixture through chromatography or selective crystallization were unsuccessful.



Scheme 2.2.19. Successful synthesis of **17** through the use of two equivalents of **1**.

Crystals of **17** suitable for X-ray analysis were grown from a mixture of CH₂Cl₂ and hexanes at -35 °C (Fig. 2.2.8). The solid state structure of **17** was quite similar to that of **2** (Fig. 2.2.2) in regard to the geometrical parameters within the borafluorene units. The B-CH₂ bond length in **17** (1.660(3) Å) was found to be slightly elongated compared to the analogous B-C_{IPr} bond in **2** (1.639(3) Å), and was found to be in agreement with a previously reported

IPrCH₂-borane adducts in our group (IPrCH₂•H₂BNMe₂•BH₃, B-C_{IPrCH₂} bond length = 1.659(3) Å).³³ The C(1)-C(2) bond length (1.473(2) Å) is inbetween that of a carbon-carbon single bond (approx. 1.54 Å) and double bond (approx. 1.3 Å)¹⁹ showing that the C(1)-C(2) bond order had decreased upon binding of the IPrCH₂ donor to boron in **17**; for comparison, the related carbon-carbon distance in free IPrCH₂ was determined to be 1.331(8) Å (avg.).³⁹

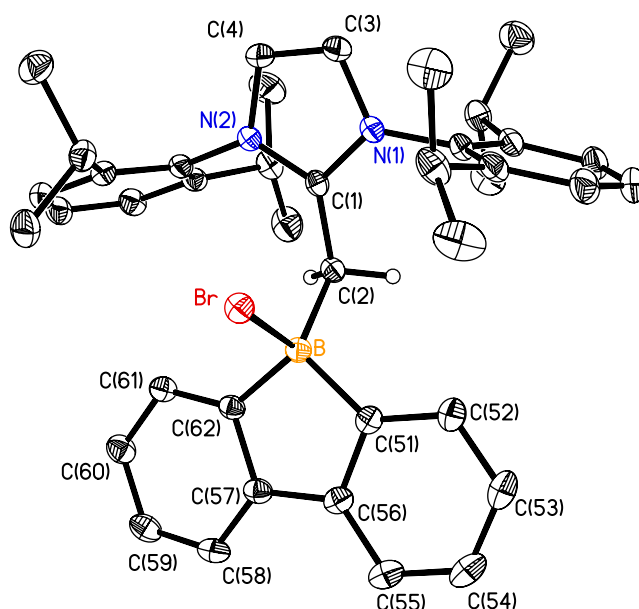
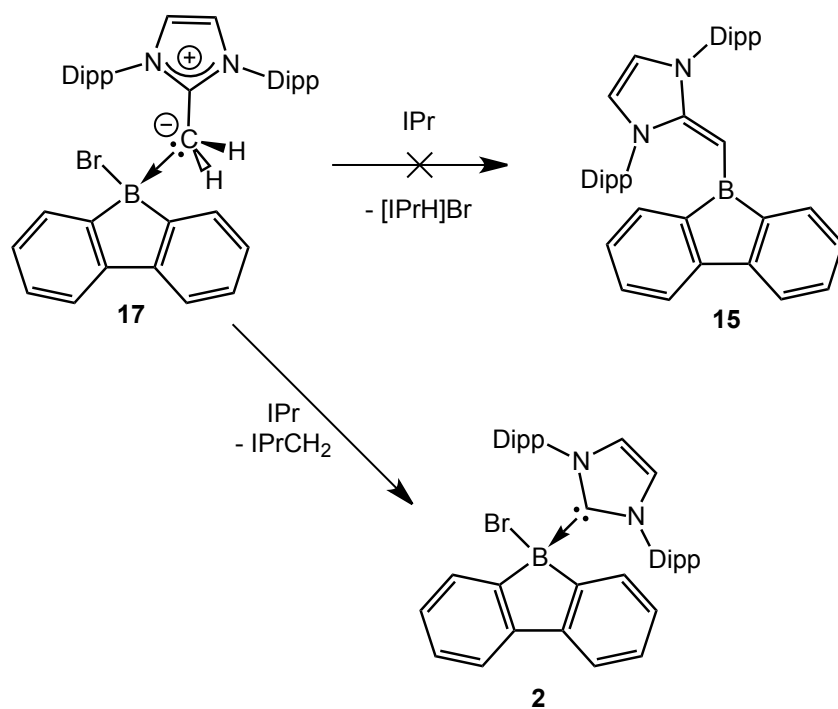


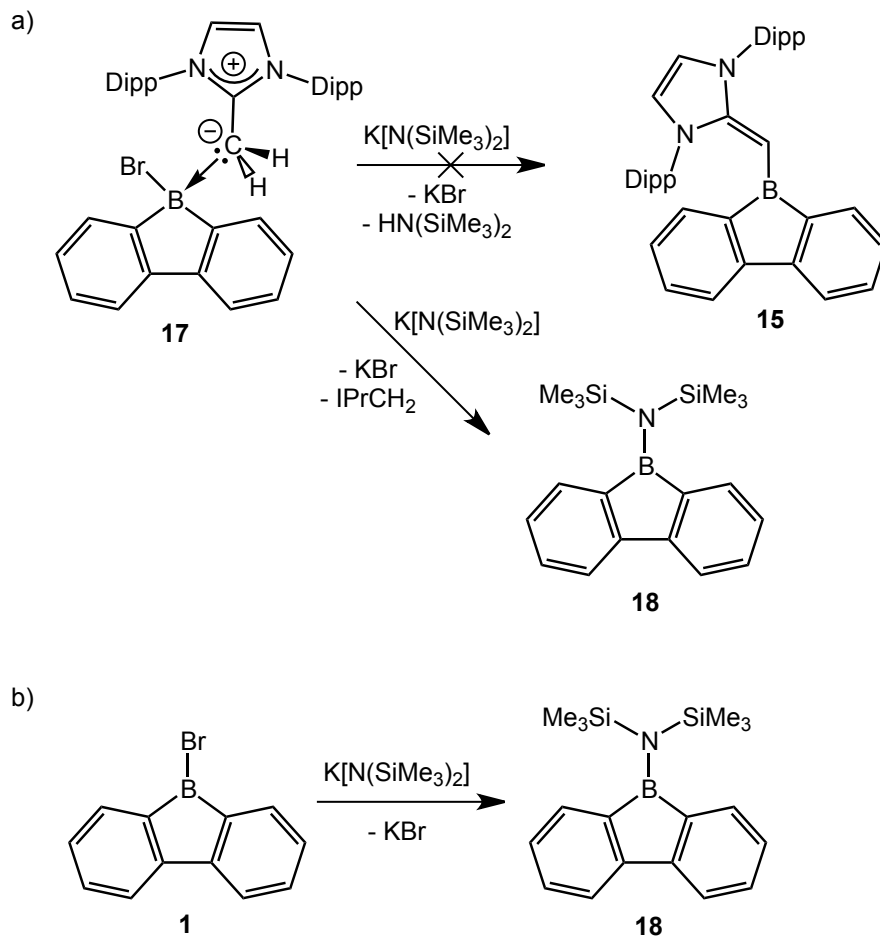
Figure 2.2.8. Thermal ellipsoid plot (30 % probability) of **17** with hydrogen atoms, except those at C(2), and CH₂Cl₂ solvate molecules omitted for clarity. Selected bond lengths (Å) and angles (°): B-Br 2.124(2), B-C(2) 1.660(3), B-C(51) 1.609(3), B-C(62) 1.610(3), C(1)-C(2) 1.473(2), C(1)-N(1) 1.354(2), C(1)-N(2) 1.349(2), C(3)-C(4) 1.343(3), C(3)-N(1) 1.386(2), C(4)-N(2) 1.389(2); C(51)-B-C(62) 100.29(15), C(51)-B-Br 106.29(12), C(62)-B-Br 106.94(13), C(51)-B-C(2) 115.38(16), C(62)-B-C(2) 116.19(15), Br-B-C(2) 110.75(12), B-C(51)-B-C(2) 121.83(15); C(1)-C(2)-B-Br torsion angle -6.7(2).

Several attempts were made to eliminate “HBr” from **17** to form the alkenyl-substituted borafluorene **15**. These included treatment of **17** with the bases IPrCH₂, IPr, benzyl potassium, 2,2,6,6-tetramethylpiperidine (TMP, along with its lithium salt), ⁱPr₂NEt, potassium phthalimide and potassium *tert*-butoxide in either THF or toluene at room temperature or under reflux for up to 24 hours. In all cases except with IPr, no reactivity was observed and only **17** was found to be present in the crude reaction mixtures. When IPr was combined with BrBFl•IPrCH₂ (**17**), it was discovered that IPr had exchanged with IPrCH₂ resulting in the formation of BrBFl•IPr (**2**) and free IPrCH₂ (Scheme 2.2.20). It was not until K[N(SiMe₃)₂] was used as a potential Brønsted base that any new products were observed (Scheme 2.2.21a). However when **17** was combined with K[N(SiMe₃)₂], free IPrCH₂ was observed in the crude reaction mixture (by ¹H NMR) in addition to a new product. A direct reaction between K[N(SiMe₃)₂] and the bromoborafluorene **1** (Scheme 2.2.21b) gave a similar product, which was shown by ¹H, ¹³C and ¹¹B{¹H} NMR spectroscopy to be the amino-substituted borafluorene ((Me₃Si)₂NBFl) **18** (Scheme 2.2.21b). At this point it was determined that the IPrCH₂ interaction with borafluorene in **17** was not strong (much weaker than the IPr interaction in **2**) and this donor could be displaced readily by exogenous nucleophiles. In addition, the presence of a π-donating -N(SiMe₃)₂ group at boron in **18** reduces the electrophilicity (and Lewis acidity) of boron, preventing coordination of IPrCH₂ from transpiring. The results suggest that the design of a different synthetic approach to **15** would be necessary. One potential avenue for future exploration would be to use alkali metals (specifically

Li, Na or K) to attempt to eliminate HBr from **17** to give hydrogen and alkali bromide salts as byproducts. As mentioned, **15** may possess interesting photophysical properties (i.e., luminescence), and might support small molecule activation chemistry, such as the heterolytic cleavage of H₂ similar to frustrated Lewis pair chemistry involving amines and boranes.⁴⁵



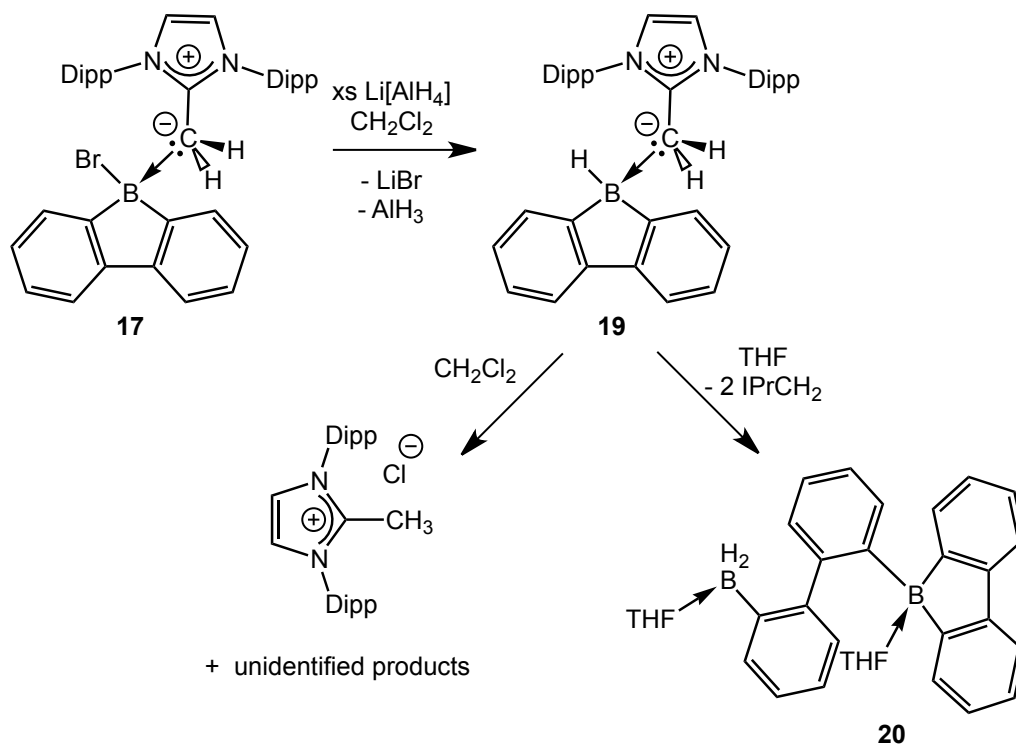
Scheme 2.2.20. Attempted removal of HBr from **17** to form **15** using IPr, which resulted in the exchange of IPr with IPrCH₂ forming **2**.



Scheme 2.2.21. a) Attempted synthesis of **15** using $\text{K}[\text{N}(\text{SiMe}_3)_2]$ as a potential base, resulting in the formation of the amino-substituted borafluorene **18**; b) formation of **18** from the direct reaction between **1** and $\text{K}[\text{N}(\text{SiMe}_3)_2]$.

Drawing inspiration from previous success with exchanging a bromide for a hydride substituent within a four-coordinate borafluorene (Scheme 2.2.8), similar reactions were conducted to determine if this would occur with compound **17** (Scheme 2.2.22). The rationale behind this was to investigate if the elimination of H_2 from an IPrCH_2 adduct of borafluorene, $\text{HBF1} \cdot \text{IPrCH}_2$ (**19**), could occur under catalytic conditions as a hydridic hydrogen on boron ($\text{B-H}^{\delta-}$) would now be

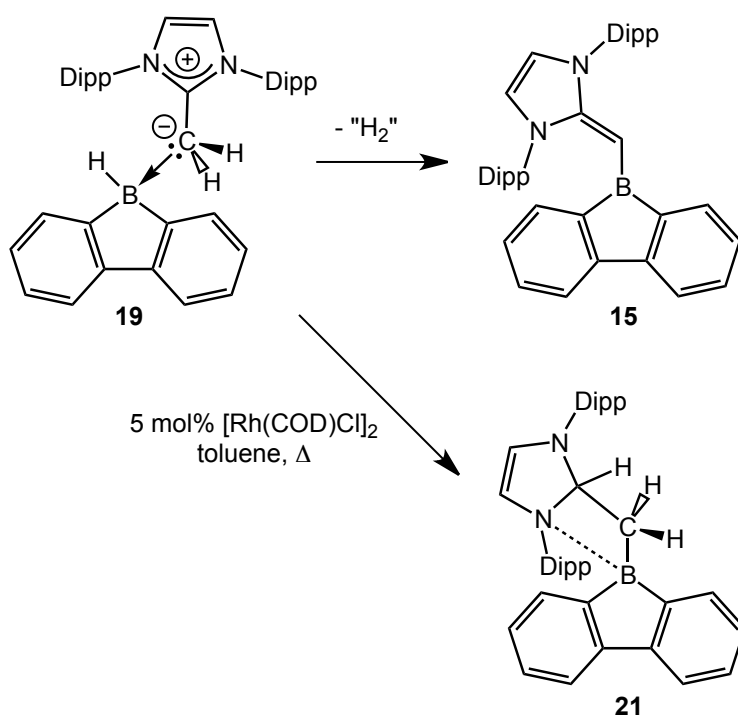
in close proximity to an acidic hydrogen on carbon ($\text{C-H}^{\delta+}$). The hydride-substituted borafluorene **19** was successfully synthesized using an almost identical procedure as used to prepare compound **8** (Scheme 2.2.8). That is, upon stirring a mixture of **17** and $\text{Li}[\text{AlH}_4]$ in CH_2Cl_2 for three days the boron hydride adduct **19** was isolated in a yield of 86 % as a colorless solid. Proton-coupled ^{11}B NMR spectroscopy strongly indicated that a hydrogen atom was now bound to the borafluorene boron as a doublet resonance was present ($\delta = -15.1$; $^1J_{\text{BH}} = 82$ Hz). Attempts to grow crystals suitable for X-ray analysis from a mixture of CH_2Cl_2 and hexanes resulted in obtaining the structure of $[\text{IPrMe}]\text{Cl}$. To verify if H/Cl exchange was transpiring between **19** and CH_2Cl_2 , a CH_2Cl_2 solution of **19** was stirred for three days in the absence of $\text{Li}[\text{AlH}_4]$. Analysis of this product showed that the $[\text{IPrMe}]\text{Cl}$ salt was present, along with several unidentified boron-containing compounds, and that **19** was not stable in CH_2Cl_2 for extended periods of time in the absence of $\text{Li}[\text{AlH}_4]$; approximately 70 % conversion to $[\text{IPrMe}]\text{Cl}$ occurs within 72 hours in CH_2Cl_2 (Scheme 2.2.22). Furthermore, it was determined that upon stirring **19** in THF for 72 hours, approximately 70 % conversion of **19** to free IPrCH_2 and a new boron-containing compound was noted (Scheme 2.2.22). The new boron-containing compound showed two ^{11}B NMR resonances at -19.1 and -7.2 ppm (as a triplet and singlet resonances, respectively) which may have been a disproportionation product (**20**) involving the ring opening of borafluorene, similar to that noted by Hübner and coworkers.⁴⁶



Scheme 2.2.22. Bromide/hydride exchange forming the hydride-substituted borafluorene **19**. Included are the decomposition reactions of **19** in CH_2Cl_2 and THF along with potential decomposition products.

The successful synthesis of **19** enabled the exploration of the potential elimination of H_2 to form **15** (Scheme 2.2.23). Efforts focused around the use of 5 mol% of $[\text{Rh}(\text{COD})\text{Cl}]_2$ (COD = 1,5-cyclooctadiene) in toluene as a potential dehydrogenative coupling catalyst as this species has been shown to be an effective pre-catalyst for the removal of H_2 from amine-boranes ($\text{R}_2\text{NH}\cdot\text{BH}_3$).⁴⁷ However, after several trials at room temperature and at reflux for up to three days, **15** was not observed although a new product from the reaction at reflux was observed by ^1H and ^{11}B NMR. According to the ^1H NMR spectrum of the new product, it appeared the boron was still most likely four-coordinate, as shown by a

single resonance at 0.2 ppm that did not exhibit any further coupling to hydrogen. The potential product of this reaction (**21**) may have been formed as the result of a boron-to-carbon hydride transfer (Scheme 2.2.23) and may involve a B-N(Dipp) interaction; related chemistry is known to occur in the adduct $\text{IPr}\cdot\text{BH}_2\text{NHDipp}$.^{20,25,48,49} As one final effort to form **15**, 3,3-dimethyl-1-butene was added to potentially react with any H_2 that may be generated during the reaction. However, all trials with 3,3-dimethyl-1-butene yielded similar results to those without.



Scheme 2.2.23. Attempted removal of H_2 from **19** and the potential product of a B-C hydride transfer upon stirring **19** in refluxing toluene in the presence of $[\text{Rh}(\text{COD})\text{Cl}]_2$; COD = 1,5-cyclooctadiene.

2.2.2 Photophysical Properties of the Neutral 9-Bromo-9-borafluorene adducts BrBFl•PPh₃ (**10**), [(DMAP)₂BFl]Br (**12**) and BrBFl•IPrCH₂ (**17**)

As borafluorene derived species featuring three-coordinate boron will tend to lose their fluorescent characteristics upon complexation with incoming Lewis bases or nucleophiles,⁶ CDCl₃ solutions of the adducts BrBFl•PPh₃ (**10**), [(DMAP)₂BFl]Br (**12**) and BrBFl•IPrCH₂ (**17**) were initially exposed to UV radiation by means of a hand-held UV lamp as a quick test to determine if a Lewis base had been incorporated. However, in all cases the clear and colorless solutions of **10**, **12**, and **17** appeared to fluoresce bright blue upon irradiation, which was initially counterintuitive as quenching of the fluorescence was expected and, thus, prompted further investigation. Figures 2.2.9-2.2.11 show the UV/Vis absorbance and fluorescence excitation and emission spectra for **10**, **12**, and **17**, respectively. The photophysical data for each luminescent adduct are tabulated in Table 2.2.1.

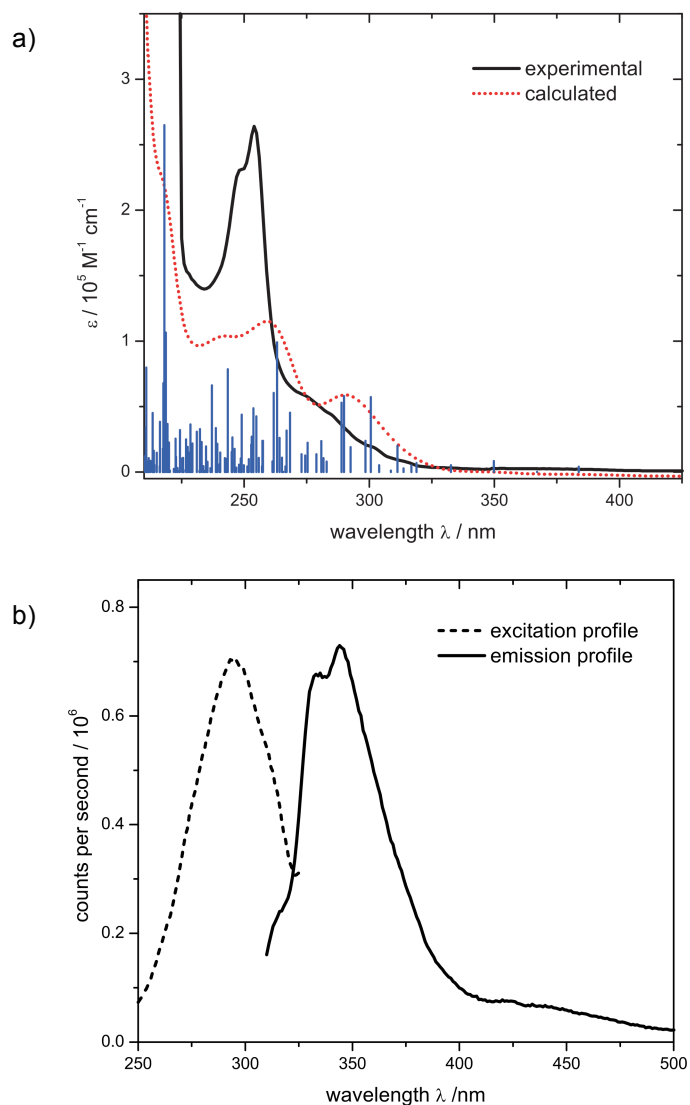


Figure 2.2.9. Photophysical spectra for BrBF₄•PPh₃ (**10**) in CH₂Cl₂. a) UV/Vis absorbance spectrum (solid line) shown with calculated (TD-DFT) spectrum (dotted line). The calculated line spectrum of the oscillator strengths for the various transitions present is shown; b) Fluorescence excitation (dashed line) and emission spectra (solid line).

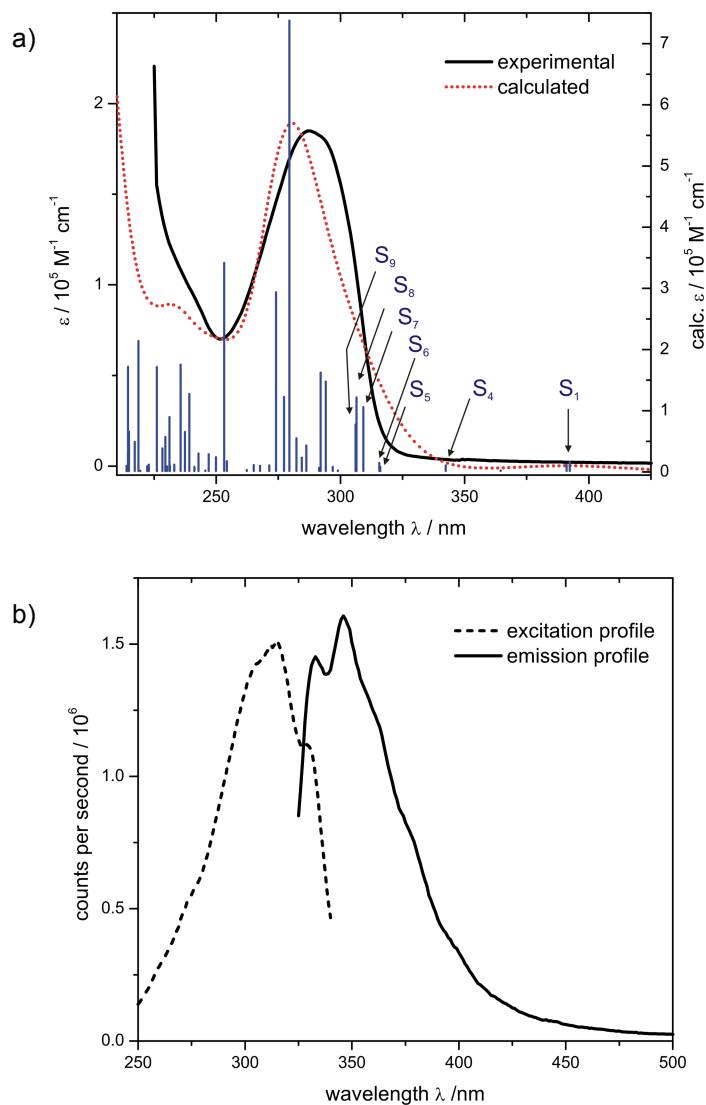


Figure 2.2.10. Photophysical spectra for [(DMAP)₂BFI]Br (**12**) in CH₂Cl₂. a) UV/Vis absorbance spectrum (solid line) shown with calculated (TD-DFT) spectrum (dotted line). The calculated line spectrum of the oscillator strengths for the various transitions present is shown. Selected electronic transitions are denoted by S_n . A difference of a factor of 3 between ϵ_{exp} and ϵ_{calc} is observed; b) Fluorescence excitation (dashed line) and emission spectra (solid line).

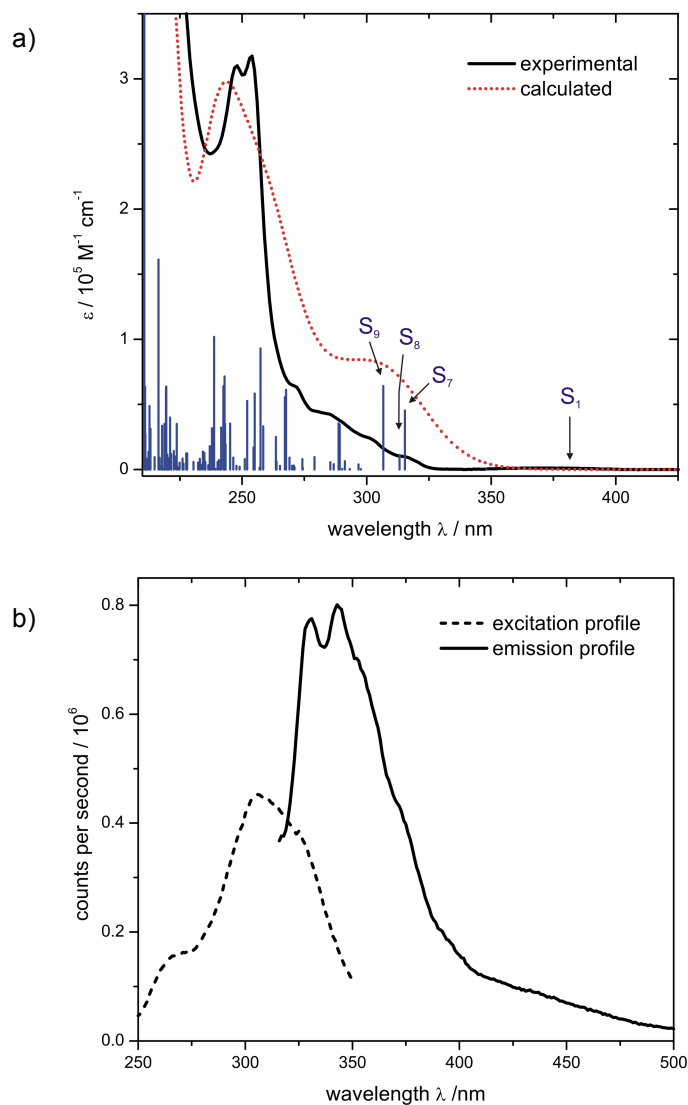


Figure 2.2.11. Photophysical spectra for BrBF1•IPrCH₂ (**17**) in CH₂Cl₂. a) UV/Vis absorbance spectrum (solid line) shown with calculated (TD-DFT) spectrum (dotted line). The calculated line spectrum of the oscillator strengths for the various transitions present is shown. Selected electronic transitions are denoted by S_n; b) Fluorescence excitation (dashed line) and emission spectra (solid line).

	BrBFl•PPh₃ (10)	[(DMAP)₂BFl]Br (12)	BrBFl•IPrCH₂ (17)
λ_{max} (nm)	248, 254	287	248, 254
ϵ ($\times 10^4$ L mol ⁻¹ cm ⁻¹)	2.30, 2.64	1.85	2.84, 2.91
λ_{ex} (nm)	285	315	306
λ_{em} (nm)	334, 344	332, 346	329, 342
Φ	0.51	0.42	0.87

Table 2.2.1. Photophysical data summary for **10**, **12** and **17**. Quantum yields (Φ) were determined relative to naphthalene in cyclohexane.⁵⁰

In all cases, the UV/Vis absorbance fell between 240 and 290 nm, well within the UV region, with only minor variations in the λ_{max} value upon changing the Lewis base species coordinated to borafluorene along with a spectral tail/shoulder occurring at longer wavelengths. This accounts for the colorless nature of the isolated compounds. The molar absorptivity coefficients were found to increase with respect to the Lewis base, in the order DMAP < PPh₃ < IPrCH₂. For compounds **10** and **17**, the presence of several very weak absorbances can be seen in the region from 270 to 320 nm. The absorbance of **12** was broad and extended over the same region. These compounds possessed two primary fluorescence emission peaks at ca. 330 and 345 nm (see Table 2.2.1). While these peaks are within the UV region, and thus would not be expected to contribute to visual luminescence, these compounds visually appeared bright blue. A closer examination of the emission spectra for these compounds shows there is significant tailing into the violet/blue region, which explains the observed blue

color. The quantum yields (measured relative to naphthalene in cyclohexane) exhibit a similar trend to that seen with the molar absorptivity and were found to be 0.42, 0.51 and 0.87 for compounds **12**, **10** and **17**, respectively. The quantum yields were in agreement with other luminescent four-coordinate BODIPY derivatives previously reported, typically range from 0.30 to > 0.90 (see Fig. 2.2.12 for representative examples).^{51,52} However, these compounds represent the first examples of fluorescent Lewis base-boratrafluorene adducts. As each complex contains reactive boron-bromine bonds, therefore functionalization to give new substituted boratrafluorenes with potentially tunable luminescence should be possible.

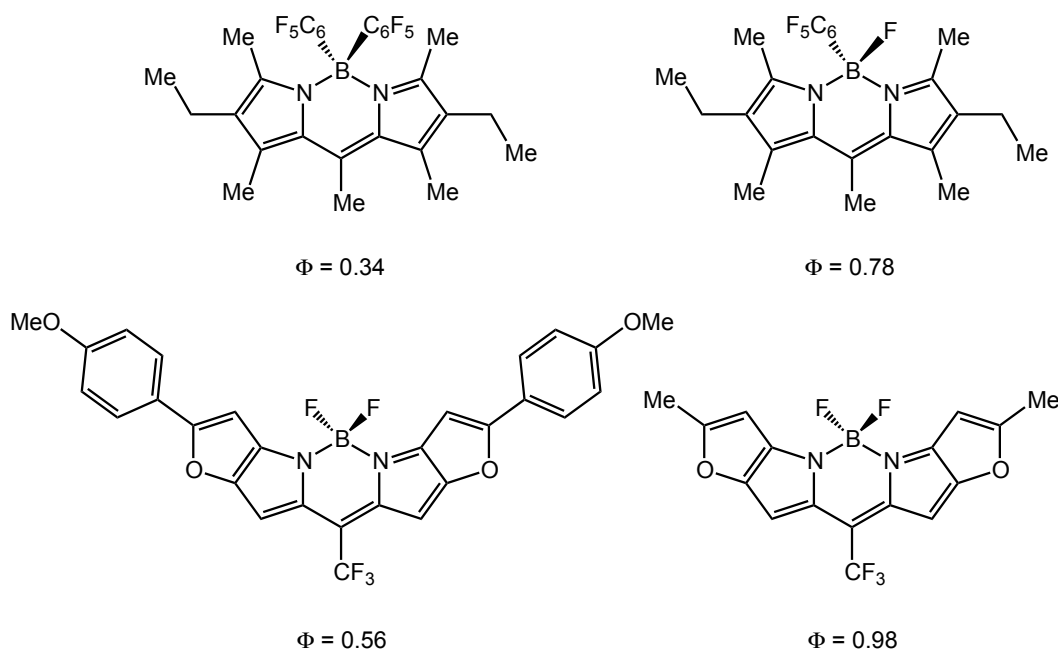


Figure 2.2.12. Representative examples of luminescent four-coordinate organoborane compounds with their quantum yields listed.

In a typical three-coordinate borafluorene system, such as those shown by Yamaguchi, *et al.*,⁶ there exists a large degree of $p\text{-}\pi^*$ conjugation between the vacant p -orbital of boron and the π -conjugation of the ancillary aryl moiety which results in an extension of the π -conjugation throughout the fused ring system.⁵³ In these cases, the HOMO is delocalized over the entirety of the borafluorene unit through the $p\text{-}\pi$ system and the LUMO is delocalized through the $p\text{-}\pi^*$ system, both factors allow for fluorescence to take place. Upon bonding with an incoming donor species (i.e., F^- or CN^-) the delocalization of the LUMO over the $p\text{-}\pi^*$ system is disrupted and the fluorescence is quenched. However, this model does not help to explain the observed fluorescence in **10**, **12** and **17**, as the four-coordinate borafluorenes would be expected not to exhibit fluorescence.

To help explain the fluorescence observed, several fluorescent BODIPY-derived systems (see Fig. 2.2.13 for a representation of the parent BODIPY) were analyzed in an effort to form a more complete picture of how the fluorescence of **10**, **12** and **17** is able to occur.^{51,52} In all instances, the conclusion drawn is quite similar: the fluorescence spectra typically show one strongly resolved emission peak that corresponds to the HOMO \rightarrow LUMO transition and a less intense peak found to correspond to the HOMO \rightarrow LUMO+1 transition, both of which represent $\pi\text{-}\pi^*$ transitions within the fused tricycle 5-6-5 atom array with no direct contribution from the boron center. In general, the luminescent properties in BODIPY frameworks are highly tunable and vary with parameters such as the introduction of bulky aryl moieties at boron, by restricting the ability of groups to rotate allowing for aggregate induced emission and extension of the π -conjugation

through the incorporation of additional fused aryl moieties at the pyrrolidine rings.⁵⁴ As a Lewis base complexed borafluorene might exhibit π conjugation akin to that of BODIPY, this served as an initial hypothesis to explain how the luminescence in these borafluorene adducts may be occurring.

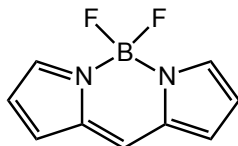


Figure 2.2.13. Unsubstituted parent BODIPY.

To confirm this hypothesis, theoretical studies (at the B3LYP/6-31G(d,p) level of theory), including TD-DFT calculations for the predicted UV/Vis spectra, were conducted to further probe the nature of the luminescence seen in compounds **10**, **12** and **17**. The calculated HOMO and LUMO molecular orbital plots are shown in Figure 2.2.12. The results of the theoretical studies for each of these three compounds were found to be consistent with each other. In general, the HOMO was found to be entirely located at the borafluorene unit and the LUMO were located on the Lewis bases. This was initially a good indication that a charge-transfer type transition may be occurring and that the HOMO/LUMO transition may have indeed been responsible for the observed fluorescence. However, upon analysis of the calculated UV/Vis spectra, this argument began to unravel. The HOMO/LUMO transition was found, in all cases, to have an oscillator frequency of 0 (see Tables 2.2.2 to 2.2.4 for a summary of selected calculated electronic transitions) and this did not seem to be participating

whatsoever in the UV/Vis absorbance. Further inspection of the calculated line spectrum revealed that the transitions responsible for the strong absorbance bands were π - π^* in nature and centered exclusively on the Lewis base present with no participation of the borafluorene unit. Upon a closer inspection of the excitation profiles (Figures 2.2.9-2.2.11) it was noted that the region involved in the excitation was found at longer wavelengths than the strong λ_{max} bands. Moreover, the regions of the UV/Vis spectra that overlapped with those involved in the excitation of **10**, **12** and **17** revealed several weak absorbance bands present (note that for **12**, the absorbance peak is quite broad and extends over the region which is active upon excitation) and, upon analyzing the line spectrum, were shown to belong to several potential transitions. Figure 2.2.14c shows selected transitions belonging to this region for **17** and indicate that the transitions involved in the fluorescence may occur between the borafluorene π system and π^* orbitals primarily situated on the Lewis base. Although not shown, similar results were found for compounds **10** and **12**, and that for **10**, **12** and **17** at least one of the calculated transitions involved electron excitation from the borafluorene π system to the borafluorene π^* system, or a π^* orbital delocalized over the entire complex. Furthermore, examination of the emission spectra indicates that multiple electronic transitions are likely responsible for the observed emission as evidenced by the two high intensity emission bands in the UV region and the significant degree of tailing into the visible spectral region. The results of these theoretical studies suggest that the nature of the fluorescence is quite complicated and, to obtain a more complete understanding, additional theoretical studies must

be carried out. However, with the data obtained, the suggestion can be made that upon altering the Lewis base may yield a facile method for tuning the emission characteristics of the newly formed adducts.

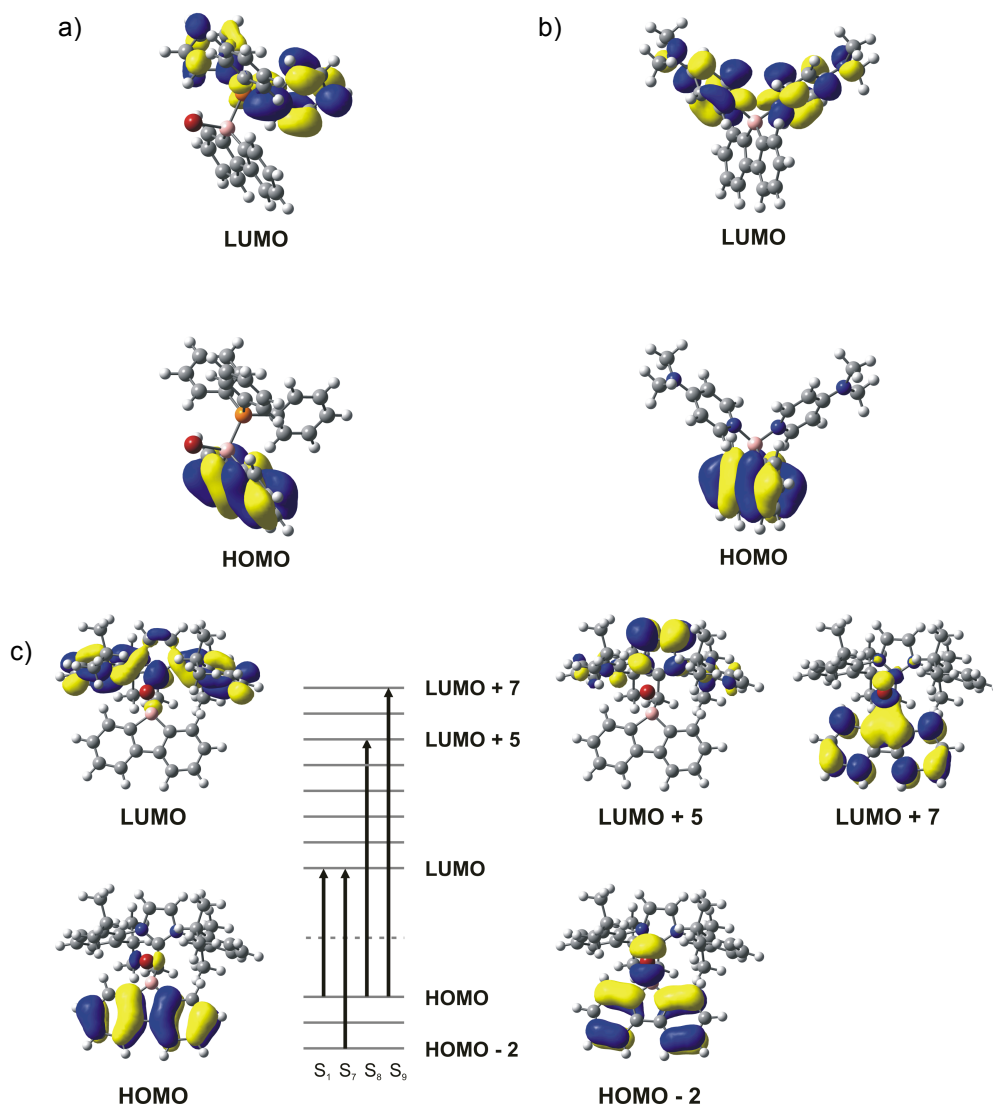


Figure 2.2.14. Calculated HOMO/LUMO plots for: a) BrBF₄•PPh₃ (**10**); b) [(DMAP)₂BF₄]Br (**12**); c) BrBF₄•IPrCH₂ (**17**). Additional molecular orbital plots are shown for **17** along with a relative energy diagram showing the HOMO/LUMO electronic transition and selected electronic transitions potentially involved in fluorescence. Similar transitions were found for compounds **10** and **12**.

BrBFl•PPh₃ (10)			
Electronic Transition	Wavelength, λ (nm)	Oscillator Strength, f	Nature of $\pi \rightarrow \pi^*$/Charge Transfer Transition
S ₁	383.69	0.0042	BFl \rightarrow PPh ₃
S ₂	367.01	0.0002	BFl \rightarrow PPh ₃
S ₃	349.83	0.0084	BFl \rightarrow PPh ₃
S ₄	332.63	0.0052	BFl \rightarrow PPh ₃
S ₅	318.86	0.0069	BFl \rightarrow mol.
S ₆	316.86	0.0051	BFl \rightarrow PPh ₃
S ₇	313.72	0.0029	BFl \rightarrow PPh ₃
S ₈	311.21	0.0202	BFl \rightarrow PPh ₃
S ₉	308.65	0.0012	BFl \rightarrow PPh ₃
S ₁₀	303.94	0.0052	BFl \rightarrow mol.
S ₁₁	300.62	0.0574	BFl \rightarrow PPh ₃
S ₁₂	298.45	0.024	BFl \rightarrow PPh ₃

Table 2.2.2. Calculated electronic transitions showing the first 12 excited states, corresponding oscillator strengths and the nature of the π - π^* /charge transfer for **10**. For the nature of the transitions BFl denotes that the molecular orbital is located on the boraflorene unit, PPh₃ denotes that the molecular orbital is located at the PPh₃ unit, and “mol.” denotes a delocalization of the molecular orbital over the whole molecule.

[(DMAP) ₂ BFl]Br (12)			
Electronic Transition	Wavelength, λ (nm)	Oscillator Strength, f	Nature of $\pi \rightarrow \pi^*$ /Charge Transfer Transition
S ₁	391.05	0.0076	BFl \rightarrow DMAP
S ₂	392.36	0.011	BFl \rightarrow DMAP
S ₃	364.52	0.0004	BFl \rightarrow DMAP
S ₄	342.38	0.0067	BFl \rightarrow DMAP
S ₅	316.07	0.0048	BFl \rightarrow DMAP
S ₆	315.67	0.0097	BFl \rightarrow DMAP
S ₇	309.19	0.0766	mol. \rightarrow DMAP
S ₈	306.45	0.0882	mol. \rightarrow DMAP
S ₉	306.06	0.0556	BFl \rightarrow BFl
S ₁₀	298.99	0.0005	BFl \rightarrow DMAP

Table 2.2.3. Calculated electronic transitions showing the first 10 excited states, corresponding oscillator strengths and the nature of the π - π^* /charge transfer for **12**. For the nature of the transitions BFl denotes that the molecular orbital is located on the boraflorene unit, DMAP denotes that the molecular orbital is located at both DMAP units, and “mol.” denotes a delocalization of the molecular orbital over the whole molecule.

BrBFl•IPrCH₂ (17)			
Electronic Transition	Wavelength, λ (nm)	Oscillator Strength, f	Nature of $\pi \rightarrow \pi^*$/Charge Transfer Transition
S₁	381.58	0	BFl \rightarrow IPrCH ₂
S₂	353.37	0	BFl \rightarrow IPrCH ₂
S₃	348.02	0.0002	BFl \rightarrow IPrCH ₂
S₄	345.99	0.0001	BFl \rightarrow IPrCH ₂
S₅	343.29	0.0001	BFl \rightarrow IPrCH ₂
S₆	318.06	0.0001	BFl \rightarrow IPrCH ₂
S₇	315.39	0.0454	BFl \rightarrow IPrCH ₂
S₈	313.25	0.0112	BFl \rightarrow IPrCH ₂
S₉	306.7	0.0643	BFl \rightarrow BFl
S₁₀	297.66	0.0005	BFl \rightarrow IPrCH ₂

Table 2.2.4. Calculated electronic transitions showing the first 10 excited states, corresponding oscillator strengths and the nature of the π - π^* /charge transfer for **17**. For the nature of the transitions BFl denotes that the molecular orbital is located on the boraflorene unit and IPrCH₂ denotes that the molecular orbital is located at IPrCH₂ unit. For S₇ and S₉, the bromine atom at the boron center is contributing to the MOs involved.

2.3 Conclusions

Although the proposed “masking” and “unmasking” of boraflorene did not proceed as expected, most likely due to the high binding affinity of the investigated Lewis bases for boraflorene, a series of novel boraflorene Lewis

base adducts were prepared and preliminary reactivity studies with these species were undertaken. Unlike IPr (in compound **2**) and PPh₃ (in compound **10**), evidence was found that a single DMAP moiety from **12** could be removed upon the addition of B(C₆F₅)₃. This implies that, upon investigation of additional Lewis bases, an ideal system can be developed to achieve the desired “masking” and “unmasking” of borafluorene, and that future investigations should be centered around the use of pyridine or pyridine derivatives (i.e. lutidine, picoline, etc.). In all cases, it was found that the bromide bound to the boron center could be exchanged for different anions (such as OTf in **9**), a hydride (as in **8** and **19**) or functionalized with an allyl group (as in **13** and **14**). This may provide an avenue through which borafluorene can ultimately be functionalized or installed into unique and potentially useful compounds such as anion and nucleophile detectors.

In addition, a series of luminescent borafluorene Lewis base adducts (**10**, **12**, and **17**) were prepared and characterized. The fluorescent characteristics of these adducts was found, through theoretical studies, to be intimately entwined with the nature of the Lewis base coordinated to the boron center of the borafluorene unit and represent a new class of luminescent tetravalent organoboranes. Furthermore, the nature of the luminescence was found to be quite complex and potentially involves several excitation and emission pathways. Additional theoretical studies will be carried out in order to further probe the nature of the fluorescence within these adducts. Moreover, the implication of these findings suggest that further investigations into the use of a wider range of Lewis bases to form adducts with borafluorene along with functionalization at the

bromide site on boron may lead to a new class of highly tunable luminescent species that could be adapted into an intriguing class of emissive materials. Specifically, the findings suggest that these emissive four-coordinate boron species and further derivatives could find use as blue, or potentially white, emitters. Furthermore, species of this nature could be adapted to be used as organic light-emitting diodes (OLEDs), however this application may be limited by their current air and moisture sensitivity. These sensitivities could be overcome through the use of bulky Lewis bases serving to provide additional protection coupled with the presence of alkyl or aryl groups at boron, thus preventing any unwanted hydrolysis or oxidation chemistry from transpiring. Future work will involve the investigation of a series of phosphine and pyridine based Lewis bases and possibly the use of nucleophilic ylides (e.g., $R_3P=CR'_2$) in order to develop novel emissive compounds.

2.4 Experimental Section

2.4.1 Experimental Methods and Procedures

General. All reactions were performed using standard Schlenk line techniques under an atmosphere of nitrogen or in an inert atmosphere glove box (MBraun Inc.). Solvents were dried using a Grubbs-type solvent purification system⁵⁵ manufactured by Innovative Technology Inc., degassed (freeze-pump-thaw method) and stored over molecular sieves under a nitrogen atmosphere prior to use. Boron tribromide (1.0 M solution in hexanes), allylmagnesium bromide (1.0 M solution in diethyl ether), *n*-butyllithium (*n*BuLi, 2.5 M solution in hexanes),

N,N-dimethylaminopyridine (DMAP), Li[AlH₄], K[N(SiMe₃)₂], HCl (5.0 M solution in Et₂O), MeI, MeOTf, Ag[OTf], and triphenylphosphine (PPh₃) were obtained from Aldrich and used as received. 1,2-Dibromobenzene was purchased from Matrix Scientific and used as received. Hydrogen bromide gas was purchased from Matheson Gas Products Canada and used as received. [Rh(COD)Cl]₂ was purchased from Strem Chemicals, Inc. and used as received. 1,3-Bis-(2,6-diisopropylphenyl)-imidazol-2-ylidene (IPr),²⁶ 1,3-bis-(2,6-diisopropylphenyl)-2-methyleneimidazoline (IPrCH₂)³⁹ and 2,2'-dibromobiphenyl¹⁶ were prepared following literature procedures. ¹¹B{¹H}, ¹¹B, ¹⁹F{¹H} and ³¹P NMR spectra were recorded on a Varian iNova-500 spectrometer referenced externally to F₃B•OEt₂ (¹¹B), CFCl₃ (¹⁹F{¹H}), Me₃SiCl (²⁹Si{¹H}) and 85% H₃PO₄ (³¹P), respectively. ¹H, ¹H{¹¹B} ¹³C{¹H} and ²⁹Si{¹H} NMR spectra were recorded on a Varian VNMRs-500 spectrometer and referenced externally to SiMe₄. Elemental analyses were performed by the Analytical and Instrumentation Laboratory at the University of Alberta. Mass spectra were obtained on an Agilent 6220 spectrometer. Melting points were measured in sealed glass capillary under nitrogen using a Meltemp melting point apparatus and are uncorrected. UV/Vis spectra were obtained from a Cary 400 UV/Vis spectrometer. Fluorescence spectra were obtained from a Photon Technology International (PTI) MP1 Fluorescence System. All quantum yields were measured relative to naphthalene in cyclohexane assuming a quantum yield (Φ) of 0.23.⁵⁰

X-ray Crystallography. Crystals of suitable quality for X-ray crystallography were removed from a vial in a glove box and coated immediately with a thin layer of hydrocarbon oil (Paratone-N). A suitable crystal was picked and mounted on a glass fiber and then quickly placed in a low temperature stream of nitrogen on the X-ray diffractometer.⁵⁶ All data were collected using a Bruker APEX II CCD detector/D8 diffractometer using with Mo K α radiation or Cu K α radiation, with crystals cooled to -100 °C. The data were corrected for absorption⁵⁷ through Gaussian integration (BrBF₄•IPr (**2**), [IPrMe]Br (**16**), BrBF₄•IPrCH₂ (**17**)) or multi-scan SADABS⁵⁸ (HBF₄•IPr (**8**)) from the indexing of the crystal faces. Structures were solved using the direct methods program SHELXD ([IPrMe]Br (**13**)), SHELXS-97 (HBF₄•IPr (**8**), BrBF₄•IPrCH₂ (**17**)), intrinsic phasing SHELXT⁵⁹ ([DMAP]₂BFI]Br (**12**)) or Patterson/structure expansion facilities within the DIRDIF-2008⁶⁰ program suite (BrBF₄•IPr (**2**)), and refined using SHELXS-97.⁵⁹ Hydrogen atoms were assigned positions based on sp² or sp³ hybridization geometries of their attached carbon atoms, and were given thermal parameters 20% greater than those of their parent atoms.

Special Refinement Conditions. For the crystal structure of [(DMAP)₂BFI]Br (**12**), attempts to refine peaks of residual electron density as disordered or partial-occupancy solvent tetrahydrofuran oxygen or carbon atoms were unsuccessful. The data were corrected for disordered electron density through use of the SQUEEZE procedure⁶¹ as implemented in *PLATON*.⁶² A total solvent-accessible void volume of 2100.4 Å³ with a total electron count of 448 (consistent with 12

molecules of solvent tetrahydrofuran, or one-half THF molecule per formula unit of the 5,5-bis(4-dimethylaminopyridine)-5*H*-dibenzo[*b,d*]borol-5-ylum ion) was found in the unit cell. Restraints were applied to distances involving the disordered 4-dimethylaminopyridine group: $d(\text{N3C}-\text{C41C}) = d(\text{N3C}-\text{C45C}) = d(\text{N3D}-\text{C41D}) = d(\text{N3D}-\text{C45D}) = 1.36(1) \text{ \AA}$; $d(\text{N3C}-\text{B1C}) = d(\text{N3D}-\text{B1C}) = 1.59(1) \text{ \AA}$; $d(\text{N4C}-\text{C46C}) = d(\text{N4C}-\text{C47C}) = d(\text{N4D}-\text{C46D}) = d(\text{N4D}-\text{C47D}) = 1.45(1) \text{ \AA}$; $d(\text{C41C}-\text{C42C}) = d(\text{C44C}-\text{C45C}) = d(\text{C41D}-\text{C42D}) = d(\text{C44D}-\text{C45D}) = 1.36(1) \text{ \AA}$; $d(\text{C42C}-\text{C43C}) = d(\text{C43C}-\text{C44C}) = d(\text{C42D}-\text{C43D}) = d(\text{C43D}-\text{C44D}) = 1.41(1) \text{ \AA}$. Distances within the disordered solvent CH_2Cl_2 molecule were restrained during refinement: $d(\text{C11S}-\text{C1S}) = d(\text{C12S}-\text{C1S}) = d(\text{C13S}-\text{C2S}) = d(\text{C14S}-\text{C2S}) = 1.75(1) \text{ \AA}$; $d(\text{C11S}\cdots\text{C12S}) = d(\text{C13S}\cdots\text{C14S}) = 2.85(1) \text{ \AA}$. For the crystal structure of [IPrMe]Br (**16**), the C–Cl distances (C2S–C13S, C2S–C14S, C3S–C15S, C3S–C16S) within the disordered dichloromethane solvent molecule were restrained to be the same.

Theoretical Studies.

All calculations were carried out using the Gaussian 09 software package at the B3LYP/6-31G(d,p) level of theory.⁶³ Implicit solvent effects were taken into account by using the integral equation formalism version of the polarizable continuum model (IEF-PCM) for dichloromethane.⁶⁴ If available, crystal structures were used as input geometries. Default convergence criteria were chosen for the geometry optimizations. The obtained optimized were confirmed to be a local energy minimum structure by performing a vibrational frequency

analysis. For the calculation of the vertical excitation spectra using TD-DFT, non-equilibrium state-specific solvation of the excited states were accounted for. The reported transition wavelengths were shifted by 25 nm to higher wavelengths compared to the calculated values. The electronic absorbance spectra were then obtained by assigning a uniform Gaussian band shape of 0.3 eV half-width at 1/e height. The molecular orbitals were extracted from the output using GaussView 5 and assuming an isovalue of 0.02.

Synthetic Procedures.

Synthesis of 9-bromo-9-borafluorene (BrBFl, 1).¹⁵ A solution of 2,2'-dibromobiphenyl (3.140 g, 10.06 mmol) in toluene (50 mL) was prepared and sparged with N₂. The solution was then cooled to -78 °C and ⁿBuLi (14.0 mL, 22.4 mmol, 1.6 M solution in hexanes) was added dropwise. The resulting mixture was allowed to slowly warm to room temperature and stir for 48 hours. The mixture was then cooled to -78 °C before BBr₃ (11.0 mL, 11.0 mmol, 1.0 M solution in hexanes) was added dropwise. The resulting mixture was allowed to slowly warm to room temperature and stir for 12 hours. The supernatant was decanted and the remaining precipitate was extracted with 3 x 50 mL of toluene and the toluene extracts were combined with the initial supernatant before the volatile components were then removed *in vacuo*. The crude product was recrystallized from hexanes at -35 °C to afford **1** as yellow needles (2.208 g, 90 %). ¹H NMR (CDCl₃, 500 MHz): δ 7.56 (d, ³J_{HH} = 7.2 Hz, 2H, ArH), 7.37 (td, ³J_{HH} = 7.6 Hz, ⁴J_{HH} = 1.2 Hz, 2H, ArH), 7.33 (d, ³J_{HH} = 7.0 Hz, 2H, ArH), 7.15

(td, $^3J_{\text{HH}} = 7.0$ Hz, $^4J_{\text{HH}} = 1.2$ Hz, 2H, ArH). $^{13}\text{C}\{^1\text{H}\}$ NMR (CDCl_3 , 125 MHz): δ 152.9 (ArC), 135.5 (ArC), 133.4 (ArC), 128.7 (ArC), 119.7 (ArC). $^{11}\text{B}\{^1\text{H}\}$ NMR (CDCl_3 , 160 MHz): δ 65.8 (s).²¹

Synthesis of BrBFI•IPr (2). To a mixture of **1** (503.9 mg, 2.074 mmol) and IPr (804.4 mg, 2.070 mmol) was added 20 mL of toluene. The mixture was allowed to stir for 12 hours during which time a colorless precipitate formed. The supernatant was decanted and the remaining solid was washed with 3 x 20 mL of toluene and the insoluble solid was dried under vacuum to afford **2** as a white powder (1.218 g, 93 %). Crystals suitable X-ray analysis were grown from a 50/50 mixture of dichloromethane and hexanes at -35 °C. ^1H NMR (C_6D_6 , 500 MHz): δ 7.43 (d, $^3J_{\text{HH}} = 7.6$ Hz, 2H, ArH), 7.25 (t, $^3J_{\text{HH}} = 7.6$ Hz, 2H, ArH), 7.01 (d, $^3J_{\text{HH}} = 7.6$ Hz, 4H, ArH), 6.97 (td, $^3J_{\text{HH}} = 7.6$ Hz, $^4J_{\text{HH}} = 1.2$ Hz, 2H, ArH), 6.57 (td, $^3J_{\text{HH}} = 7.6$ Hz, $^4J_{\text{HH}} = 1.2$ Hz, 2H, ArH), 6.40 (d, $^3J_{\text{HH}} = 7.2$ Hz, 2H, ArH), 6.28 (s, 2H, -N-CH-), 2.79 (septet, $^3J_{\text{HH}} = 6.8$ Hz, 4H, CH(CH₃)₂), 1.08 (d, $^3J_{\text{HH}} = 6.4$ Hz, 12H, CH(CH₃)₂), 0.90 (d, $^3J_{\text{HH}} = 7.2$ Hz, 12H, CH(CH₃)₂). $^{13}\text{C}\{^1\text{H}\}$ NMR (C_6D_6 , 125 MHz): δ 149.7 (ArC), 146.2 (ArC), 136.1 (ArC), 134.3 (ArC), 131.1 (ArC), 129.1 (ArC), 126.5 (ArC), 125.1 (ArC), 124.8 (ArC), 118.7 (-N-CH-), 30.2 (CH(CH₃)₂), 29.3 (CH(CH₃)₂), 26.0 (CH(CH₃)₂), 22.2 (CH(CH₃)₂). $^{11}\text{B}\{^1\text{H}\}$ NMR (C_6D_6 , 160 Hz): δ -6.4 (s). HR-MS EI (positive mode, m/z): Calcd. for [M-Br]⁺: 551.35974. Found: 551.35892 ($\Delta\text{ppm} = 1.5$). Anal. calcd. for C₃₉H₄₄BBrN₂: C, 74.18; H, 7.02; N, 4.44. Found: C, 73.53; H, 7.17; N, 4.28. Mp (°C): no melting or decomposition up to 340.

Synthesis of HBF₄•IPr (8). To a mixture of **2** (102.2 mg, 0.162 mmol) and Li[AlH₄] (24.5 mg, 0.646 mmol) was added 15 mL of toluene. The resulting mixture was allowed to stir for 5 days. The mixture was then filtered through a small (ca. 1 cm) plug of silica gel. The volatile components were removed from the filtrate *in vacuo* and the remaining crude solid was washed with 5 mL of diethyl ether to yield **8** as a white solid (24.2 mg, 27 %). Crystals suitable for X-ray analysis were grown from a 50/50 mixture of dichloromethane and hexanes at -35 °C. ¹H NMR (CDCl₃, 500 MHz): δ 7.34 (d, ³J_{HH} = 6.5 Hz, 2H, ArH), 7.28 (d, ³J_{HH} = 7.5 Hz, 2H, ArH), 7.23 (d, ³J_{HH} = 6.0 Hz, 4H, ArH), 7.10 (s, 2H, -N-CH-), 7.08 (d, ³J_{HH} = 8.0 Hz, 4H, ArH), 6.94 (td, ³J_{HH} = 7.5 Hz, ⁴J_{HH} = 1.5 Hz, 2H, ArH), 6.90 (td, ³J_{HH} = 7.5 Hz, ⁴J_{HH} = 1.5 Hz, 2H, ArH), 2.81 (septet, ³J_{HH} = 7.0 Hz, 4H, CH(CH₃)₂), 1.17 (d, ³J_{HH} = 7.0 Hz, 12H, CH(CH₃)₂), 1.11 (d, ³J_{HH} = 6.5 Hz, 12H, CH(CH₃)₂). ¹³C{¹H} NMR (CDCl₃, 125 MHz): δ 149.2 (ArC), 145.2 (ArC), 134.2 (ArC), 131.4 (ArC), 130.1 (ArC), 124.9 (ArC), 124.1 (ArC), 123.5 (ArC), 118.4 (-N-CH-), 29.8 (CH(CH₃)₂), 29.0 (CH(CH₃)₂), 26.4 (CH(CH₃)₂), 22.3 (CH(CH₃)₂). ¹¹B{¹H} NMR (CDCl₃, 160 MHz): δ -19.1 (s). ¹¹B NMR (CDCl₃, 160 MHz): δ -19.1 (d, ¹J_{BH} = 84 Hz). HR-MS EI (positive mode, m/z): Calcd. for [M]⁺: 552.36755. Found: 552.36558 (Δppm = 3.6). Anal. calcd. for C₃₉H₄₅BBrN₂: C, 84.77; H, 8.21; N, 5.07. Found: C, 84.77; H, 8.30; N, 5.13. Mp (°C): 308-310.

Synthesis of [BFl•IPr]OTf (9). To a mixture of **2** (500.1 mg, 0.792 mmol) and Ag[OTf] (203.1 mg, 0.791 mmol) was added dichloromethane (15 mL). The reaction mixture was protected from light and allowed to stir for 12 hours. The resulting mixture was filtered and all volatiles were removed from the filtrate *in vacuo* to afford the crude product as a pale yellow solid. The crude product was recrystallized from 10 mL of a 50/50 mixture of dichloromethane/hexanes at -35 °C to afford **9** as a colorless solid (250.9 mg, 45 %). ¹H NMR (CDCl₃, 500 MHz): δ 7.35 (t, ³J_{HH} = 7.6 Hz, 2H, ArH), 7.27 (d, ³J_{HH} = 6.8 Hz, 2H, ArH), 7.15 (d, ³J_{HH} = 7.6 Hz, 2H, ArH), 7.11 (s, 2H, -N-CH-), 7.10 (d, ³J_{HH} = 7.6 Hz, 4H, ArH), 7.02 (td, ³J_{HH} = 7.2 Hz, ⁴J_{HH} = 1.2 Hz, 2H, ArH), 6.96 (td, ³J_{HH} = 7.2 Hz, ⁴J_{HH} = 1.2 Hz, 2H, ArH), 2.68 (septet, ³J_{HH} = 6.8 Hz, 4H, CH(CH₃)₂), 1.22 (d, ³J_{HH} = 6.8 Hz, 12H, CH(CH₃)₂), 1.09 (d, ³J_{HH} = 6.8 Hz, 12H, CH(CH₃)₂). ¹³C{¹H} NMR (CDCl₃, 125 MHz): δ 150.0 (ArC), 144.6 (ArC), 134.0 (ArC), 131.0 (ArC), 130.7 (ArC), 127.9 (ArC), 126.5 (ArC), 125.4 (ArC), 123.8 (ArC), 119.0 (-N-CH-), 29.8 (CH(CH₃)₂), 29.2 (CH(CH₃)₂), 26.6 (CH(CH₃)₂), 22.0 (CH(CH₃)₂). ¹¹B{¹H} NMR (CDCl₃, 160 MHz): δ 2.3 (s). ¹⁹F{¹H} NMR (CDCl₃, 376 MHz): δ -77.8 (s). HR-MS EI (positive mode, m/z): Calcd. for [M]⁺: 700.31177. Found: 700.31221 (Δppm = 0.6). Anal. calcd. for C₄₀H₄₄BF₃N₂O₃S: C, 68.57; H, 6.33; N, 4.00. Found: C, 68.35; H, 6.43; N, 4.03. Mp (°C): 312 (decomp.).

Synthesis of BrBFl•PPh₃ (10). To a mixture of **1** (93.1 mg, 0.383 mmol) and PPh₃ (100.0 mg, 0.381 mmol) was added 15 mL of toluene. The resulting mixture was allowed to stir for 12 hours. All volatile components were removed *in vacuo*

and the remaining solid was washed with 10 mL of hexanes and dried before the **10** was isolated as a white solid (176.7 mg, 92 %). ^1H NMR (CDCl_3 , 500 MHz): δ 7.57 (dd, $^3J_{\text{HP}} = 9.2$ Hz, $^3J_{\text{HH}} = 7.5$ Hz, 6H, ArH in PPh_3), 7.49 (td, $^3J_{\text{HH}} = 7.0$ Hz, $^4J_{\text{HH}} = 1.5$ Hz, 2H, ArH), 7.42 (d, $^3J_{\text{HH}} = 7.5$ Hz, 2H, ArH), 7.37-7.32 (m, 9H, ArH in PPh_3), 7.14 (tt, $^3J_{\text{HH}} = 7.5$ Hz, $^4J_{\text{HH}} = 1.0$ Hz, 2H, ArH), 6.99 (td, $^3J_{\text{HH}} = 7.0$ Hz, $^4J_{\text{HH}} = 1.0$ Hz, 2H, ArH). $^{13}\text{C}\{^1\text{H}\}$ NMR (CDCl_3 , 125 MHz): δ 148.8 (d, $^3J_{\text{CP}} = 7.0$ Hz, ArC), 134.2 (d, $^3J_{\text{CP}} = 8.2$ Hz, ArC), 132.2 (d, $^5J_{\text{CP}} = 1.8$ Hz, ArC), 131.8 (d, $^4J_{\text{CP}} = 2.5$ Hz, ArC), 128.6 (d, $^2J_{\text{CP}} = 10.3$ Hz, ArC), 127.8 (d, $^4J_{\text{CP}} = 2.0$ Hz, ArC), 126.5 (d, $^4J_{\text{CP}} = 2.3$ Hz, ArC), 125.4 (d, $^1J_{\text{CP}} = 59.3$ Hz, ArC), 119.4 (s, ArC). $^{11}\text{B}\{^1\text{H}\}$ NMR (CDCl_3 , 160 MHz): δ -7.4 (s). $^{31}\text{P}\{^1\text{H}\}$ NMR (CDCl_3 , 202 MHz): δ 1.8 (s). UV/Vis (in CH_2Cl_2): $\lambda_{\text{max}} = 248$ nm ($\epsilon = 2.30 \times 10^4$ L mol $^{-1}$ cm $^{-1}$), 254 nm ($\epsilon = 2.64 \times 10^4$ L mol $^{-1}$ cm $^{-1}$). Fluorescence emission (in CH_2Cl_2): $\lambda_{\text{em}} = 334, 344$ nm, fluorescence quantum yield: $\Phi = 0.51$, relative to naphthalene in cyclohexane. HR-MS EI (positive mode, m/z, %): 262.0909 (M^+ - BrBFI, 100), 184.0411 (Ph_2P^+ , 9), 183.0363 (Ph_2P^+ - H, 51), 152.0627 (Ph_2^{2+} , 9), 108.0128 (PhP^+ , 25), 91.0548 (BrB^+ , 3), 77.0389 (Ph^+ , 4). Anal. calcd. for $\text{C}_{30}\text{H}_{23}\text{BBrP}$: C, 71.32; H, 4.59. Found: C, 72.18; H, 4.81. Mp ($^\circ\text{C}$): 209-212.

Synthesis of [(DMAP) $_2$ BFI]Br (12). To a mixture of **1** (199.4 mg, 0.821 mmol) and *N,N*-dimethylaminopyridine (DMAP, 202.8 mg, 1.660 mmol) was added 15 mL of toluene. The resulting mixture was allowed to stir for 12 hours. The supernatant was decanted and the remaining solid was washed with 15 mL of toluene and dried *in vacuo* to afford **12** as a white solid (354.3 mg, 89 %).

Crystals suitable for X-ray analysis were grown from a 50/50 mixture of dichloromethane and tetrahydrofuran at -35 °C. ^1H NMR (CDCl_3 , 500 MHz): δ 8.05 (m, 4H, ArH in DMAP), 7.64 (dt, $^3J_{\text{HH}} = 7.5$ Hz, $^4J_{\text{HH}} = 0.5$ Hz, 2H, ArH), 7.49 (dt, $^3J_{\text{HH}} = 7.5$ Hz, $^4J_{\text{HH}} = 0.5$ Hz, 2H, ArH), 7.31 (td, $^3J_{\text{HH}} = 7.5$ Hz, $^4J_{\text{HH}} = 1.0$ Hz, 2H, ArH), 7.20 (td, $^3J_{\text{HH}} = 7.5$ Hz, $^4J_{\text{HH}} = 1.0$ Hz, 2H, ArH), 6.80 (m, 4H, ArH in DMAP), 3.16 (s, 12H, $\text{N}(\text{CH}_3)_2$ in DMAP). $^{13}\text{C}\{^1\text{H}\}$ NMR (CDCl_3 , 125 MHz): δ 156.3 (ArC), 149.2 (ArC), 143.4 (ArC), 130.2 (ArC), 128.9 (ArC), 128.2 (ArC), 127.5 (ArC), 125.3 (ArC), 120.0 (ArC), 40.1 ($\text{N}(\text{CH}_3)_2$). $^{11}\text{B}\{^1\text{H}\}$ NMR (CDCl_3 , 160 MHz): δ 4.6 (s). UV/Vis (in CH_2Cl_2): $\lambda_{\text{max}} = 287$ nm ($\epsilon = 1.85 \times 10^4$ $\text{L mol}^{-1} \text{cm}^{-1}$). Fluorescence (in CH_2Cl_2): $\lambda_{\text{em}} = 332, 346$ nm, fluorescence quantum yield: $\Phi = 0.42$, relative to naphthalene in cyclohexane. HR-MS ES (positive mode, m/z): $[\text{M}-\text{Br}]^+$; 407.2399. Anal. calcd. for $\text{C}_{26}\text{H}_{28}\text{BBrN}_4$: C, 64.09; H, 5.79; N, 11.50. Found: C, 65.30; H, 5.81; N, 10.31. Mp ($^\circ\text{C}$): 144-147.

Allylation of 10: Synthesis of (allyl)BFI•PPh₃ (13). A solution of **10** (101.4 mg, 0.201 mmol) in 10 mL of THF was prepared in a 20 mL scintillation vial and frozen in a liquid nitrogen-cooled cold well in a glove box. The solution was removed from the cold well and immediately after the solution had thawed, allylmagnesium bromide (1.0 M solution in diethyl ether, 0.196 mL, 0.196 mmol) was added slowly with stirring. The resulting mixture was allowed to warm to room temperature and stirred overnight. The volatiles were removed *in vacuo* and the resulting white solid, **13**, was washed with 2 x 10 mL of diethyl ether and dried *in vacuo* (crude yield: 43.4 mg). ^1H NMR (CDCl_3 , 500 MHz): δ 7.51 (dt,

$^3J_{\text{HH}} = 7.5$ Hz, $^4J_{\text{HH}} = 1.0$ Hz, 2H, ArH), 7.43 (td, $^3J_{\text{HH}} = 6.5$ Hz, $^4J_{\text{HH}} = 1.0$ Hz, 2H, ArH), 7.20-7.35 (m, 15H, ArH in PPh₃), 7.13 (td, $^3J_{\text{HH}} = 7.5$ Hz, $^4J_{\text{HH}} = 1.0$ Hz, 2H, ArH), 6.96 (td, $^3J_{\text{HH}} = 7.5$ Hz, $^4J_{\text{HH}} = 1.0$ Hz, 2H, ArH), 5.56 (m, 1H, -CH=CH₂), 4.65 (dd, $^2J_{\text{HH}} = 0.5$ Hz, $^3J_{\text{HH}} = 16.5$ Hz, 1H, -CH=CHH), 4.44 (dd, $^2J_{\text{HH}} = 1.5$ Hz, $^3J_{\text{HH}} = 10.5$ Hz, 1H, -CH=CHH), 2.29 (d, $^3J_{\text{HH}} = 7.0$ Hz, 2H, -CH₂-). $^{13}\text{C}\{^1\text{H}\}$ NMR (CDCl₃, 125 MHz): δ 150.0 (ArC), 140.9 (ArC), 137.9 (ArC), 133.9 (d, $^1J_{\text{CP}} = 9.6$ Hz, ArC), 130.9 (ArC), 128.5 (d, $^2J_{\text{CP}} = 9.4$ Hz, ArC), 126.1 (ArC), 125.2 (ArC), 119.1 (ArC), 110.7 (allylC), 107.6 (allylC), 30.4 (-CH₂-). $^{11}\text{B}\{^1\text{H}\}$ NMR (CDCl₃, 160 MHz): δ -9.7 (s). $^{31}\text{P}\{^1\text{H}\}$ NMR (CDCl₃, 160 MHz): δ 11.2 (s). See Figures 2.4.1-2.4.3 in Section 2.4.3 for NMR spectra of the crude product. HR-MS EI (positive mode, m/z): Calcd. for [(allyl)BFI]⁺: 204.11104. Found: 204.11109 ($\Delta\text{ppm} = 0.3$). Calcd. for [PPh₃]⁺: 262.09113. Found: 262.09159 ($\Delta\text{ppm} = 1.8$).

Allylation of 12: Synthesis of (allyl)BFI•DMAP (14). A suspension of **12** (100.1 mg, 0.206 mmol) in 10 mL of THF was prepared in a 20 mL scintillation vial and frozen in a liquid nitrogen-cooled cold well in a glove box. The frozen mixture was then removed from the cold well and immediately after the THF solvent had thawed allylmagnesium bromide (1.0 M solution in diethyl ether, 0.205 mL, 0.205 mmol) was added slowly with stirring. The resulting mixture was allowed to stir overnight, after which it had become clear and orange. The volatiles were removed *in vacuo* and the resulting orange residue was washed with 2 x 10 mL of diethyl ether and dried *in vacuo*. The remaining orange solid was washed with 2 x

10 mL toluene and dried *in vacuo* to afford crude **14** as a pale orange solid (crude yield: 38.8 mg). ^1H NMR (CDCl_3 , 500 MHz): δ 8.20 (d, $^3J_{\text{HH}} = 7.5$ Hz, 2H, ArH in DMAP), 7.66 (d, $^3J_{\text{HH}} = 7.5$ Hz, 2H, ArH), 7.48 (d, $^3J_{\text{HH}} = 7.0$ Hz, 2H, ArH), 7.21 (td, $^3J_{\text{HH}} = 7.5$ Hz, $^4J_{\text{HH}} = 1.0$ Hz, 2H, ArH), 7.13 (td, $^3J_{\text{HH}} = 7.0$ Hz, $^4J_{\text{HH}} = 1.0$ Hz, 2H, ArH), 6.54 (d, $^3J_{\text{HH}} = 6.0$ Hz, 2H, ArH in DMAP), 6.05 (m, 1H, -CH=CH₂), 4.71 (dd, $^2J_{\text{HH}} = 3.0$ Hz, $^3J_{\text{HH}} = 16.9$ Hz, 1H, -CH=CHH), 4.64 (dd, $^2J_{\text{HH}} = 2.0$ Hz, $^3J_{\text{HH}} = 12.0$ Hz, 1H, -CH=CHH), 3.05 (s, 6H, -N(CH₃)₂), 1.83 (d, $^3J_{\text{HH}} = 8.0$ Hz, 2H, -CH₂-CH=CH₂). $^{13}\text{C}\{^1\text{H}\}$ NMR (CDCl_3 , 125 MHz): δ 155.5 (ArC), 148.4 (ArC), 144.5 (ArC), 130.2 (ArC), 126.3 (ArC), 125.9 (ArC), 119.1 (ArC), 106.7 (allylC), 106.4 (allylC), 39.3 (N(CH₃)₂) 30.4 (-CH₂-). $^{11}\text{B}\{^1\text{H}\}$ NMR (CDCl_3 , 160 MHz): δ -0.7 (s). See Figures 2.4.4-2.4.6 in Section 2.4.3 for NMR spectra of the crude product. HR-MS EI (positive mode, m/z): Calcd. for [DMAP]⁺: 121.07658. Found: 121.07664 ($\Delta\text{ppm} = 0.5$). Calcd. for [(allyl)BF₄]⁺: 204.11104. Found: 204.11014 ($\Delta\text{ppm} = 4.4$).

Synthesis of IPrCH₂.³⁹ To a white slurry of 1,3-bis-(2,6-diisopropylphenyl)-imidazolium chloride, [IPrH]Cl (4.007 g, 9.43 mmol) in 50 mL THF at -78 °C was added ⁿBuLi (4.5 mL, 11.25 mmol, 2.5 M solution in hexanes) dropwise by syringe (10 mL capacity) at a rate of approx. 2 drops per second. The resulting mixture was removed from the cold bath immediately after the addition and allowed to stir for 20 minutes during which time the mixture became orange and clear. The mixture was cooled to -78 °C and stirred for 20 minutes before MeI (0.70 mL, 11.22 mmol) was added dropwise. The resulting mixture was removed

from the cold bath immediately after addition and allowed to stir for 20 minutes during which time a white precipitate formed. The mixture was cooled to $-78\text{ }^{\circ}\text{C}$ and stirred for 20 minutes before $n\text{-BuLi}$ (4.5 mL, 11.25 mmol, 2.5 M solution in hexanes) was added dropwise by syringe at a rate of approx. 2 drops per second. The resulting mixture was removed from the cold bath immediately after the addition and allowed to stir for 20 minutes during which time the mixture became orange and clear. Volatile components were removed *in vacuo* and the remaining residue was extracted with 3 x 50 mL of hexanes and each extract was filtered through Celite. The hexanes extracts were combined and a white solid remained after all volatile components were removed. Recrystallization of the crude product from 20 mL of hexanes at $-35\text{ }^{\circ}\text{C}$ afforded pure IPrCH_2 (3.238 g, 85 %). ^1H NMR (C_6D_6 , 500 MHz): δ 7.22 (t, $^3J_{\text{HH}} = 7.0\text{ Hz}$, 2H, ArH), 7.17 (d, $^3J_{\text{HH}} = 7.0\text{ Hz}$, 4H, ArH), 5.85 (s, 2H, N-CH-), 3.35 (septet, $^3J_{\text{HH}} = 6.9\text{ Hz}$, 4H, $\text{CH}(\text{CH}_3)_2$), 2.42 (s, 2H, =CH₂), 1.36 (d, $^3J_{\text{HH}} = 6.9\text{ Hz}$, 12H, $\text{CH}(\text{CH}_3)_2$), 1.22 (d, $^3J_{\text{HH}} = 6.9\text{ Hz}$, 12H, $\text{CH}(\text{CH}_3)_2$). $^{13}\text{C}\{^1\text{H}\}$ NMR (C_6D_6 , 125 MHz): δ 152.5 (N-C-N), 148.9 (ArC), 134.9 (ArC), 129.3 (ArC), 124.5 (ArC), 114.6 (-N-CH-), 44.3 (=CH₂), 28.8 ($\text{CH}(\text{CH}_3)_2$), 24.3 ($\text{CH}(\text{CH}_3)_2$), 23.8 ($\text{CH}(\text{CH}_3)_2$).³⁹

Synthesis of [IPrMe]Br (16). Gaseous HBr was bubbled through a solution of IPrCH_2 (100.2 mg, 0.249 mmol) in 10 mL of toluene until a colorless precipitate formed (approx. 30 seconds). The resulting precipitate was isolated by filtration and dried *in vacuo* to give **16** as a white solid (115.3 mg, 96 %). ^1H NMR (CDCl_3 , 500 MHz): δ 8.15 (s, 2H, -N-CH-), 7.62 (t, $^3J_{\text{HH}} = 7.5\text{ Hz}$, 2H, ArH), 7.39 (d, $^3J_{\text{HH}}$

= 7.5 Hz, 4H, ArH), 2.28 (septet, $^3J_{\text{HH}} = 7.0$ Hz, 4H, CH(CH₃)₂), 2.08 (s, 3H, -CH₃), 1.28 (d, $^3J_{\text{HH}} = 7.0$ Hz, 12H, CH(CH₃)₂), 1.18 (d, $^3J_{\text{HH}} = 7.0$ Hz, 12H, CH(CH₃)₂). ¹³C{¹H} NMR (CDCl₃, 125 MHz): δ 145.0 (N-C-N), 144.9 (ArC), 132.6 (ArC), 129.1 (ArC), 126.8 (ArC), 125.4 (-N-CH-), 29.2 (CH(CH₃)₂), 24.8 (CH(CH₃)₂), 23.5 (CH(CH₃)₂), 11.0 (-CH₃). HR-MS EI (positive mode, m/z): Calcd. for [IPrMe]⁺: 403.3108. Found: 403.3101 (Δppm = 1.6). Anal. calcd. for C₂₈H₃₉BrN₂: C, 69.55; H, 8.13; N, 5.79. Found: C, 70.46; H, 7.80; N, 4.92. Mp (°C): 225 (decomp.).

Synthesis of BrBFI•IPrCH₂ (17). To a mixture of **1** (504.5 mg, 2.08 mmol) and IPrCH₂ (412.7 mg, 1.03 mmol) was added 20 mL of toluene. The mixture was allowed to stir for 72 hours during which time a colorless precipitate formed. The supernatant was decanted and the remaining solid was washed with 3 x 15 mL of toluene. All volatile components were removed from the solid *in vacuo* to afford **17** as a white powder (638.5 mg, 96 %). Crystals suitable for X-ray analysis were grown from a 50/50 mixture of dichloromethane and hexanes at -35 °C. ¹H NMR (CDCl₃, 500 MHz): δ 7.68 (t, $^3J_{\text{HH}} = 8.0$ Hz, 2H, ArH), 7.50 (d, $^3J_{\text{HH}} = 8.0$ Hz, 4H, ArH), 7.36 (d, $^3J_{\text{HH}} = 7.5$ Hz, 2H, ArH), 7.22 (s, 2H, -N-CH-), 6.95 (td, $^3J_{\text{HH}} = 7.0$ Hz, $^4J_{\text{HH}} = 1.5$ Hz, 2H, ArH), 6.69 (td, $^3J_{\text{HH}} = 7.0$ Hz, $^4J_{\text{HH}} = 1.5$ Hz, 2H, ArH), 5.94 (d, $^3J_{\text{HH}} = 9.0$ Hz, 2H, ArH), 3.05 (septet, $^3J_{\text{HH}} = 7.0$ Hz, 4H, CH(CH₃)₂), 2.66 (s, 2H, -CH₂-B), 1.34 (d, $^3J_{\text{HH}} = 6.5$ Hz, 12H, CH(CH₃)₂), 1.37 (d, $^3J_{\text{HH}} = 7.0$ Hz, 12H, CH(CH₃)₂). ¹³C{¹H} NMR (CDCl₃, 125 MHz): δ 160.5 (ArC), 146.7 (ArC), 146.1 (ArC), 131.6 (ArC), 131.5 (ArC), 129.3 (ArC), 126.1

(ArC), 125.8 (ArC), 125.7 (ArC), 122.1 (ArC), 118.5 (-N-CH-), 29.2 (-CH₂-B), 26.4 (CH(CH₃)₂), 22.9 (CH(CH₃)₂). ¹¹B{¹H} NMR (CDCl₃, 160 MHz): δ -1.4 (s). UV/Vis (in CH₂Cl₂): λ_{max} = 248 nm (ε = 2.84 x 10⁴ L mol⁻¹ cm⁻¹), 254 nm (ε = 2.91 x 10⁴ L mol⁻¹ cm⁻¹). Fluorescence emission (in CH₂Cl₂): λ_{em} = 329, 342, fluorescence quantum yield: Φ = 0.87, relative to naphthalene in cyclohexane. HR-MS EI (positive mode, m/z): Calcd. for [BrBFI]⁺: 243.98819. Found: 243.98620 (Δppm = 8.2). Calcd. for [IPrCH₂]⁺: 402.30350. Found: 402.30281 (Δppm = 1.7). Anal. calcd. for C₄₀H₄₆BBrN₂: C, 74.42; H, 7.18; N, 4.34. Found: C, 73.15; H, 7.05; N, 4.20. Mp (°C): 228-231.

Synthesis of (Me₃Si)₂NBFI (18). To a solution of **1** (45.5 mg, 0.187 mmol) in 5 mL of toluene was added a solution of K[N(SiMe₃)₂] (32.9 mg, 0.165 mmol) in 5 mL of toluene. The resulting mixture was allowed to stir overnight before being filtered. The volatile components were removed *in vacuo* to afford **18** as a pale orange semi-solid (crude yield: 40.6 mg, 76 %). ¹H NMR (CDCl₃, 500 MHz): δ 7.76 (dt, ³J_{HH} = 7.2 Hz, ⁴J_{HH} = 1.2 Hz, 2H, ArH), 7.29 (dt, ³J_{HH} = 7.2 Hz, ⁴J_{HH} = 1.2 Hz, 2H, ArH), 7.11 (td, ³J_{HH} = 7.6 Hz, ⁴J_{HH} = 1.2 Hz, 2H, ArH), 7.02 (td, ³J_{HH} = 7.6 Hz, ⁴J_{HH} = 1.2 Hz, 2H, ArH), 0.30 (s, 18H, Si-CH₃). ¹³C{¹H} NMR (CDCl₃, 125 MHz): δ 153.3 (ArC), 133.4 (ArC), 132.5 (ArC), 119.7 (ArC), 4.5 (Si-CH₃). ¹¹B{¹H} NMR (CDCl₃, 160 MHz): δ 54.2 (s). ²⁹Si{¹H} NMR (CDCl₃, 100 MHz): δ 3.4 (s). Calcd. for [SiNBFI]⁺: 205.05191. Found: 205.05243 (Δppm = 2.5).

Synthesis of HBF₄•IPrCH₂ (19). To a mixture of **17** (202.2 mg, 0.313 mmol) and Li[AlH₄] (25.7 mg, 0.677 mmol) was added 10 mL of CH₂Cl₂. The resulting mixture was allowed to stir for 5 days. The mixture was then filtered through a small (ca. 1 cm) plug of silica gel. The volatile components were removed from the filtrate *in vacuo* to yield **19** as a white solid (152.4 mg, 86 %). ¹H{¹¹B} NMR (CDCl₃, 500 MHz): δ 7.64 (t, ³J_{HH} = 8.0 Hz, 2H, ArH), 7.49 (d, ³J_{HH} = 7.5 Hz, 2H, ArH), 7.43 (d, ³J_{HH} = 8.0 Hz, 4H, ArH), 7.08 (s, 2H, -N-CH-), 6.94 (td, ³J_{HH} = 7.5 Hz, ⁴J_{HH} = 1.0 Hz, 2H, ArH), 6.73 (td, ³J_{HH} = 7.5 Hz, ⁴J_{HH} = 1.0 Hz, 2H, ArH), 6.12 (d, ³J_{HH} = 7.0 Hz, 2H, ArH) 2.77 (septet, ³J_{HH} = 7.0 Hz, 4H, CH(CH₃)₂), 2.35 (broad, 1H, -BH, assignment made by broadband ¹H{¹¹B} decoupling), 2.15 (d, ³J_{HH} = 3.5 Hz, 2H, -CH₂-B) 1.25 (d, ³J_{HH} = 7.0 Hz, 12H, CH(CH₃)₂), 1.21 (d, ³J_{HH} = 6.5 Hz, 12H, CH(CH₃)₂). ¹³C{¹H} NMR (CDCl₃, 125 MHz): δ 163.5 (ArC), 148.1 (ArC), 145.8 (ArC), 131.6 (ArC), 131.3 (ArC), 130.1 (ArC), 125.2 (ArC), 124.3 (ArC), 123.5 (ArC), 121.5 (ArC), 118.2 (-N-CH-), 29.2 (CH(CH₃)₂), 25.8 (CH(CH₃)₂), 22.6 (CH(CH₃)₂). ¹¹B{¹H} NMR (CDCl₃, 160 MHz): δ -15.1 (s). ¹¹B NMR (CDCl₃, 160 MHz): δ -15.1 (d, ¹J_{BH} = 82 Hz). See Figures 2.4.7-2.4.9 in Section 2.4.3 for NMR spectra. UV/Vis (in CH₂Cl₂): λ_{max} = 315 nm (ε = 8.64 x 10³ L mol⁻¹ cm⁻¹). Fluorescence emission (in CH₂Cl₂): λ_{em} = 329, 341, 434 nm, fluorescence quantum yield: Φ = 0.38, relative to naphthalene in cyclohexane. HR-MS EI (positive mode, m/z): Calcd. for [M]⁺: 566.38324. Found: 566.38218 (Δppm = 1.9). Anal. calcd. for C₄₀H₄₇BN₂: C, 84.79; H, 8.36; N, 4.94. Found: C, 79.65; H, 8.04; N, 4.56. Mp (°C): 218-220. Despite repeated

attempts, combustion analysis gave consistently low values for carbon content (lower by ca. 5 %).

Decomposition of **19 in THF and CH₂Cl₂.** It must be noted that **19** is prone to decomposition in THF and in CH₂Cl₂ in the absence of Li[AlH₄]. A solution of 27.4 mg (0.048 mmol) of **19** in 10 mL of THF was prepared and allowed to stir for 3 days. ¹¹B NMR spectroscopy revealed that ~70 % decomposition had occurred and the emergence of three new boron environments were noted. ¹¹B NMR (C₆D₆, 160 MHz): δ 3.3 (br, new environment), -6.1 (s, new environment), -14.5 (d, ¹J_{BH} = 82 Hz, **19**, 30 %) -19.1 (t, ¹J_{BH} = 83 Hz, new environment).

A solution of 29.6 mg (0.052 mmol) of **19** in 10 mL of CH₂Cl₂ was prepared and allowed to stir for 3 days. ¹H NMR spectroscopy revealed that ~70 % conversion to [IPrMe]Cl³⁸ had occurred and ¹¹B NMR spectroscopy revealed two new boron environments. ¹¹B NMR (CDCl₃, 160 MHz): δ 2.3 (br, new environment), -6.7 (s, new environment), -15.1 (d, ¹J_{BH} = 82 Hz).

Thermal Treatment of HBFl•IPrCH₂ (19**).** To a suspension of 46.4 mg (0.081 mmol) of **19** in 30 mL of toluene was added a solution of 2.9 mg (0.0059 mmol) of [Rh(COD)Cl]₂ in 1 mL of toluene. The resulting mixture was heated to reflux overnight. The volatile components were removed *in vacuo* and a brown/orange solid remained and was not purified further (crude yield: 44.0 mg). ¹H NMR (CDCl₃, 500 MHz): δ 7.72 (s) 7.69 (t, ³J_{HH} = 8.0 Hz, 2H, ArH), 7.62 (t, ³J_{HH} = 8.0

Hz, 1H, -N-CH(CH₂)-N-), 7.50 (d, ³J_{HH} = 8.0 Hz, 4H, ArH), 7.38 (d, ³J_{HH} = 7.5 Hz, 2H, ArH), 7.33 (d, ³J_{HH} = 6.0 Hz, 2H, ArH), 7.21 (s, 2H, -N-CH-), 6.92 (td, ³J_{HH} = 7.0 Hz, ⁴J_{HH} = 1.5 Hz, 2H, ArH), 6.80 (td, ³J_{HH} = 7.5 Hz, ⁴J_{HH} = 1.0 Hz, 2H, ArH), 5.92 (d, ³J_{HH} = 7.0 Hz, 2H, ArH), 3.0 (broad, 4H, CH(CH₃)₂), 2.52 (s, 2H, -CH₂-B), 2.23 (septet, ³J_{HH} = 6.5 Hz, 2H, CH(CH₃)₂), 1.32 (d, ³J_{HH} = 6.5 Hz, 12H, CH(CH₃)₂), 1.25 (d, ³J_{HH} = 7.0 Hz, 6H, CH(CH₃)₂), 1.19 (d, ³J_{HH} = 6.5 Hz, 12H, CH(CH₃)₂), 1.15 (d, ³J_{HH} = 7.0 Hz, 6H, CH(CH₃)₂). ¹¹B{¹H} NMR (CDCl₃, 160 MHz): δ 0.2 (s). See Figures 2.4.10 and 2.4.11 for NMR spectra of the crude product.

Attempted “Unmasking” of BrBF1•IPr (2), BrBF1•PPh₃ (10) and [(DMAP)₂BF1]Br (12). Several attempts were made to remove the Lewis base (either DMAP or PPh₃) from the boron center in **2**, **10** and **12**. In a typical experiment, the Lewis base-borafluorene adduct (approx. 0.1 mmol) was dissolved in a 20 mL of CH₂Cl₂ and the desired “unmasking agent” was added followed by stirring overnight. The volatile components were then removed *in vacuo* and the products were then analyzed by NMR. The results are tabulated below:

Table 2.4.1. Attempted “unmasking” of BrBFl•IPr (**2**).

Reagent Added (1:1 mole ratio)/Conditions	Result
HCl/room temp in toluene	No Reaction
MeI/room temp in toluene; reflux in hexanes	No Reaction
MeOTf/room temp and reflux in toluene	No Reaction
BEt ₃ /room temp in CH ₂ Cl ₂	No Reaction

Table 2.4.2. Attempted “unmasking” of BrBFl•PPh₃ (**10**).

Reagent Added (1:1 mole ratio)/Conditions	Result
BEt ₃ /room temp in CH ₂ Cl ₂	No Reaction
B(C ₆ F ₅) ₃ /room temp in CH ₂ Cl ₂	Mostly (> 80 %) starting material. New Product observed by ¹¹ B NMR ^a (free BrBFl and (C ₆ F ₅) ₃ B•PPh ₃ not observed ³⁵)

a) ¹¹B NMR spectroscopy showed a new peak at -10.8 ppm as a singlet suggesting one new boron environment, however ¹⁹F NMR spectroscopy revealed that up to 4 new compounds may be present. ¹H NMR contained several overlapping peaks that could not be resolved.

Table 2.4.3. Attempted “unmasking” of [(DMAP)₂BFI]Br (**12**) (both addition of 1 and 2 equivalents of each reagent have been added, in all cases, results are the same).

Reagent Added (1:1 and 2:1 mole ratios)/Conditions	Result (regardless of mole ratio, results were the same)
HCl (in Et ₂ O)/room temp and reflux in CH ₂ Cl ₂	No Reaction
MeOTf/room temp and reflux in CH ₂ Cl ₂	No Reaction
MeI/room temp	No Reaction
B(C ₆ F ₅) ₃ /room temp	> 50 % Starting Material; (C ₆ F ₅) ₃ B•DMAP ³⁶ observed with addition of both one and two equivalents; additional product observed when one equivalent added (possibly BrBFI•DMAP) ^a

a) ¹¹B NMR spectroscopy showed a new peak at -9.6 ppm as a singlet suggesting one new, unidentified boron environment, however ¹⁹F NMR spectroscopy revealed that up to 4 new compounds may be present. ¹H NMR contained several overlapping peaks that could not be resolved.

2.4.2 Crystallographic Tables

Table 2.4.4. Crystallographic Data for Compounds **2**, **8** and **12**.

	2 • CH ₂ Cl ₂	8	12 • 1/3 CH ₂ Cl ₂ • 1/2 THF
empirical formula	C ₄₀ H ₄₆ BBrCl ₂ N ₂	C ₃₉ H ₄₅ BN ₂	C _{28.33} H _{32.67} BBrCl _{0.67} N ₄ O _{0.5}
fw	716.41	552.58	551.60
cryst. dimens. (mm)	0.41 x 0.24 x 0.23	0.45 x 0.42 x 0.35	0.30 x 0.26 x 0.18
cryst. syst.	monoclinic	monoclinic	monoclinic
space group	<i>P2₁/c</i>	<i>P2₁/n</i>	<i>C2/c</i>
unit cell			
<i>a</i> (Å)	11.4012 (4)	11.3096 (4)	29.9685 (7)
<i>b</i> (Å)	21.2295 (8)	14.8357 (6)	12.7445 (3)
<i>c</i> (Å)	15.8472 (6)	20.1829 (8)	43.8064 (10)
α (°)			
β (°)		104.2470 (10)	91.3286 (4)
γ (°)			
<i>V</i> (Å ³)	103.6023 (5)	3282.3 (2)	16726.6 (7)
<i>Z</i>	4	4	24
ρ_{calcd} (g cm ⁻³)	1.276	1.118	1.314
μ (mm ⁻¹)	1.276	0.064	1.564
<i>T</i> (K)	173(1)	173(1)	173(1)
$2\theta_{\text{max}}$ (°)	52.82	52.80	52.95
total data	29726	26087	66493
unique data (<i>R</i> _{int})	7649 (0.0406)	6735 (0.0214)	17236 (0.0370)
observed data [I > 2σ(I)]	6154	5571	11962
params.	415	383	897
<i>R</i> ₁ [I > 2σ(I)] ^a	0.0374	0.0400	0.0659
w <i>R</i> ₂ [all data] ^a	0.0940	0.1090	0.1996
Difference map $\Delta\rho$ (e Å ⁻³)	0.782 / -0.886	0.217 / -0.183	1.510 / -1.198

$$^a R_1 = \frac{\sum ||F_o| - |F_c||}{\sum |F_o|}; wR_2 = \left[\frac{\sum w(F_o^2 - F_c^2)^2}{\sum w(F_o^4)} \right]^{1/2}$$

Table 2.4.5. Crystallographic Data for Compounds **16** and **17**.

	16 • 2 CH₂Cl₂	17 • 2 CH₂Cl₂
empirical formula	C ₃₀ H ₄₃ BrCl ₄ N ₂	C ₄₂ H ₅₀ BBrCl ₄ N ₂
fw	653.37	815.36
cryst. dimens. (mm)	0.31 x 0.13 x 0.07	0.36 x 0.14 x 0.11
cryst. syst.	triclinic	monoclinic
space group	<i>P</i> $\bar{1}$	<i>P</i> 2 ₁ / <i>n</i>
unit cell		
<i>a</i> (Å)	11.6745 (3)	12.5593 (9)
<i>b</i> (Å)	12.1104 (3)	22.5211 (15)
<i>c</i> (Å)	12.2440 (3)	15.1550 (10)
α (°)	79.3360 (10)	
β (°)	85.4340 (10)	101.145 (3)
γ (°)	89.7850 (10)	
<i>V</i> (Å ³)	1695.69 (7)	4205.7 (5)
<i>Z</i>	2	4
ρ_{calcd} (g cm ⁻³)	1.280	1.288
μ (mm ⁻¹)	4.698	3.895
<i>T</i> (K)	173(1)	173(1)
2 θ_{max} (°)	136.70	140.43
total data	11375	27177
unique data (<i>R</i> _{int})	5928 (0.0125)	7844 (0.0217)
observed data [<i>I</i> > 2 σ (<i>I</i>)]	5299	7335
params.	362	452
<i>R</i> ₁ [<i>I</i> > 2 σ (<i>I</i>)] ^a	0.0419	0.0350
<i>wR</i> ₂ [all data] ^a	0.1166	0.0914
Difference map $\Delta\rho$ (e Å ⁻³)	0.674 / -0.533	0.877 / -0.625

^a $R_1 = \sum ||F_o| - |F_c|| / \sum |F_o|$; $wR_2 = [\sum w(F_o^2 - F_c^2)^2 / \sum w(F_o^4)]^{1/2}$

2.4.3 NMR Spectra

Figure 2.4.1. Crude ^1H NMR Spectrum for (allyl)BF $_4$ •PPh $_3$ (**13**).

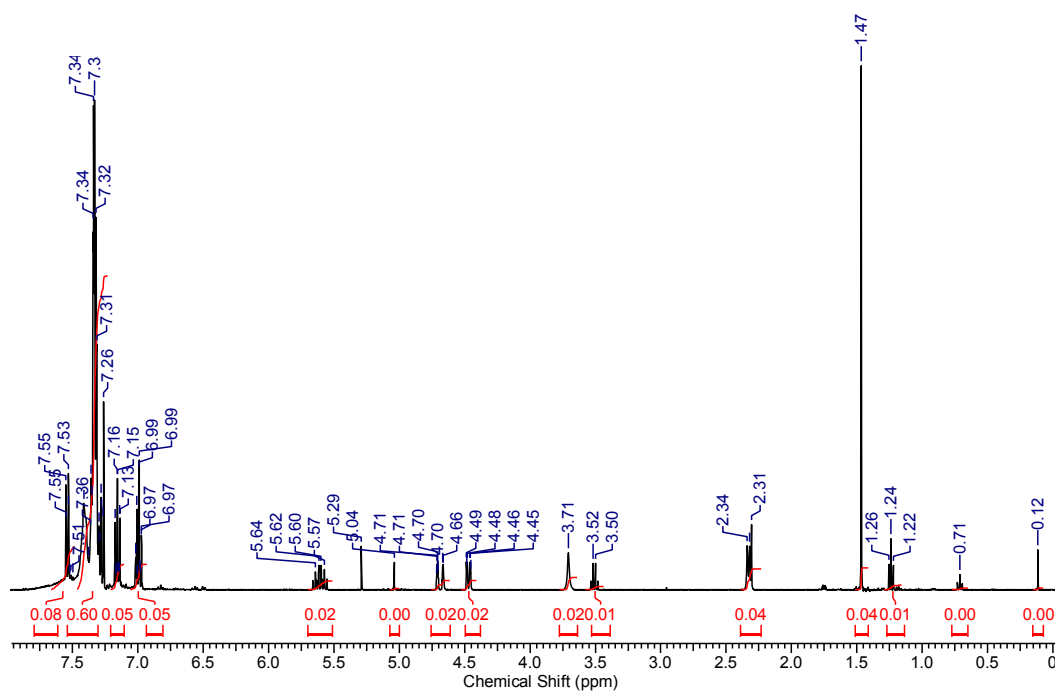


Figure 2.4.2. Crude ^{13}C NMR Spectrum for (allyl)BF $_4$ •PPh $_3$ (**13**).

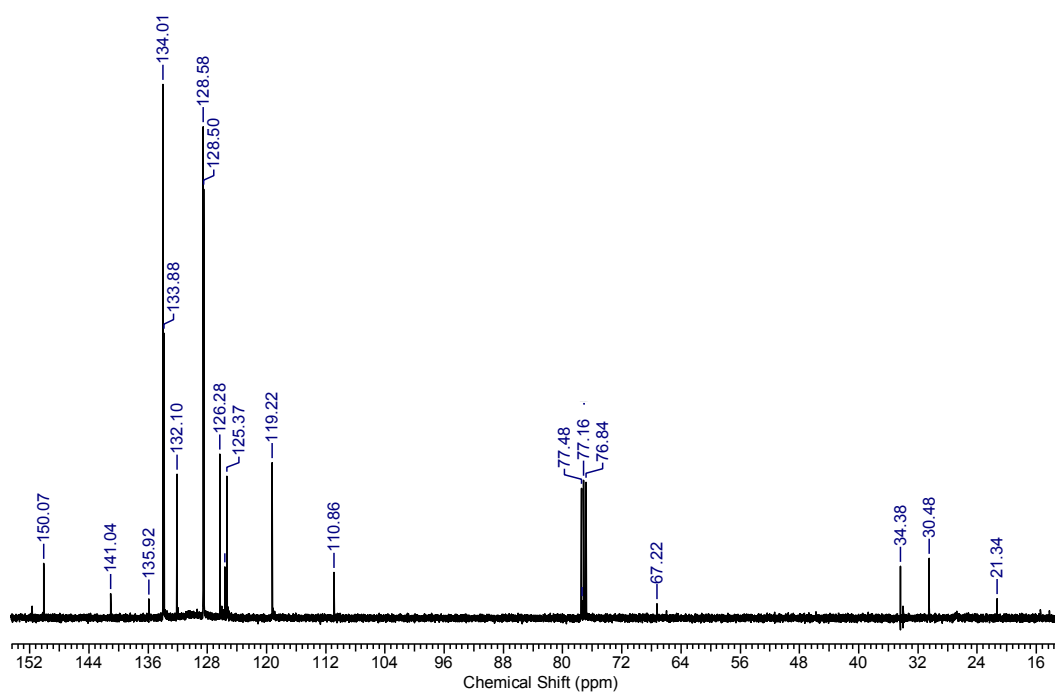


Figure 2.4.3. Crude $^{11}\text{B}\{^1\text{H}\}$ NMR Spectrum for (allyl)BF $_4$ •PPh $_3$ (**13**).

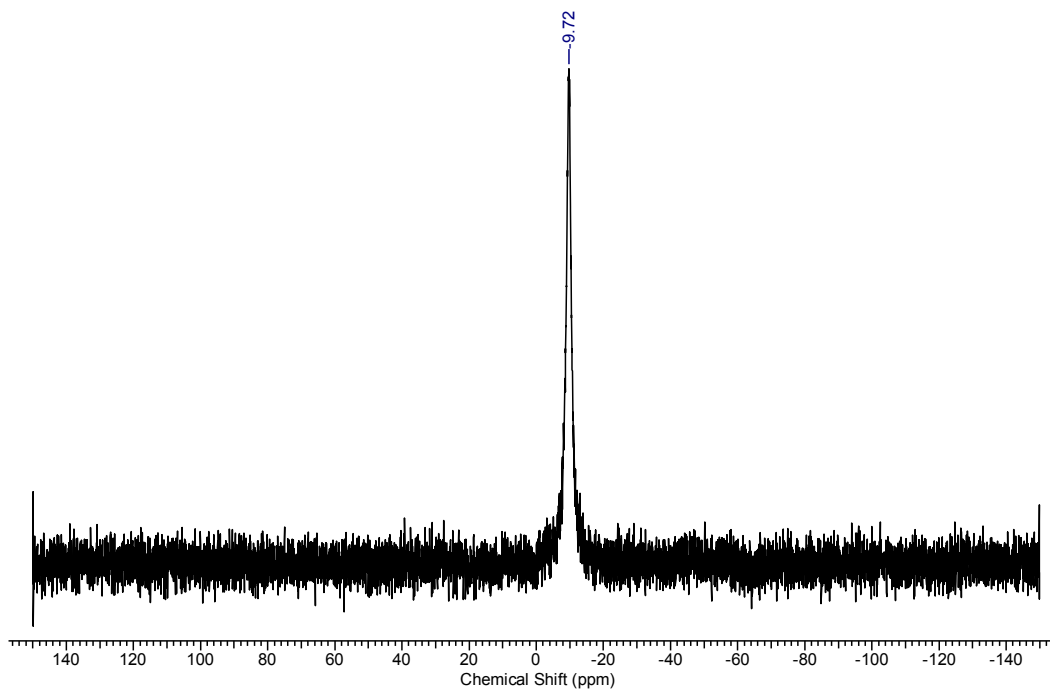


Figure 2.4.4. Crude ^1H NMR Spectrum for (allyl)BF $_4$ •DMAP (**14**).

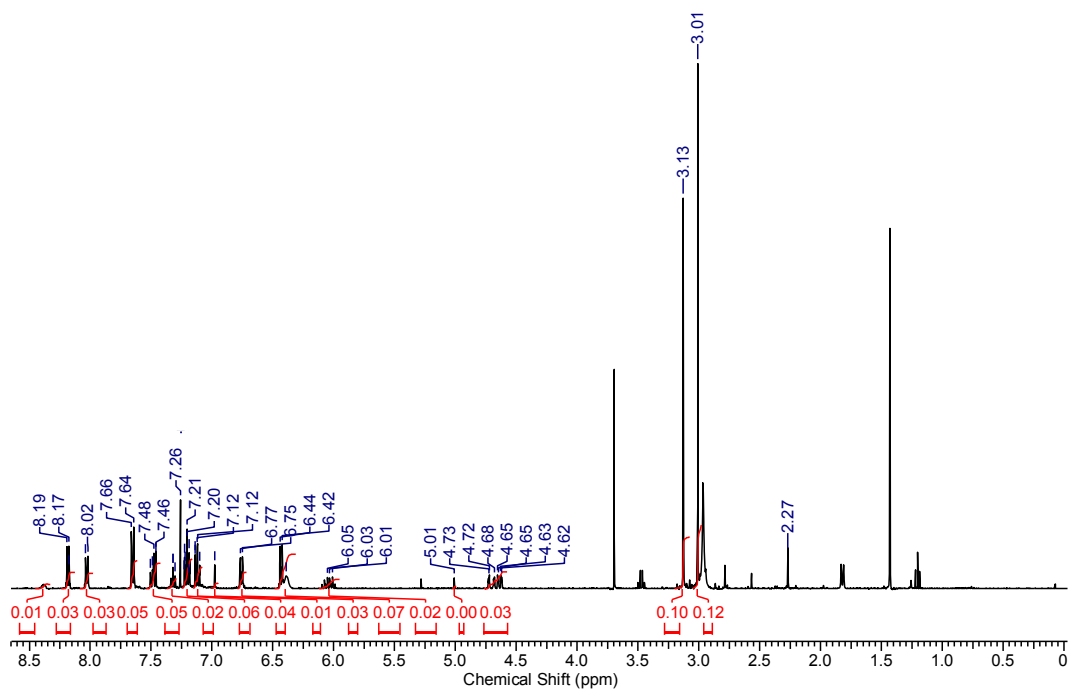


Figure 2.4.5. Crude ^{13}C NMR Spectrum for (allyl)BF $_4$ •DMAP (14).

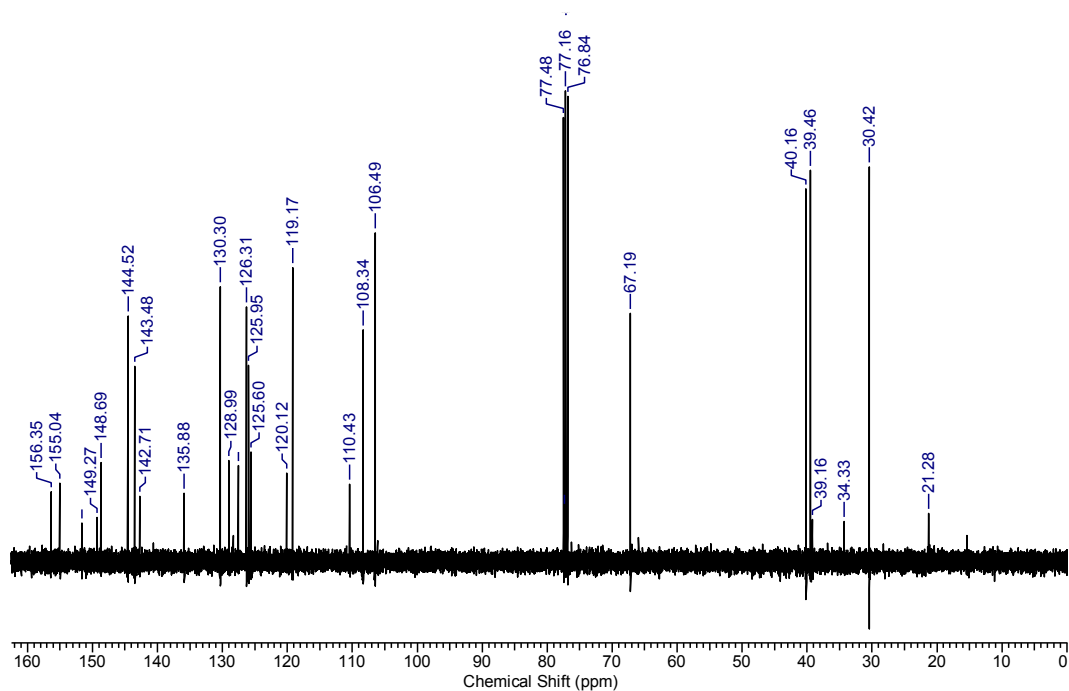


Figure 2.4.6. Crude $^{11}\text{B}\{^1\text{H}\}$ NMR Spectrum for (allyl)BF $_4$ •DMAP (14).

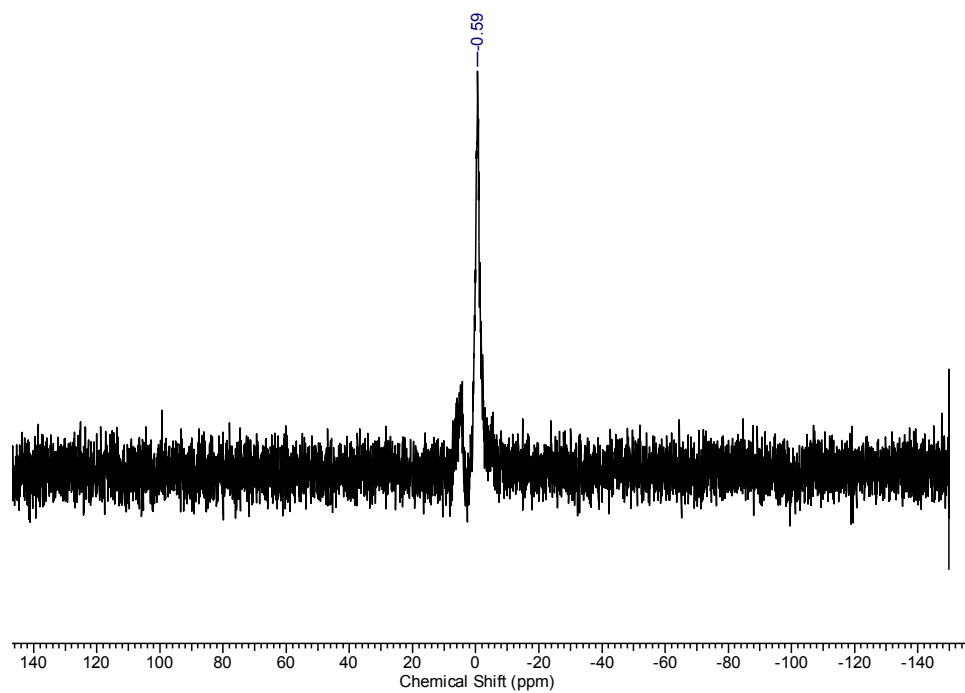


Figure 2.4.7. ^1H NMR Spectrum for $\text{HBF}_4 \cdot \text{IPrCH}_2$ (**19**).

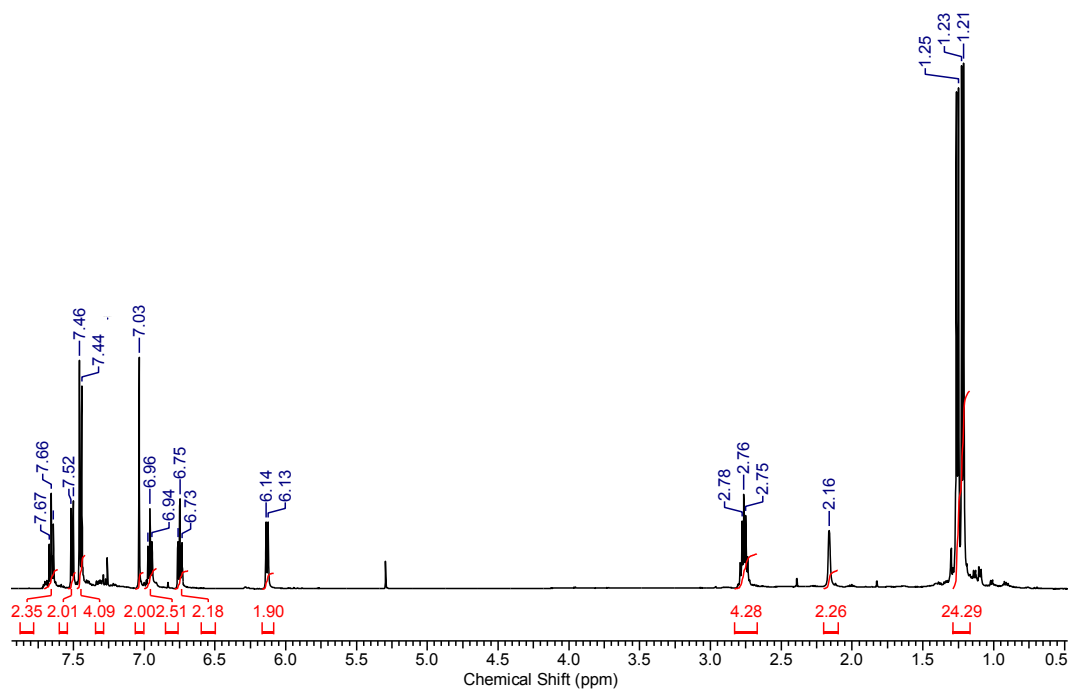


Figure 2.4.8. ^{13}C NMR Spectrum for $\text{HBF}_4 \cdot \text{IPrCH}_2$ (**19**).

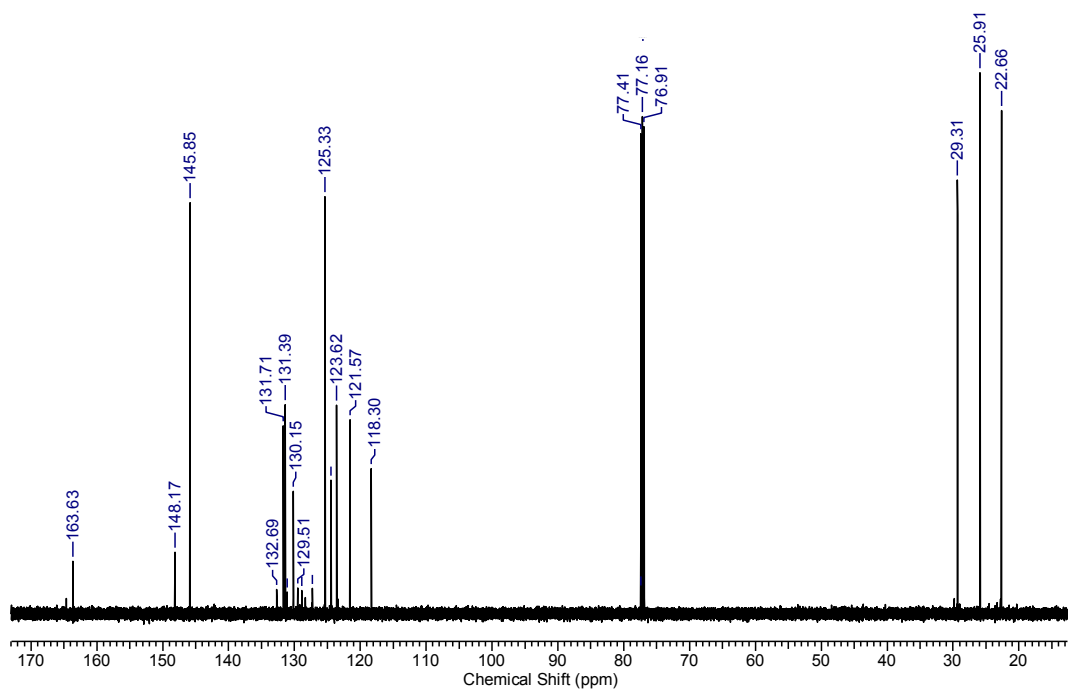


Figure 2.4.9. Proton-Coupled ^{11}B NMR Spectrum for $\text{HBF}_4 \cdot \text{IPrCH}_2$ (19).

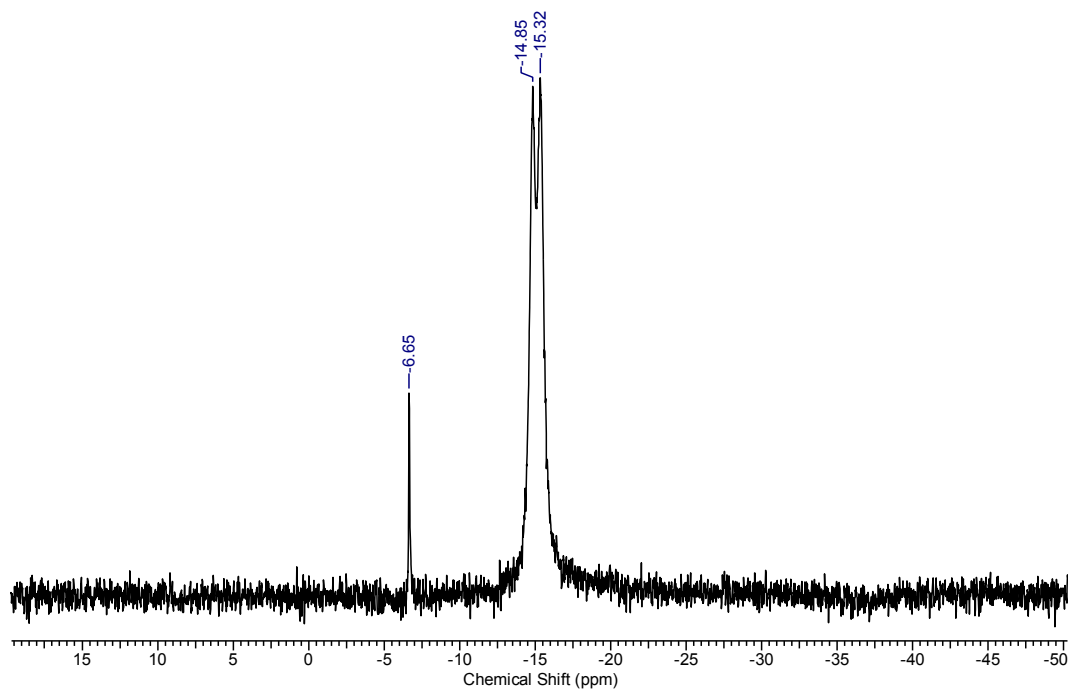


Figure 2.4.10. ^1H NMR spectrum for the thermal treatment of $\text{HBF}_4 \cdot \text{IPrCH}_2$ (19).

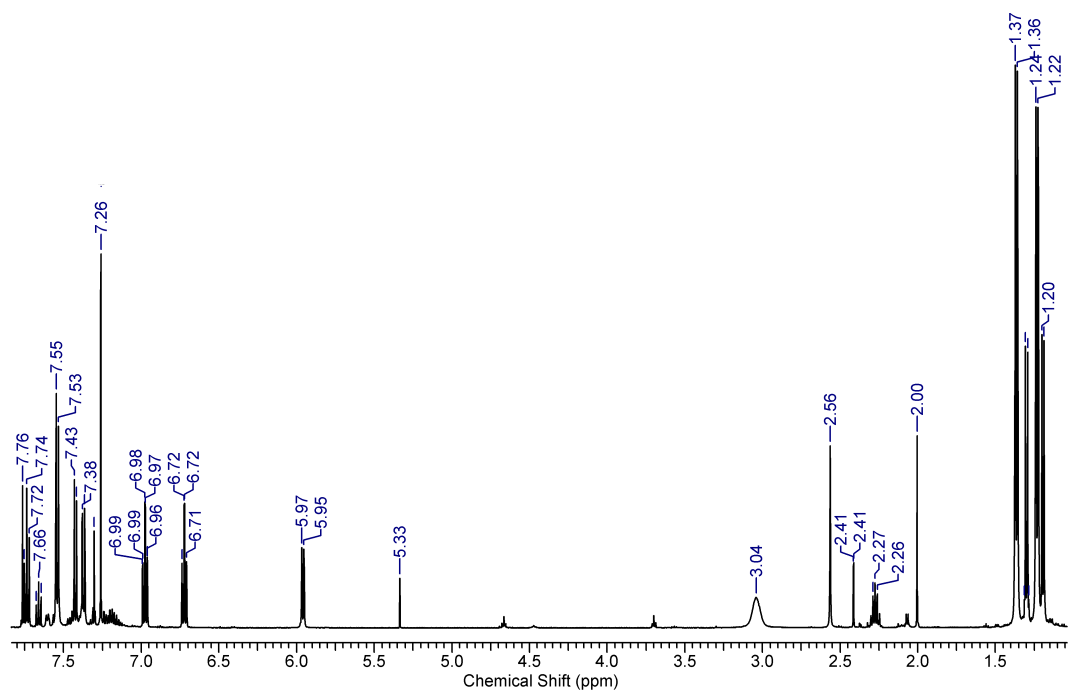
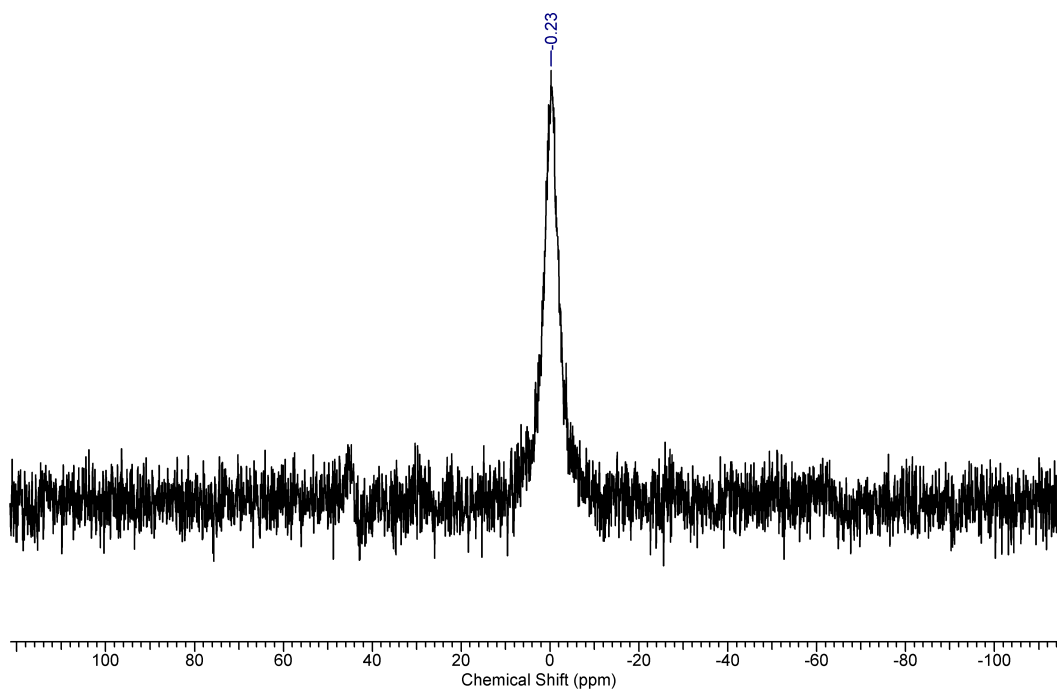


Figure 2.4.11. $^{11}\text{B}\{^1\text{H}\}$ NMR spectrum for the thermal treatment of $\text{HBF}_4 \cdot \text{IPrCH}_2$ (19).



2.5 References

- (1) Cho, D.-G.; Sessler, J. L. *Chem. Soc. Rev.* **2009**, *38*, 1647.
- (2) Li, H.; Lalancette, R. A.; Jäkle, F. *Chem. Commun.* **2011**, *47*, 9378.
- (3) Acheampong, M.; Paksirajan, K.; Lens, P. L. *Environ. Sci. Pollut. Res.* **2013**, *20*, 3799.
- (4) Lloyd, L. *Handbook of Industrial Catalysts*; Springer Science + Business Media, LLC: New York, NY, USA, 2011.
- (5) Burnworth, M.; Rowan, S. J.; Weder, C. *Chem. Eur. J.* **2007**, *13*, 7828.
- (6) Yamaguchi, S.; Shirasaka, T.; Akiyama, S.; Tamao, K. *J. Am. Chem. Soc.* **2002**, *124*, 8816.

- (7) Wade, C. R.; Broomsgrove, A. E. J.; Aldridge, S.; Gabbai, F. P. *Chem. Rev.* **2010**, *110*, 3958.
- (8) Hudson, Z. M.; Wang, S. *Acc. Chem. Res.* **2009**, *42*, 1584.
- (9) Chase, P. A.; Romero, P. E.; Piers, W. E.; Parvez, M.; Patrick, B. O. *Can. J. Chem.* **2005**, *83*, 2098.
- (10) Iida, A.; Yamaguchi, S. *J. Am. Chem. Soc.* **2011**, *133*, 6952.
- (11) Jäkle, F. *Coord. Chem. Rev.* **2006**, *250*, 1107.
- (12) Sainsbury, T.; Satti, A.; May, P.; Wang, Z.; McGovern, I.; Gun'ko, Y. K.; Coleman, J. J. *J. Am. Chem. Soc.* **2012**, *134*, 18758.
- (13) Braïda, B.; Derat, E.; Chaquin, P. *ChemPhysChem* **2013**, DOI: 10.1002/cphc.201300361.
- (14) Zhang, Z.-C.; Chung, T. C. M. *Macromolecules* **2006**, *39*, 5187.
- (15) Biswas, S.; Oppel, I. M.; Bettinger, H. F. *Inorg. Chem.* **2010**, *49*, 4499.
- (16) Dougherty, T. K.; Lau, K. S. Y.; Hedberg, F. L. *J. Org. Chem.* **1983**, *48*, 5273.
- (17) Du, C. J. F.; Hart, H.; Ng, K. K. D. *J. Org. Chem.* **1986**, *51*, 3162.
- (18) Saednya, A.; Hart, H. *Synthesis* **1996**, 1455.
- (19) Lide, D. *CRC Handbook of Chemistry and Physics: A Ready-Reference Book of Chemical and Physical Data*; 85th ed.; CRC Press: Boca Raton, Fla., 2004.
- (20) Curran, D. P.; Solovyev, A.; Makhlof Brahmi, M.; Fensterbank, L.; Malacria, M.; Lacôte, E. *Angew. Chem. Int. Ed.* **2011**, *50*, 10294.
- (21) Narula, C. K. N., H. *J. Organomet. Chem.* **1985**, *281*, 131.

- (22) Biswas, S.; Maichle-Mossmer, C.; Bettinger, H. F. *Chem. Commun.* **2012**, 48, 4564.
- (23) Das, A.; Hübner, A.; Weber, M.; Bolte, M.; Lerner, H.-W.; Wagner, M. *Chem. Commun.* **2011**, 47, 11339.
- (24) Köhl, O. *Chem. Soc. Rev.* **2007**, 36, 592.
- (25) Heuclin, H.; Ho, S. Y. F.; Le Goff, X. F.; So, C.-W.; Mézailles, N. *J. Am. Chem. Soc.* **2013**, 135, 8774.
- (26) Jafarpour, L. S., E. D.; Nolan, S. P. *J. Organomet. Chem.* **2000**, 606, 49.
- (27) Hübner, A.; Lerner, H.-W.; Wagner, M.; Bolte, M. *Acta Crystallogr.* **2010**, E66, 0444.
- (28) Braunschweig, H.; Chiu, C.-W.; Damme, A.; Ferkinghoff, K.; Kraft, K.; Radacki, K.; Wahler, J. *Organometallics* **2011**, 30, 3210.
- (29) Braunschweig, H.; Chiu, C.-W.; Radacki, K.; Kupfer, T. *Angew. Chem. Int. Ed.* **2010**, 49, 2041.
- (30) Hudnall, T. W.; Gabbaï, F. P. *Chem. Commun.* **2008**, 4596.
- (31) Bonnier, C.; Piers, W. E.; Parvez, M.; Sorensen, T. S. *Chem. Commun.* **2008**, 4593.
- (32) Someya, C. I.; Inoue, S.; Präsang, C.; Irran, E.; Driess, M. *Chem. Commun.* **2011**, 47, 6599.
- (33) Malcolm, A. C.; Sabourin, K. J.; McDonald, R.; Ferguson, M. J.; Rivard, E. *Inorg. Chem.* **2012**, 51, 12905.
- (34) Boshra, R.; Sundararaman, A.; Zakharov, L. N.; Incarvito, C. D.; Rheingold, A. L.; Jäkle, F. *Chem. Eur. J.* **2005**, 11, 2810.

- (35) Jacobsen, H.; Berke, H.; Döring, S.; Kehr, G.; Erker, G.; Fröhlich, R.; Meyer, O. *Organometallics* **1999**, *18*, 1724.
- (36) Lesley, M. J. G.; Woodward, A.; Taylor, N. J.; Marder, T. B.; Cazenobe, I.; Ledoux, I.; Zyss, J.; Thornton, A.; Bruce, D. W.; Kakkar, A. K. *Chem. Mater.* **1998**, *10*, 1355.
- (37) Kuhn, N.; Bohnen, H.; Kreutzberg, J.; Blaser, D.; Boese, R. *J. Chem. Soc., Chem. Commun.* **1993**, *0*, 1136.
- (38) Al-Rafia, S. M. I.; Ferguson, M. J.; Rivard, E. *Inorg. Chem.* **2011**, *50*, 10543.
- (39) Al-Rafia, S. M. I.; Malcolm, A. C.; Liew, S. K.; Ferguson, M. J.; McDonald, R.; Rivard, E. *Chem. Commun.* **2011**, *47*, 6987.
- (40) Al-Rafia, S. M. I.; Momeni, M. R.; Ferguson, M. J.; McDonald, R.; Brown, A.; Rivard, E. *Organometallics* **2013**, DOI: 10.1021/om400361n.
- (41) Coluccini, C.; Sharma, A. K.; Caricato, M.; Sironi, A.; Cariati, E.; Righetto, S.; Tordin, E.; Botta, C.; Forni, A.; Pasini, D. *PCCP* **2013**, *15*, 1666.
- (42) Weber, L.; Eickhoff, D.; Kahlert, J.; Bohling, L.; Brockhinke, A.; Stammler, H.-G.; Neumann, B.; Fox, M. A. *Dalton Trans.* **2012**, *41*, 10328.
- (43) Achelle, S.; Barsella, A.; Baudequin, C.; Caro, B.; Robin-le Guen, F. *J. Org. Chem.* **2012**, *77*, 4087.
- (44) Fan, C.; Piers, W. E.; Parvez, M. *Angew. Chem. Int. Ed.* **2009**, *48*, 2955.
- (45) Sumerin, V.; Schulz, F.; Nieger, M.; Leskelä, M.; Repo, T.; Rieger, B. *Angew. Chem. Int. Ed.* **2008**, *47*, 6001.

- (46) Hübner, A.; Qu, Z.-W.; Englert, U.; Bolte, M.; Lerner, H.-W.; Holthausen, M. C.; Wagner, M. *J. Am. Chem. Soc.* **2011**, *133*, 4596.
- (47) Staubitz, A.; Sloan, M. E.; Robertson, A. P. M.; Friedrich, A.; Schneider, S.; Gates, P. J.; Auf der Günne, J. S.; Manners, I. *J. Am. Chem. Soc.* **2010**, *132*, 13332.
- (48) Al-Rafia, S. M. I.; McDonald, R.; Ferguson, M. J.; Rivard, E. *Chem. Eur. J.* **2012**, *18*, 13810.
- (49) Frey, G. D.; Masuda, J. D.; Donnadiou, B.; Bertrand, G. *Angew. Chem. Int. Ed.* **2010**, *49*, 9444.
- (50) Brouwer, A. M. *Pure Appl. Chem.* **2011**, *83*, 2213.
- (51) Umezawa, K.; Nakamura, Y.; Makino, H.; Citterio, D.; Suzuki, K. *J. Am. Chem. Soc.* **2008**, *130*, 1550.
- (52) Bonnier, C.; Piers, W. E.; Al-Sheikh Ali, A.; Thompson, A.; Parvez, M. *Organometallics* **2009**, *28*, 4845.
- (53) Allinger, N. L.; Siefert, J. H. *J. Am. Chem. Soc.* **1975**, *97*, 752.
- (54) Loudet, A.; Burgess, K. *Chem. Rev.* **2007**, *107*, 4891.
- (55) Pangborn, A. B.; Giardello, M. A.; Grubbs, R. H.; Rosen, R. K.; Timmers, F. *J. Organometallics* **1996**, *15*, 1518.
- (56) Hope, H. *Prog. Inorg. Chem.* **1995**, *43*, 1.
- (57) Blessing, R. H. *Acta Crystallogr.* **1995**, *A51*, 33.
- (58) Sheldrick, G. M. *SADABS, version 2008/1*; Universität Göttingen: Göttingen, Germany, 2008.
- (59) Sheldrick, G. M. *Acta Crystallogr.* **2008**, *A64*, 112.

- (60) Beurkens, P. T. B., G.; de Gelder, R.; Smits, J. M. M.; Garcia-Granda, S.; Gould, R. O. *DIRDIF-2008*; Crystallography Laboratory, Radboud University: Nijmegen, The Netherlands, 2008.
- (61) van der Sluis, P. S., A. L. *Acta Crystallogr.* **1990**, *A64*, 194.
- (62) *PLATON - a multipurpose crystallographic tool*; Utrecht University: Utrecht, The Netherlands.
- (63) Frisch, M. J.; Trucks, G. W.; Schlegel, H. B.; Scuseria, G. E.; Robb, M. A.; Cheeseman, J. R.; Scalmani, G.; Barone, V.; Mennucci, B.; Petersson, G. A.; Nakatsuji, H.; Caricato, M.; Li, X.; Hratchian, H. P.; Izmaylov, A. F.; Bloino, J.; Zheng, G.; Sonnenberg, J. L.; Hada, M.; Ehara, M.; Toyota, K.; Fukuda, R.; Hasegawa, J.; Ishida, M.; Nakajima, T.; Honda, Y.; Kitao, O.; Nakai, H.; Vreven, T.; J. A. Montgomery, J.; Peralta, J. E.; Ogliaro, F.; Bearpark, M.; Heyd, J. J.; Brothers, E.; Kudin, K. N.; Staroverov, V. N.; Keith, T.; Kobayashi, R.; Normand, J.; Raghavachari, K.; Rendell, A.; Burant, J. C.; Iyengar, S. S.; Tomasi, J.; Cossi, M.; Rega, N.; Millam, J. M.; Klene, M.; Knox, J. E.; Cross, J. B.; Bakken, V.; Adamo, C.; Jaramillo, J.; Gomperts, R.; Stratmann, R. E.; Yazyev, O.; Austin, A. J.; Cammi, R.; Pomelli, C.; Ochterski, J. W.; Martin, R. L.; Morokuma, K.; Zakrzewski, V. G.; Voth, G. A.; Salvador, P.; Dannenberg, J. J.; Dapprich, S.; Daniels, A. D.; Farkas, O.; Foresman, J. B.; Ortiz, J. V.; Cioslowski, J.; Fox, D. J.; Gaussian, Inc.: Wallingford CT, 2010.
- (64) Tomasi, J.; Mennucci, B.; Cammi, R. *Chem. Rev.* **2005**, *105*, 2999.

Chapter 3: Summary and Future Work

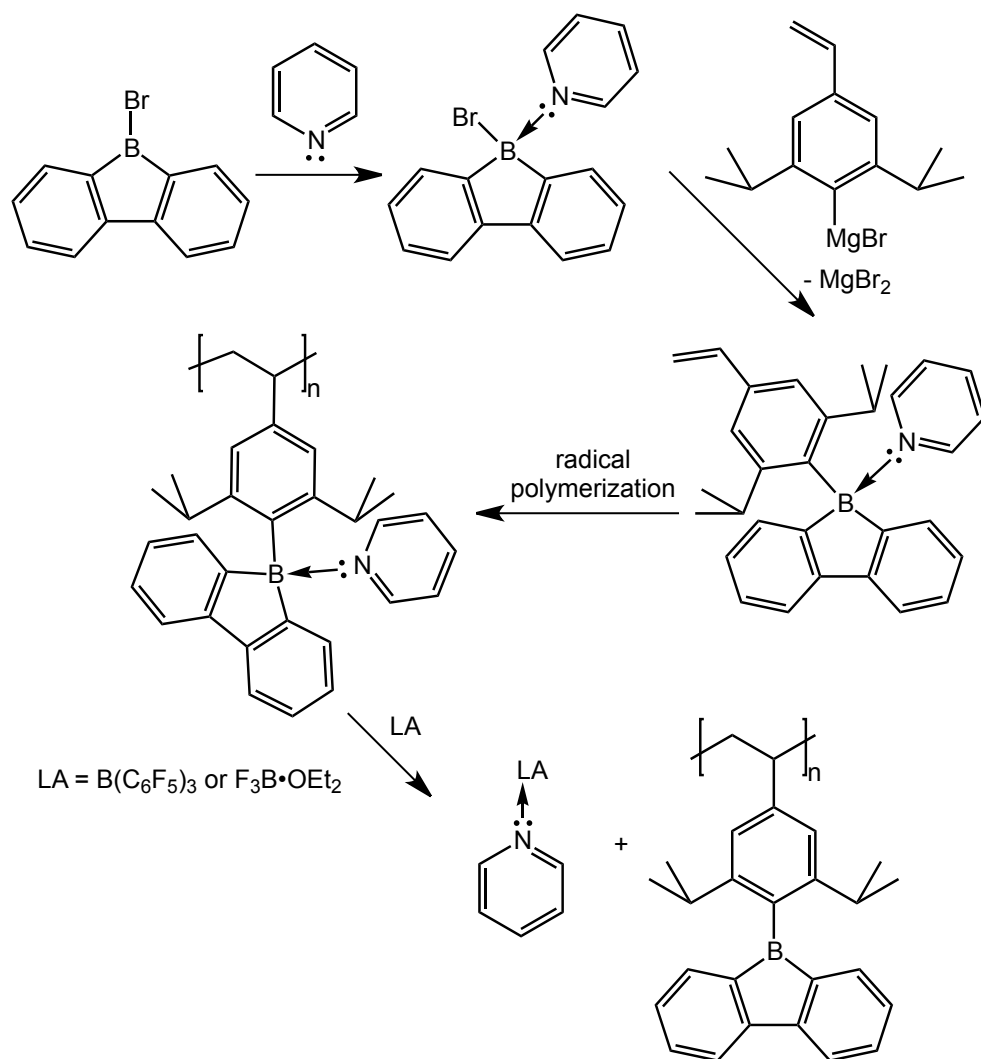
3.1 Summary

As described throughout Chapter 2, several Lewis base adducts of 9-bromo-9-borafluorene were prepared and preliminary reactivity studies were conducted to not only determine the viability of functionalizing the reactive boron-bromine bond but also explore their potential use in the “masking” and “unmaking” approach towards the incorporation of borafluorene as a pendant group within a polymer. Although the removal of the Lewis base proved to be more difficult than anticipated, the mono-adducts $\text{BrBFl}\cdot\text{PPh}_3$ and $\text{BrBFl}\cdot\text{IPrCH}_2$, along with the bis-adduct $[(\text{DMAP})_2\text{BFl}]\text{Br}$, were found to possess interesting luminescent properties. The nature of the observed luminescence was further investigated through theoretical studies, which revealed that both the borafluorene unit and the bound Lewis base were potentially involved in the emissive pathways representing a new class of emissive materials.

3.2 Future Work Towards Incorporating Borafluorene into a Polymeric Scaffold

Although attempt to remove bound Lewis bases from borafluorene were not as facile as anticipated, the removal of at least one DMAP group from the bis-adduct $[(\text{DMAP})_2\text{BFl}]\text{Br}$ did seem to occur in the presence of $\text{B}(\text{C}_6\text{F}_5)_3$. With this in mind, future attempts toward the “masking/unmasking” approach to incorporate the borafluorene unit into a polymeric scaffold will most likely be centered on the use of pyridinyl-based Lewis bases, such as pyridine, picoline or

lutidine (Scheme 3.2.1). The use of such Lewis bases should lead to mono-adducts and their weaker donor ability, compared to DMAP, could be exploited and a strong Lewis acids (such as $B(C_6F_5)_3$ or $F_3B \cdot OEt_2$) could be used to liberate the borafluorene after the desired functionalization of the boron-bromine bond and polymerization had occurred. Furthermore, the polymer system originally sought out may potentially be air and moisture sensitive resulting in the limited use of such polymers for the detection of nucleophiles, especially in moisture rich environments. In effort to prevent any unwanted reactivity, the vacant *p*-orbital on boron must be protected. To achieve this, an avenue that may be explored in the future would involve the incorporation of bulky styrene based groups at a four-coordinate boron center within borafluorene prior to polymerization (Scheme 3.2.1).



Scheme 3.2.1. Representative “masking” and “unmasking” pathway utilizing pyridine as a Lewis base and featuring the incorporation of a bulky aryl group at boron.

3.3 Future Research Involving Luminescent Lewis Base Adducts of Borfluorene

The luminescent properties of the Lewis base - borfluorene adducts BrBFl•PPh₃, [(DMAP)₂BFl]Br and BrBFl•IPrCH₂ showed to be much more complex than initially anticipated. Future efforts to form a deeper understanding

of the possible emission pathways of these adducts should be focused on more in depth theoretical studies of the luminescent systems presented in Section 2.2.2, which can be achieved through calculating excited state configurations of these adducts and examining their potential to contribute to the overall observed fluorescence. The emissive nature of these species should be analyzed via luminescence lifetime measurements. Examination of their potential for electroluminescence, and their ability to maintain their luminescent characteristics over time, may reveal that these compounds could be quite robust and potentially find use as organic light-emitting diode (OLED) displays or even as white emitters for panel lighting. The potential also exists to incorporate these luminescent four-coordinate boron species into polymeric scaffold, similar to those suggested in Section 3.2 although without the removal of the Lewis base, to achieve polymer based OLEDs. Furthermore, the tuning of the fluorescence and incorporation of copolymerization agents can potentially lead to emission in either the green or even red visible regions of the electromagnetic spectrum and ultimately result in the creation of borafluorene-based displays.